Osmotic Mass Exchangers for Power Generation and Energy Recovery: Analysis and Analogy to Heat Exchangers

by

Leonardo David Banchik

B.S., Mechanical Engineering
University of Nevada, Las Vegas, 2010

Submitted to the Department of Mechanical Engineering
in partial fulfillment of the requirements for the degree of

Master of Science in Mechanical Engineering

at the

MASSACHUSETTS INSTITUTE OF TECHNOLOGY

June 2013

Author .....
Department of Mechanical Engineering
May 21, 2013

Certified by .....
John H. Lienhard V
Collins Professor of Mechanical Engineering
Thesis Supervisor

Accepted by .....
David E. Hardt
Chairman, Committee on Graduate Students

Osmotic Mass Exchangers for Power Generation and Energy Recovery: Analysis and Analogy to Heat Exchangers

by

Leonardo David Banchik

Submitted to the Department of Mechanical Engineering
on May 21, 2013, in partial fulfillment of the
requirements for the degree of
Master of Science in Mechanical Engineering

Abstract

Desalination is an important separation process which can provide water scarce regions with clean water for drinking or for agricultural use. Thermal distillation has historically been the dominant method for obtaining pure water, but today, reverse osmosis (RO) produces a greater percentage of the total desalinated water worldwide by a large margin. Fundamentally, an RO system is a membrane-based osmotic mass exchanger. Another type of membrane-based osmotic process, a subset of forward osmosis (FO) called pressure retarded osmosis (PRO), currently exhibits promise for making desalination more energy efficient and is receiving attention in the literature. PRO exchangers are capable of producing power from two streams of different salinity and recovering energy from the brine stream of any desalination process when paired with water pumps and turbines. RO and PRO exchangers are essentially mass exchangers with a hydraulic or osmotic pressure difference across a membrane acting as the predominant driving potential.

Using a simple resistance model for mass transfer applied across an ideal RO and PRO membrane, closed form expressions are developed which relate the performance of a one-dimensional membrane as a function of membrane properties, membrane area, inlet salinities, operating conditions, and flow configuration. These closed form expressions are analogous to the effectiveness versus number of transfer unit (ε-NTU) models which have been used for decades in the rating and sizing of heat exchangers. The closed form expressions, along with numerical simulations for validating the models, are used to determine the limits of permeate flux in one-dimensional RO, PRO, and FO membranes; analyze the power performance of a one-dimensional PRO membrane; and determine the viability of using a PRO-based energy recovery device to reduce the net power consumption for RO desalination.

The closed-form solutions for determining the performance of the RO and PRO membranes require that osmotic pressure be defined as a linear function of salinity. It is found that for a seawater RO process with a typical recovery ratio of 50% or less, the maximum error associated with linearization is less than 6.1%. For brackish water desalination, where processes typically operate at very high recovery ratios but have

brine salinities lower than those encountered in seawater desalination, the error does not exceed 1.8%. For PRO membranes, using varying linearization curves, maximum errors for flux performance of less than 5.5% are incurred by the linear approximation. It is also found that the maximum Second Law efficiency of the power achievable from a one-dimensional PRO membrane is 66.48%. For large membrane areas, the maximum power for a PRO membrane occurs at a hydraulic pressure difference that is not equal to exactly one-half the osmotic pressure difference as reported in literature for zero-dimensional PRO membranes. For PRO membranes used for brine chemical energy recovery from an RO plant treating a feed stream of 35 g/kg, it is found that a wastewater salinity of less than 20 g/kg is required to recover power. Because the membranes within this study have been assumed as ideal, the performance results for flux, power, and power recovery can serve as informative upper bounds.

Thesis Supervisor: John H. Lienhard V
Title: Collins Professor of Mechanical Engineering

Acknowledgments

I dedicate my first words of gratitude to whichever benevolent creator or spark set this awe inspiring universe in motion. Life is truly the greatest gift and these are marvelous times in which we live.

I sincerely thank all of my past engineering mentors whom have guided me through the scientific process and showed me how to become a better researcher: Prof. Robert Boehm, Dr. Jay James, and Dr. Omar Abdelaziz. To my current advisor, Prof. John Lienhard V: I am grateful for your guidance, wisdom, and trust in my abilities when you chose me to join the Center for Clean Water and Energy. I would also like to thank Dr. Mostafa Sharqawy for his contributions to this work and to King Fahd University of Petroleum and Minerals for funding this research through the Center for Clean Water and Clean Energy at MIT and KFUPM.

Gracias a mis padres, Carlos y Adriana, por la paciencia que tuvieron en criarme, porque no era un niño fácil de criar; por el amor inmenso y el apoyo que me siguen dando; y por inspirarme con su fuerza y valor ejemplificado por actos como establecer una vida en un país extraño, empezar una empresa exitosa, o tomar roles de liderazgo en la sinagoga, en los deportes, y en organizaciones profesionales y comunitarias. Gracias por servir como modelos de cómo ser una persona de bien. Tambien doy gracias a mis dos hermanos, Anna y Marcos, quienes me siguen inspirando con sus propios éxitos y a todos las otras personas, inumerables de mencionar, que ayudaron a que este momento sea una realidad. Los quiero muchísimo.

THIS PAGE INTENTIONALLY LEFT BLANK

Contents

THIS PAGE INTENTIONALLY LEFT BLANK

List of Figures

List of Tables

Nomenclature

Roman symbols		Units
A	water permeability coefficient	kg/s-m^2-kPa
A_m	total membrane surface area	m^2
b	molality - moles of solute per kilogram of solvent	mol/kg
C	modified van 't Hoff coefficient	kPa-kg/g
c	molarity - moles of solute per cubic meter of solution	mol/m^3
CF	concentration factor	-
g	specific Gibbs free energy	kJ/kg
h	specific enthalpy	kJ/kg
i	van 't Hoff factor	-
K	solute resistance to diffusion	s/m
k	mass transfer coefficient	m/s
$\dot{m}$	solution mass flow rate	kg/s
M	molecular weight	g/mol or kg/mol
MR	mass flow rate ratio	-
MTU	number of mass transfer units	-
N	number of elements in a numerical exchanger	-
P	hydraulic pressure	kPa
P^*	pressure ratio	-
PR	permeation ratio	-
$\dot{Q}$	heat transfer rate	kW
R	universal gas constant	kJ/mol-K
RR	recovery ratio	-
s	specific entropy	kJ/kg-K
SR	osmotic pressure ratio	-
T	temperature	K or °C
w	salinity - grams of solute per kilogram of solution	g/kg
$\dot{W}$	work transfer rate or power	kW

Greek symbols		**Units**
α	first quadratic root	
β	second quadratic root	
Δ	a difference	
ε	effectiveness	-
η	isentropic efficiency	-
θ	modified osmotic pressure ratio	-
κ	first quadratic root	
λ	second quadratic root	
π	osmotic pressure	kPa
ρ	density	kg/m^3
ϕ	osmotic coefficient	-
ω	Lambert or omega function	

Subscripts

0	environmental property
actual	actual operation
A	system A
B	system B
b	brine stream
comp	compression
d	draw stream
db	diluted brine stream
exp	expansion
f	feed stream
i	pertaining to the i^{th} section of a one-dimensional exchanger
in	inlet
j	pertaining to the j^{th} solute in a solution
least	reversible operation
max	maximum

net	net system work
opt	optimum
out	outlet
p	permeate or product stream
pump	associated with a pump
pure	property of pure water
rec	work recovered by use of energy recovery device
recipe	corresponds to a reference of seawater constituents
rev	reversible
s	salt
sep	separation
turb	associated with a turbine
ww	wastewater stream

Superscripts		**Units**
$'$	modified variable	
$''$	flux (per unit area)	$1/m^2$
rev	reversible	

Acronyms

ECP	external concentration polarization
ERD	energy recovery device
FO	forward osmosis
ICP	internal concentration polarization
NTU	number of transfer units
PRO	pressure retarded osmosis
PX	pressure exchanger
RO	reverse osmosis
SGE	salinity gradient engine

Chapter 1

Introduction

1.1 Water crisis

"Water, water, everywhere, nor any drop to drink"

So cried Samuel Coleridge's ocean stranded ancient mariner, but for many living in the world today, this is not fiction but a stark reality. According to the United Nations, almost one-fifth of the world population currently lives in areas of physical water scarcity and one-quarter lives in developing countries which face water scarcity due to a lack of adequate water related infrastructure [1]. In addition to scarcity, the quality of available water in certain parts of the world is so low that in 2010 the Secretary-General of the United Nations declared that dirty water kills more people than war [2]. There are solutions, however, to quench the world's thirst.

1.2 Existing solutions

Conservation and wastewater recycling are crucial first steps for reducing water demands in water stressed regions. Where these efforts are insufficient or unsuccessful, however, desalination plays an essential role in providing fresh water for potable use and for agriculture. Desalination is any process that separates ions from saline waters. Figure 1-1 shows the total worldwide installed capacity by desalination technology

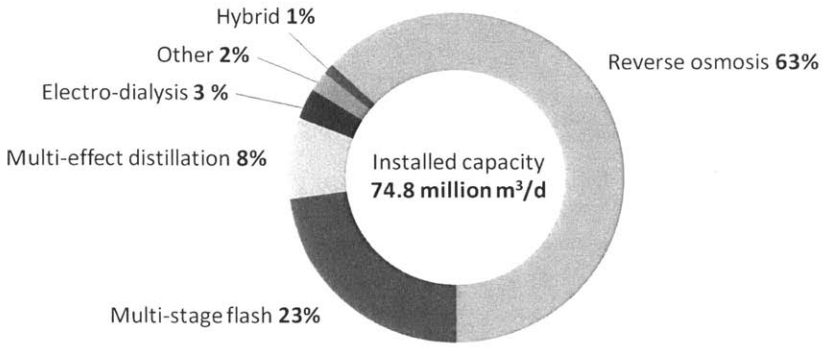

Figure 1-1: Total worldwide installed capacity by desalination technology for 2012.

in 2012 [3]. The desalination technologies shown here can be categorized by their primary driving potential: temperature, for multi-stage flash and multi-effect distillation; voltage, for electro-dialysis; or hydraulic pressure, for reverse osmosis.

Of the nearly 75 billion liters per day currently produced by desalination, reverse osmosis (RO) systems produce the lion's share of 47 billion liters per day. Because RO dominates the global installed capacity, this work will focus on ways to improve reverse osmosis systems in order to alleviate worldwide water scarcity.

1.2.1 Osmotic mass exchangers

Figure 1-2 depicts the two osmotic mass exchangers which will be the focus of this work. Figure 1-2a shows a basic representation of a reverse osmosis mass exchanger. In a reverse osmosis system, a feed stream to be purified, typically seawater or brackish water, is first pre-treated to prevent membrane damage. In this step, anti-scalants are added and foulants are removed. The pre-treated feed stream is then pumped to a high pressure and sent into the exchanger.

The RO exchanger is comprised of a semi-permeable membrane which allows water to pass through but not salts or other dissolved solids. Water is forced through the membrane via a large trans-membrane hydraulic pressure difference. This hydraulic pressure difference, $\Delta P = P_{\text{feed}} - P_{\text{product}}$, must be greater than the difference in trans-membrane osmotic pressure, $\Delta\pi = \pi_{\text{feed}} - \pi_{\text{product}}$, in order for the water to flow in the direction of lower salt concentration.

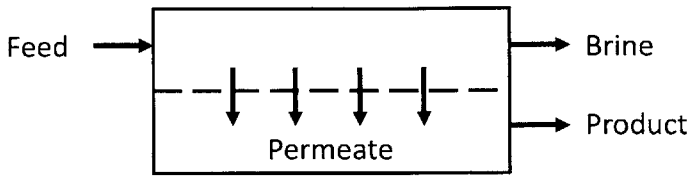

(a) Representation of a reverse osmosis exchanger

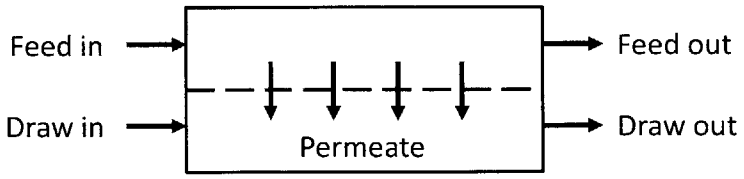

(b) Representation of a forward osmosis exchanger

Figure 1-2: Schematic drawing of a reverse and forward osmosis exchanger.

The osmotic pressure of a stream is a function of the local amount of dissolved salts. The phenomenon of osmosis is a mass transfer process in which water travels through a membrane impermeable to salts from a region of low salt concentration to a region of high salt concentration. The high salinity region is said to have high osmotic pressure, whereas the low salinity region is said to have low osmotic pressure. Inside of the reverse osmosis exchanger, the feed is concentrated and the product is very pure. This corresponds to a high osmotic pressure feed and a low osmotic pressure product, which, in the absence of a hydraulic pressure difference, will serve to force permeate from the product side to the feed side. For the RO process, as long as the applied hydraulic pressure difference is larger than the osmotic pressure difference, the permeate will flow through the membrane in the intended direction. The remaining feed exits as a concentrated brine and the permeate is collected as the product. In practice, each exchanger unit is a pressure vessel comprised of one or more spiral wound membranes. There may be multiple pressure vessels in series and in parallel in an RO plant.

Figure 1-2b shows a typical forward osmosis (FO) exchanger. Like an RO system, a semi-permeable membrane is used which allows water, but not salts, to pass

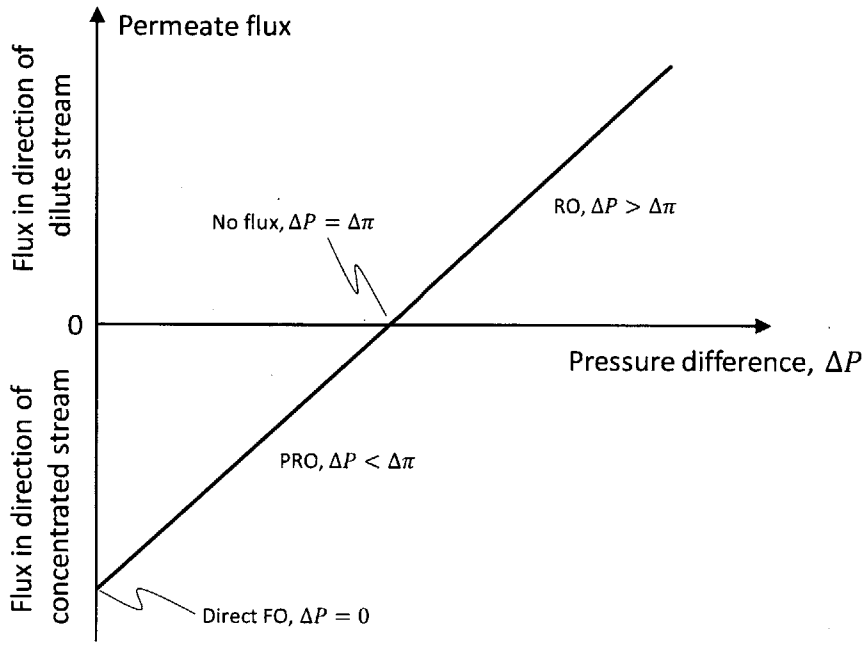

Figure 1-3: Qualitative plot of the various operating regimes of osmotic membrane-based mass exchangers. Figure adapted from Lee et al. [4].

through. Unlike RO, however, the permeate flows into the more concentrated stream due to an osmotic pressure difference which is higher than the hydraulic pressure difference. The term forward osmosis specifically means that the permeate flows through the membrane in the direction of the more concentrated stream. The value of the hydraulic pressure difference, $\Delta P = P_{\text{draw}} - P_{\text{feed}}$, relative to the osmotic pressure difference, $\Delta\pi = \pi_{\text{draw}} - \pi_{\text{feed}}$, is what denotes whether the exchanger operates in the pressure retarded osmosis (PRO) or direct forward osmosis regime as illustrated in Fig. 1-3. An exchanger operates in direct forward osmosis when both streams are at the same hydraulic pressure and in the PRO regime when $0 < \Delta P < \Delta\pi$. Throughout this work, the terms direct FO and FO both denote the regime of operation where $\Delta P = 0$.

The second chapter of this work will present a method for rating and sizing RO exchangers which is similar to a model used for heat exchangers. This model can allow RO system designers to select the appropriate amount of membrane area for given operating conditions, membrane properties, and desired performance. The third

chapter extends the method of rating and sizing RO exchangers to FO exchangers operating in the PRO regime. These types of exchangers can be used for either power production or for recovering chemical energy from the brine stream of a desalination process. The final two chapters examine the limits of FO performance, the limits of PRO power production, and the viability of using PRO membranes for brine chemical energy recovery from a reverse osmosis system.

THIS PAGE INTENTIONALLY LEFT BLANK

Chapter 2

Analogy of Reverse Osmosis Mass Exchangers to Heat Exchangers

Leonardo D. Banchik, Mostafa H. Sharqawy [1], and John H. Lienhard V

Chapter abstract

A strong analogy exists between heat exchangers and osmotic mass exchangers. The ε-NTU method is well-known for the design of heat exchangers. In the present chapter, a similar method, called ε-MTU (effectiveness-mass transfer units), is developed for osmotic mass exchangers in order to design RO systems. This method is used to relate the size, applied hydraulic pressure, inlet salinity, and other parameters to the recovery ratio and a newly defined effectiveness parameter for such mass exchangers. The governing equations for an RO mass exchanger are nondimensionalized assuming ideal membrane characteristics and a linearized form of the osmotic pressure function for seawater. A closed form solution is found which relates three dimensionless groups: the mass transfer units for an RO device, MTU, which is equivalent to an effective size of the exchanger; a pressure ratio, SR, which relates osmotic and hydraulic pressures; and the recovery ratio, RR, which relates the permeate to the inlet feed flow rate. In addition, the effectiveness of an RO exchanger is defined as the recovery ratio divided by the maximum recovery ratio. A one-dimensional numerical model of an RO exchanger is developed in order to establish the range of validity of the analytical model based on a linearized osmotic pressure approximation. The analytical ε-MTU model for the RO exchanger can be easily used for design or performance evaluation.

[1] Dr. Sharqawy contributed to the work in this chapter by assisting in the development of the equations, developing the reverse osmosis effectiveness definition, and providing the design example.

2.1 Introduction

Reverse osmosis (RO) is a separation process commonly used for the production of pure water from brackish water or seawater. In RO, a saline source of water, the feed stream, is pumped to a high hydraulic pressure and allowed to flow across one side of a semi-permeable membrane within a pressure vessel, while lower pressure is maintained on the other side. The membrane is permeable to water diffusion but highly resistant to salt permeation so that, along the length of the membrane, pure water flows through the membrane from the feed to the lower pressure, permeate side. The permeate is collected as a product at the outlet whereas the feed stream exits the vessel as a concentrated brine. The process is called reverse osmosis because the input hydraulic pressure of the feed stream must be greater than the osmotic pressure difference between the brine and permeate streams which would otherwise cause an osmotic flow of water from the permeate to the feed.

There are many mathematical models for the mass transport process through the RO membrane and which relate the performance of the RO system to the operating conditions. A well-known model for the membrane transport is the solution-diffusion model of Lonsdale et al. [5]. This model assumes that the membrane is a non-porous material into which molecules dissolve and diffuse through. This diffusion theory applies to both the solvent and solute molecules. Other mathematical models for RO include the porous model [6], the capillary flow model [7], and the irreversible thermodynamic model [8]. Much research has been conducted on the physics of the solution-diffusion model [9–13] and many numerical studies have been applied to account for the more complex effects of concentration polarization, salt diffusion, and fouling [14–18]. Others have applied the solution-diffusion model for the design of RO modules such as spiral wound and hollow fiber modules [19–22]. In addition, the solution-diffusion model has been used together with relevant conservation laws to optimize the operation of RO systems and minimize the specific power consumption

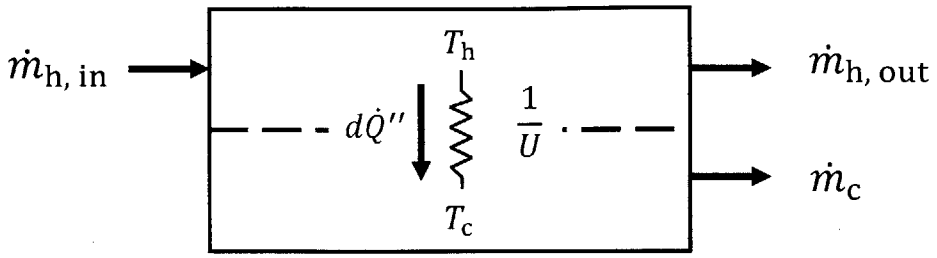

(a) Single inlet stream heat exchanger

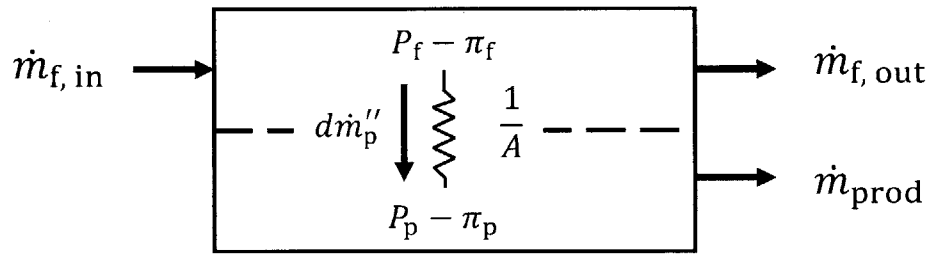

(b) Single inlet stream osmotic mass exchanger

Figure 2-1: Schematic drawing of a single inlet heat and osmotic mass exchanger.

of a plant [23–28].

In the heat exchanger shown in Fig. 2-1a, the temperature difference between a hot and cold fluid is the driving potential for a differential amount of heat transfer. The resistance to heat flow per unit area is the reciprocal of the overall heat transfer coefficient, U. The exchanger shown here is for a phase change process which has a fixed cold temperature throughout the length of the exchanger. The analogous system for an osmotic mass exchanger is the RO system shown in Fig. 2-1b. A feed solution of a high salinity and high osmotic and hydraulic pressure enters the left side of the exchanger. Along the length of the exchanger, permeate is forced through a semipermeable membrane, leaving the salts behind. At the exit of the exchanger, the feed is recovered as a concentrated brine and the product is recovered as the accumulated amount of pure permeate. The driving potential for mass transfer is the difference in hydraulic and osmotic pressures. The resistance to the mass transfer per unit area is the reciprocal of the water permeability coefficient, A.

In heat exchangers, the effectiveness-number of transfer units (ε-NTU) method

developed by Kays and London [29] is a well-known design method that determines the required surface area of a heat exchanger for a fixed effectiveness and inlet conditions. The method uses three dimensionless groups: the effectiveness, which is the ratio of actual heat exchange to the maximum heat exchange possible; a heat capacity rate ratio, which is the heat capacity rate of the minimum capacity rate stream divided by that of the maximum capacity rate stream; and the number of transfer units, which is an effective size of the heat exchanger.

This chapter develops an ε-NTU method for an RO mass exchanger. The governing equations for permeate flow in an RO exchanger are nondimensionalized and solved to provide closed form analytical expressions which relate the effective size of the exchanger, the performance of the exchanger, and the input operating conditions. A new dimensionless performance indicator, the effectiveness of the RO exchanger, is defined. These new dimensionless groups are discussed, and the analogy to heat exchangers is drawn. Because the analytical model requires a linearization of the osmotic pressure, a numerical model using the nonlinear osmotic pressure is also applied to quantify the errors associated with using the linear approximation. Finally, a design example is given to illustrate the use of the present approach as a tool for design of an RO system.

2.2 Reverse osmosis mass exchanger model

Figure 2-2 is a schematic drawing of an osmotic mass exchanger working in the RO mode. A feed solution with a high salt concentration flows through a channel alongside a semi-permeable membrane. The hydraulic pressure difference (ΔP) is greater than the osmotic pressure difference ($\Delta\pi$) across the membrane, so that water flows from the feed side to the permeate side. The inlet conditions of the feed stream are given as the mass flow rate, hydraulic pressure, and osmotic pressure (which is a function of

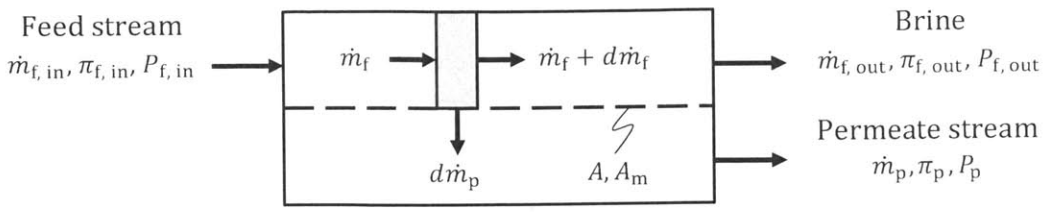

Figure 2-2: Schematic drawing of a membrane-based RO osmotic mass exchanger.

the local stream salinity) as indicated in Fig. 2-2. The total membrane area (A_m) and water permeability (A) of the membrane material are also given. The model makes the following assumptions:

- The water permeability coefficient (A) is constant.
- Concentration polarization is neglected, so that the salt concentration near the membrane surface is equal to the bulk concentration of the associated stream.
- Hydraulic pressure drop through the flow channels is negligible.
- Salt rejection is 100%, so that only pure water diffuses through the membrane.
- The osmotic pressure follows van 't Hoff's equation which is linearly proportional to the salt concentration (see Appendix A).

2.2.1 Governing equations

The permeate flow rate in the direction of the permeate stream through a differential membrane area is given by Eq. (2.1)

$$d\dot{m}_p = A \cdot (\Delta P - \Delta\pi)\, dA_m \tag{2.1}$$

where

- $d\dot{m}_p$, is the permeate mass flow rate through the membrane in kg/s,

- A, is the modified[2] water permeability coefficient of the membrane in kg/s-m^2-kPa,
- ΔP is the hydraulic pressure difference between the feed and permeate (i.e., $P_\mathrm{f} - P_\mathrm{p}$) in kPa,
- $\Delta\pi$ is the local osmotic pressure difference between the feed and permeate (i.e., $\pi_\mathrm{f} - \pi_\mathrm{p}$) in kPa, and
- A_m is the membrane surface area in m^2.

The osmotic pressure for a solution [30] is given by

$$\pi = \phi(RT\rho_{\text{solvent}}) \sum_{j=\text{solutes}} b_j \tag{2.2}$$

where ϕ is the osmotic coefficient, predominantly a function of temperature and salinity; R is the universal gas constant; T is the absolute temperature; ρ_{solvent} is the solvent density (pure water); and $\sum_{j=\text{solutes}} b_j$ is the sum of the molalities of each solute. A detailed derivation of the osmotic pressure for seawater is given in Appendix B.

Equation (2.2) shows that osmotic pressure is a nonlinear function of salinity. In order to facilitate our analysis, we use van 't Hoff's equation to linearize the osmotic pressure. In the second half of this chapter, this assumption will be checked for its validity by comparing results to a numerical model which uses the nonlinear osmotic pressure. Checking for the validity of the linearization assumption will be especially important for ranges of operation which encounter high salinities. Expressing the osmotic pressure as a linear function of salinity yields:

$$\Delta\pi = \pi_\mathrm{f} - \pi_\mathrm{p} = C(w_\mathrm{f} - w_\mathrm{p}) \tag{2.3}$$

[2]It is important to note that the water permeability coefficient (A) is often given in units of m/s-bar or L/m^2-hr-bar [16], which is the permeate water volume flux per unit pressure difference; however, for the present model, we express this coefficient on a mass basis (equivalent to multiplying it by the density of pure water and some obvious SI conversion factors).

where w is the salinity (mass of solutes per total mass of solution) in g/kg and C is a modified van 't Hoff's coefficient (see Appendix A). The modified van 't Hoff's coefficient can adjusted by range to address for nonlinearity. Substituting Eq. (2.3) into Eq. (2.1),

$$d\dot{m}_{\mathrm{p}} = A \cdot [\Delta P - C(w_{\mathrm{f}} - w_{\mathrm{p}})]\, dA_{\mathrm{m}} \tag{2.4}$$

Applying conservation of solutes for the feed side between the inlet and any arbitrary location along the flow channel:

$$\dot{m}_{\mathrm{s,\,f}} = \dot{m}_{\mathrm{f,\,in}} \times w_{\mathrm{f,\,in}} = \dot{m}_{\mathrm{f}} \times w_{\mathrm{p}} \tag{2.5}$$

At the same arbitrary location, conservation of mass requires that

$$\dot{m}_{\mathrm{f,\,in}} = \dot{m}_{\mathrm{f}} + \dot{m}_{\mathrm{p}} \tag{2.6}$$

Substitution of Eq. (2.6) into Eq. (2.5) yields

$$w_{\mathrm{f}} = \frac{\dot{m}_{\mathrm{f,\,in}} \times w_{\mathrm{f,\,in}}}{\dot{m}_{\mathrm{f,\,in}} - \dot{m}_{\mathrm{p}}} \tag{2.7}$$

Under the assumed condition of 100% salt rejection, only pure water permeates through the membrane; hence the salinity of the permeate and its osmotic pressure are zero. Substituting Eq. (2.7) into Eq. (2.4) and setting $w_{\mathrm{p}} = 0$ yields

$$d\dot{m}_{\mathrm{p}} = A \left[\Delta P - C \frac{\dot{m}_{\mathrm{f,\,in}} \times w_{\mathrm{f,\,in}}}{\dot{m}_{\mathrm{f,\,in}} - \dot{m}_{\mathrm{p}}}\right] dA_{\mathrm{m}} \tag{2.8}$$

We now proceed to cast Eq. (2.8) in a dimensionless form. Three dimensionless parameters are introduced for this purpose.

2.2.2 Dimensionless parameters

Recovery ratio, RR

$$\mathrm{RR} \equiv \frac{\dot{m}_{\mathrm{p}}}{\dot{m}_{\mathrm{f,\,in}}} \tag{2.9}$$

The recovery ratio is a primary performance metric of an RO mass exchanger as it represents the amount of pure water recovered from the feed stream. (In so far as the inlet mass flow rate is greater than the maximum amount of permeate that can be recovered, the recovery ratio should not be confused with the effectiveness which will be described in the next section.)

Osmotic pressure ratio, SR

$$\mathrm{SR}_{\mathrm{f}} \equiv \frac{\pi_{\mathrm{f,\,in}}}{\Delta P} \tag{2.10}$$

The osmotic pressure ratio is the ratio of the osmotic pressure at the feed inlet to the trans-membrane hydraulic pressure difference. This ratio should always be less than one since in the RO system the hydraulic pressure difference must be greater than the osmotic pressure of the feed.

Mass transfer units, MTU

$$\mathrm{MTU} \equiv \frac{A\,A_{\mathrm{m}}\,\Delta P}{\dot{m}_{\mathrm{f,\,in}}} \tag{2.11}$$

The *number of mass transfer units* (MTU) is a dimensionless parameter for a membrane mass exchanger similar to the *number of transfer units* (NTU) used in heat exchanger design. The total membrane area, A_{m}, is analogous to the total heat exchanger surface area and A, the overall water permeability coefficient, is analogous to the overall heat transfer coefficient in heat exchangers. Therefore, the MTU in the membrane-based mass exchanger will play the same role that NTU plays in ε-NTU analysis of heat exchangers.

Dividing Eq. (2.8) by $\dot{m}_{\mathrm{f,\,in}}$ and substituting Eqs. (2.9)–(2.11) yields

$$d\mathrm{RR} = \left(1 - \frac{\mathrm{SR_f}}{1 - \mathrm{RR}}\right) d\mathrm{MTU} \tag{2.12}$$

Assuming no pressure drop through the flow channels, the hydraulic pressure difference between the feed and permeate sides (ΔP) is fixed. With the boundary condition that RR = 0 where MTU = 0 (at the inlet), Eq. (2.12) can be integrated to give the mass transfer units as follows

$$\mathrm{MTU} = \mathrm{RR} + \mathrm{SR_f}\,\ln\left(\frac{\mathrm{SR_f} - 1}{\mathrm{SR_f} + \mathrm{RR} - 1}\right) \tag{2.13}$$

Alternatively, an explicit solution for the recovery ratio can be obtained from Eq. (2.13) as follows

$$\mathrm{RR} = 1 - \mathrm{SR_f} - \mathrm{SR_f} \cdot \omega\left[\left(\frac{1 - \mathrm{SR_f}}{\mathrm{SR_f}}\right)\exp\left(\frac{1 - \mathrm{SR_f} - \mathrm{MTU}}{\mathrm{SR_f}}\right)\right] \tag{2.14}$$

where ω is the Lambert, or omega, function in which $\omega(x)$ is the solution to $x = \omega e^{\omega}$. Equation (2.13) can be used to design an RO membrane mass exchanger where the required mass transfer units (hence the effective membrane surface area) is given as an explicit relation of the form

$$\mathrm{MTU} = \mathrm{fn}(\mathrm{RR},\, \mathrm{SR_f}) \tag{2.15}$$

Figure 2-3 shows the variation of the recovery ratio (RR) with mass transfer units (MTU) for varying osmotic pressure ratios at a temperature of 25°C. For salinities of feed which are close to seawater, the $\mathrm{SR_f} = 0.1$ contour will result in brine that is highly saline at MTU values of greater than 1. In this range, the osmotic pressure of the brine stream significantly deviates from the linearized value. Seawater RO

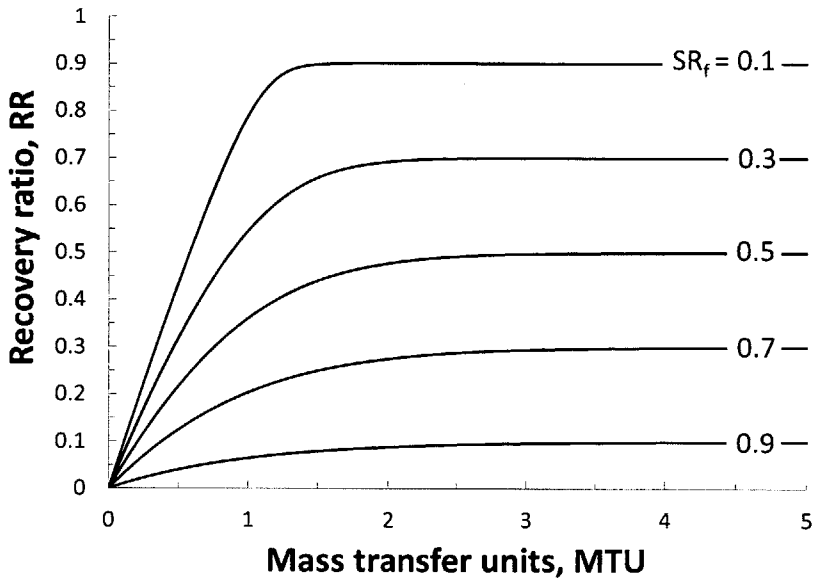

Figure 2-3: Recovery ratio vs. mass transfer units at various osmotic pressure ratios.

systems, however, typically operate at recovery ratios of about 60% and lower.

The outlet feed (or brine) salinity, $w_{\mathrm{f,\,out}}$, can be expressed as a function of the recovery ratio and the inlet feed salinity:

$$w_{\mathrm{f,\,out}} = \frac{w_{\mathrm{f,\,in}}}{1 - \mathrm{RR}} \tag{2.16}$$

The concentration factor, CF, can be defined as the ratio of the brine to inlet feed salinity. From Eq. (2.16), we have

$$\mathrm{CF} \equiv \frac{w_{\mathrm{f,\,out}}}{w_{\mathrm{f,\,in}}} = \frac{1}{1 - \mathrm{RR}} \tag{2.17}$$

The concentration factor (CF) is a crucial design parameter in desalination technologies, in that too high a CF can lead to scale formation. In practice, for seawater desalination, the CF rarely exceeds 3, whereas for brackish water desalination this figure can be increased to 5 or even 10 depending on the characteristics of the feed

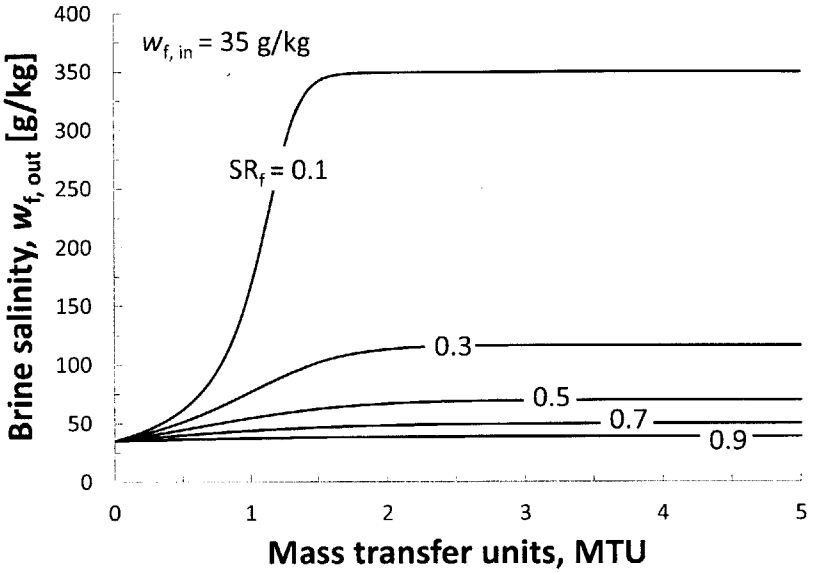

Figure 2-4: Salinity of rejected brine vs. mass transfer units at different osmotic pressure ratios when the inlet feed salinity is 35 g/kg.

water. Figure 2-4 shows the brine salinity as a function of the mass transfer units with varying osmotic pressure ratio for a fixed inlet feed salinity representative of seawater. It can be seen that the contour of $SR_f = 0.1$ provides an unacceptably high brine salinity for MTU greater than 1. However, it is very unlikely that a seawater RO system will be designed to operate at such high recovery ratios required to produce a brine in this salinity range. Figure 2-5 shows the concentration factor plotted versus the mass transfer units for varying osmotic pressure ratios.

It is clear from Eq. (2.15) that the three dimensionless parameters are similar to effectiveness-NTU representations of heat exchangers in which NTU is a function of the effectiveness and the heat capacity rate ratio; however, an additional derivation will be needed to reach a parameter analogous to effectiveness. This will be presented in the subsequent section.

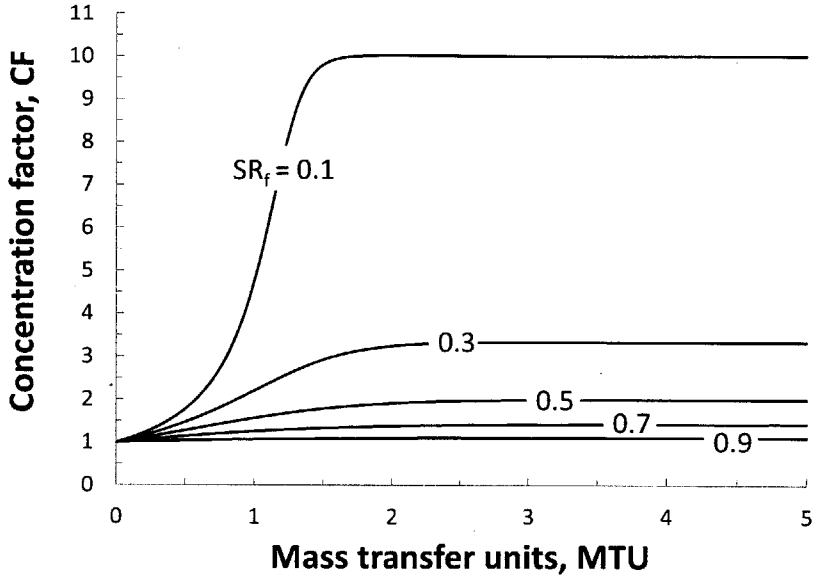

Figure 2-5: Concentration factor vs. mass transfer units for varying osmotic pressure ratio and arbitrary feed salinity.

2.3 Reverse osmosis effectiveness (ε-MTU model)

The effectiveness of the RO system can be defined as the ratio of the permeate flow rate actually achieved by an exchanger of a given size to the maximum possible permeate flow rate for a given hydraulic pressure and inlet osmotic pressure. The effectiveness so defined is the same as the ratio of the actual recovery ratio to the maximum possible recovery ratio. This definition is evident in Fig. 2-3, in which the recovery ratio reaches a maximum value for a given osmotic pressure ratio as the MTU becomes large. The exchanger effectiveness approaches one in this limit.

In this section, we wish to derive a relation for the maximum recovery ratio in order to write an equation for the effectiveness. We note that the maximum permeate flow rate will be reached when the osmotic pressure difference between the feed and permeate rises to the point that the net driving force ($\Delta P - \Delta\pi$) equals zero at the outlet of the membrane channel. From Eq. (2.1), this fixes the outlet osmotic pressure

as

$$\Delta P = \Delta\pi = \pi_{\mathrm{f,\,out}} \tag{2.18}$$

The relation between the inlet and outlet osmotic pressure can be obtained using conservation of solution and solute on the feed stream as follows

$$\pi_{\mathrm{f,\,out}} = \frac{\pi_{\mathrm{f,\,in}}}{1 - \mathrm{RR}} \tag{2.19}$$

Substituting Eq. (2.18) into Eq. (2.19), the following relation for the maximum recovery ratio is obtained

$$\mathrm{RR}_{\mathrm{max}} = 1 - \mathrm{SR}_{\mathrm{f}} \tag{2.20}$$

Equation (2.20) gives the maximum recovery ratio as a function of the osmotic pressure ratio. Now, the effectiveness is defined as

$$\varepsilon \equiv \frac{\mathrm{RR}}{\mathrm{RR}_{\mathrm{max}}} \tag{2.21}$$

Substituting Eqs. (2.20) and (2.21) into Eq. (2.13), an expression for MTU as a function of the effectiveness can be obtained as given in Eq. (2.22):

$$\mathrm{MTU} = \varepsilon(1 - \mathrm{SR}_{\mathrm{f}} - \mathrm{SR}_{\mathrm{f}}\,\ln(1 - \varepsilon)) \tag{2.22}$$

Figure 2-6 shows the variation of effectiveness with the mass transfer units for various osmotic pressure ratios. It may be observed that for small values of MTU, the effectiveness is approximately equal to MTU. This result can be found mathematically by taking the derivative of Eq. (2.22) with respect to effectiveness and taking the limit to where effectiveness approaches zero. The result can also be found, as shown in Eq. (2.23), by substituting the integrated form of the zero-dimensional transport equation, Eq. (2.1), along with Eq. (2.20) into Eq. (2.21) while noting that $\Delta\pi \rightarrow \pi_{\mathrm{f,\,in}}$

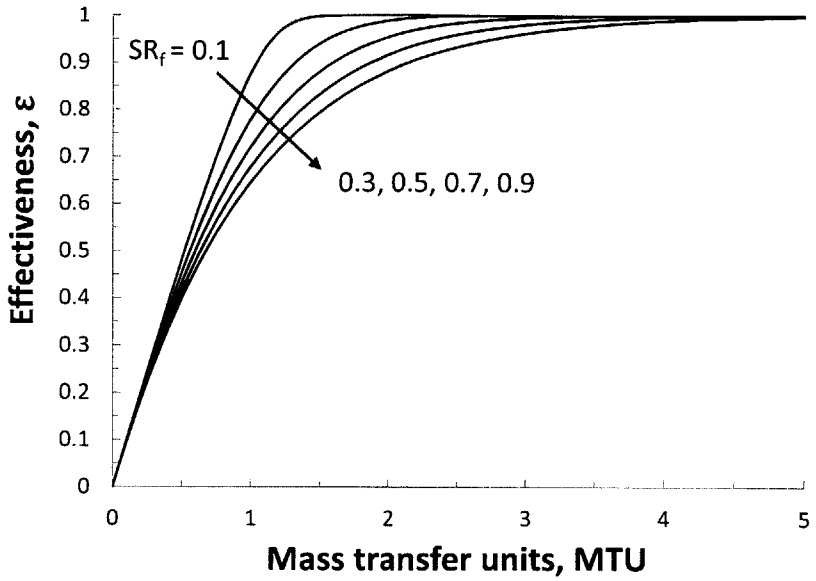

Figure 2-6: Effectiveness vs. mass transfer units for varying osmotic pressure ratios.

for a zero-dimensional exchanger with pure permeate.

$$\text{at MTU} << 1,\ \varepsilon = \frac{\text{RR}_{\text{zero-dimensional}}}{\text{RR}_{\text{max}}} = \frac{A \times A_{\text{m}}(\Delta P - \Delta\pi)}{\dot{m}_{\text{f, in}}\left(1 - \frac{\pi_{\text{f, in}}}{\Delta P}\right)} = \text{MTU} \qquad (2.23)$$

This is analogous to the well-known limit for heat exchangers where the effectiveness is equal to NTU as NTU approaches zero [31].

2.3.1 Numerical model of RO mass exchanger

The analytical expressions required that a linear relationship between osmotic pressure and salinity be assumed. This assumption is acceptable for relatively dilute solutions, but for more saline waters, the variation is somewhat nonlinear. In this section, a numerical model of a one-dimensional reverse osmosis mass exchanger is developed using a nonlinear function for the osmotic pressure, so as to determine the deviation of the analytical results given earlier. The model applies a discretized version of the transport equation, Eq. (2.1), and conservation of solutes and solution

Table 2.1: Data input for RO numerical model

Input	Symbol	Value/Range
Ambient temperature	T_0	25 °C
Modified water permeability coefficient	A	3.61×10^{-6} kg/s-m^2-kPa
Feed mass flow rate	$\dot{m}_{\mathrm{f,in}}$	1 kg/s
Inlet feed salinity	$w_{\mathrm{f,in}}$	5 g/kg and 35 g/kg
Trans-membrane pressure difference	ΔP	0.60–3.08 MPa
Membrane area	A_{m}	0–3.46×10^3 m^2

to N membrane elements in series. The number of elements was increased to 50 at which point the results were grid independent. The total amount of permeate is calculated by numerically integrating the permeate mass flow rate produced by all elements. The development of the nonlinear osmotic pressure function used in this numerical model is given in Appendix B.

The numerical model is used to estimate the error in the analytical model that results from using a linearized osmotic pressure function. All other assumptions made for the analytical model are also made for the numerical model. An additional assumption is that the RO membranes can withstand arbitrary net driving pressures. Two cases are considered: brackish water, $w_{\mathrm{f,\,in}} = 5$ g/kg, and seawater, $w_{\mathrm{f,\,in}} = 35$ g/kg. The input parameters for the numerical calculation are given in Table 2.1. The water permeability coefficient used is representative of a typical spiral wound seawater membrane [14].

To determine the effectiveness from the numerical model, we once again note that the maximum recovery ratio, $\mathrm{RR_{max}}$, is achieved when the equality from Eq. (2.18) holds. Applying conservation of solutes and solution to the feed stream yields the following expression:

$$\mathrm{RR_{max}} = 1 - \frac{w_{\mathrm{f,\,in}}}{w_{\mathrm{f,\,out,\,max}}} \tag{2.24}$$

The maximum outlet salinity, $w_{\mathrm{f,\,out,\,max}}$, is determined by Eq. (2.20) of which the

osmotic pressure at the outlet, $\pi_{f,\,out}$, is a function. The effectiveness can now be determined by Eq. (2.19) using the maximum recovery ratio defined by Eq. (2.24).

2.3.2 Results and discussion

Figure 2-7 shows the recovery ratio versus mass transfer units for varying osmotic pressure ratios. The black solid lines are the same curves displayed in Fig. 2-3, and the circles and triangles are for the brackish water and seawater cases using the nonlinear function for osmotic pressure. As shown in this figure, the maximum deviation of the analytical result from the seawater numerical result is about 7.98% at the lowest value of SR_f. This is because for a high salinity feed stream (i.e., the seawater case), and at higher recovery ratio ($RR = 0.9$ at this large deviation), the exit brine has a very high salinity, hence the actual osmotic pressure deviates significantly from the linear model. Because the actual osmotic pressure is higher than the linearized pressure at high salinities (see Fig. A-1 in Appendix A.1), the amount of permeate is reduced and the maximum achievable recovery ratio declines. The observed deviation is generally acceptable because it occurs at high inlet feed salinity and low osmotic pressure ratio conditions that are not found in practical operation. As previously mentioned, the highest recovery ratio for seawater RO plants is typically in the range of 40 to 60% [32, 33]. From Fig. 2-7, the maximum deviation between the analytical and numerical solution for recovery ratios less than 50% does not exceed 6.1%.

Current RO technologies use a recovery ratio of about 80–90% for low salinity surface water and municipal wastewater [32, 33]. The recovery ratio for brackish water varies between the two ranges subject to the feed salinity. Even for these high recovery ratios, however, the deviations in recovery ratio for the brackish water case do not exceed 1.8% from the analytical model. This is because the osmotic pressure is nearly linear with salinity for low salinity feeds such as brackish water and municipal wastewater.

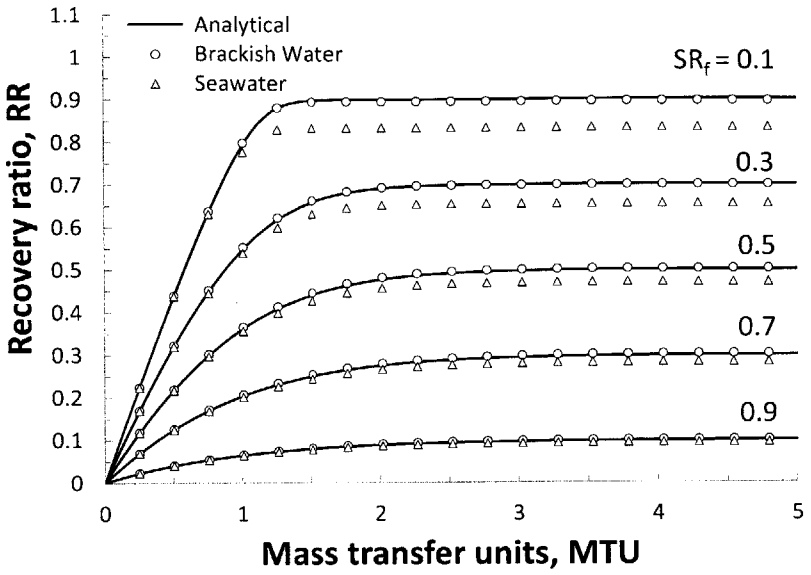

Figure 2-7: Recovery ratio vs. mass transfer units with contours of osmotic pressure ratio for (1) analytical Eq. (2.14), (2) brackish water with a nonlinear osmotic pressure function, and (3) seawater with a nonlinear osmotic pressure function.

Figure 2-8 shows a comparison of the concentration factor from the analytical model to those resulting from the numerical brackish and seawater cases. The same trend as in Fig. 2-7 is evident in Fig. 2-8, where the greatest deviation incurred by the analytical model is for high salinity feed solutions and low osmotic pressure ratios. However, there is less deviation associated with the brackish water case because the osmotic pressure is nearly linear with low salinity feed solutions. As previously mentioned, CF will normally be limited in order to avoid precipitation of sparingly soluble salts from the feed stream.

Figure 2-9 shows the effectiveness as a function of MTU varying with osmotic pressure ratios for both the analytical and numerical cases. Again it is found that the greatest deviation associated with linearization is for high salinity feed solutions and low osmotic pressure ratios. For the seawater case, a maximum deviation of 7.8% was found for an osmotic pressure ratio of 0.1. For the brackish water case, a maximum

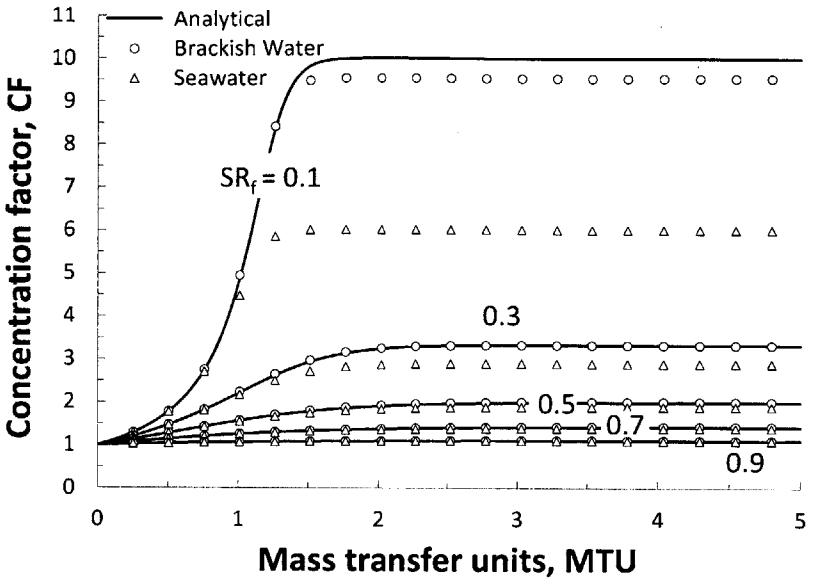

Figure 2-8: Concentration factor vs. mass transfer units with contours of osmotic pressure ratio for: (1) analytical solution, Eq. (2.17); (2) brackish water with a nonlinear osmotic pressure function; and (3) seawater with a nonlinear osmotic pressure function.

deviation of 1.65% was found.

2.3.3 Design example

The following is a brief example which illustrates the use of the analytical expression for design of an RO system using the ε-MTU method. The provided data are adapted from [33].

Find: Calculate the membrane area required for an RO system operating at the following conditions:

- Feed pressure is 6,500 kPa
- Inlet feed salinity is 42 g/kg
- Permeate pressure is 101 kPa
- Water permeability coefficient is 2×10^{-6} kg/s-m^2-kPa

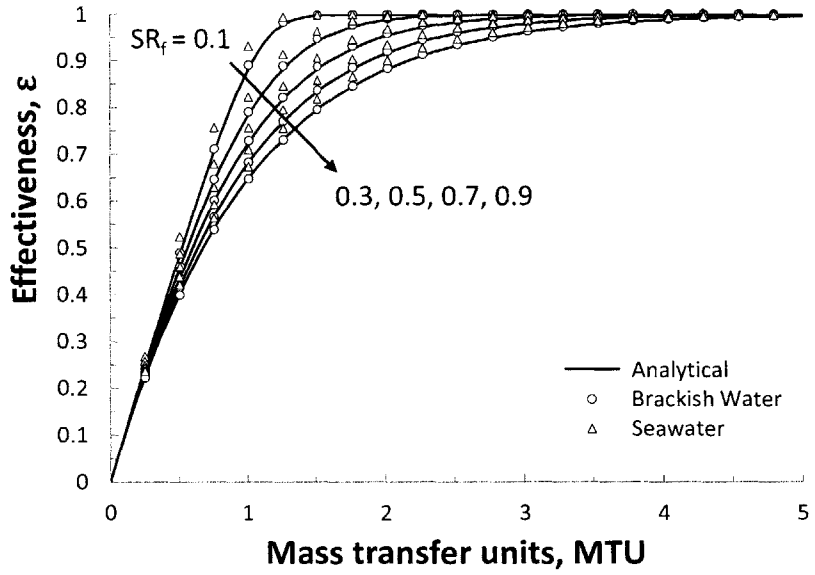

Figure 2-9: Effectiveness vs. mass transfer units with contours of osmotic pressure ratio for: (1) analytical Eq. (2.22); (2) brackish water with a nonlinear osmotic pressure function; and (3) seawater with a nonlinear osmotic pressure function.

- System temperature is 25°C
- Feed flow rate is 2.5 kg/s
- Permeate flow rate is 1 kg/s
- Pure water density is 1,000 kg/m^3

Solution: From the given feed and permeate flow rates, we can calculate the recovery ratio as

$$\mathrm{RR} = 1/2.5 = 0.4 \tag{2.25}$$

The osmotic pressure ratio can be calculated as follows:

$$\mathrm{SR_f} = \pi_{\mathrm{f,\,in}}/\Delta P = 73.45 \times 42/(6,500 - 101) = 0.48 \tag{2.26}$$

From Fig. 2-3, the MTU is 1.1 at RR = 0.4 and SR$_f$ = 0.48. Using the definition of MTU given by Eq. (2.11), one can calculate the total membrane area to be 217.5 m^2.

In comparison, the result obtained in [33] is 206.1 m^2 based on assuming an average osmotic pressure difference throughout the exchanger. El-Dessouky's approach results in a slightly underestimated membrane area according to the present model.

2.4 Conclusions

The major conclusions of this chapter are as follow:

1. A closed form analytical solution for a one-dimensional reverse osmosis mass exchanger was developed. The equation expresses the recovery ratio of the membrane as a function of two dimensionless groups: the osmotic pressure ratio and the number of mass transfer units.

2. A robust analogy exists between heat exchangers and osmotic mass exchangers in which the effectiveness can be expressed by three dimensionless groups. The new ε-MTU model developed for osmotic mass exchangers can be used as a design method for RO systems using a linear osmotic pressure function and ideal membrane characteristics.

3. The maximum deviation of recovery ratio between the linearized analytical expression and the numerical solution that uses the nonlinear osmotic pressure function is 7.98%. This maximum deviation occurs for seawater feed only at very high recovery ratios ($\sim$90%), which is not practically applied. However, at a typically used recovery ratio of 50% the deviation is less than 6.1%. For the brackish water case, where plants typically operate at very high recovery ratios, the deviation does not exceed 1.8%.

Chapter 3

Analogy of Pressure Retarded Osmosis Mass Exchangers to Heat Exchangers

Mostafa H. Sharqawy[1], Leonardo D. Banchik, and John H. Lienhard V

Chapter abstract

Forward osmosis (FO) and pressure retarded osmosis (PRO) systems are being used in desalination, water treatment, and energy production. These systems work on the basis of mass transfer through a semi-permeable membrane which passes water and rejects salts and other substances. These membrane-based devices are essentially mass exchangers which are analogous to heat exchangers. The driving potentials in these mass exchangers are the concentration and pressure differences, whereas in heat exchangers the driving potential is the temperature difference. Closed form solutions of the permeation rate through an ideal PRO mass exchanger are obtained for parallel and counter flow configurations. The permeation ratio, PR, is obtained as a function of dimensionless parameters such as the number of mass transfer units, MTU; the mass flow rate ratio, MR; and the osmotic pressure ratio, SR. The resulting mathematical expressions form an effectiveness-NTU model for osmotic mass exchangers. These

[1]Dr. Sharqawy contributed to the work in this chapter by deriving the analytical model and developing the pressure retarded osmosis effectiveness.

expressions are analogous to those for heat exchangers and can be used for the initial design and rating of PRO membrane-based mass exchange devices.

3.1 Introduction

Pressure retarded osmosis systems are mass exchangers which are currently receiving great attention for their capabilities to produce renewable power from two streams of different salinities. In a PRO system, the higher salinity solution is called the draw stream and the lower salinity solution is called the feed stream. For power production, seawater and river water are typically used as the draw and feed streams, respectively. These streams enter a mass exchanger where a semi-permeable membrane allows water to pass through, but not salts. As opposed to RO operation, the difference in osmotic pressure drives pure water, or permeate, from the feed stream, through the membrane, and into the pressurized draw stream to dilute it. The pressurized diluted draw stream can be depressurized through a hydroturbine, such as a Pelton wheel, to produce power. In this chapter, we investigate the performance of the PRO exchanger relative to the amount of permeate and develop a sizing methodology similar to that commonly used for heat exchangers.

The concept of PRO was first proposed by Loeb [34]. Since then, numerous mathematical models have been developed and experiments implemented to determine the work and permeate flux performance of PRO membranes. Mehta and Loeb were early to recognize internal concentration polarization, a resistance to mass transfer which occurs inside the support layer of the membrane, as significant in a model developed for diffusion through a PRO membrane [35]. Lee et al. more rigorously investigated concentration polarization in PRO membranes and developed equations to determine the maximum work density and flux for zero-dimensional ideal membranes and membranes with internal concentration polarization [4]. Two decades later, McCutcheon and Elimelech developed a model which incorporates internal and external concen-

tration polarization for a zero-dimensional FO and PRO membrane [36]. Currently, PRO related research is being conducted to determine the effect of fouling on flux performance [37–39] and the viability of novel materials for new membranes and hollow fibers [40–42]. The performance of one- and two-dimensional forward and pressure retarded osmosis experimental studies have also been numerically investigated very recently [43–47].

The operation of an osmotic mass exchanger looks very similar to a heat exchanger when both systems are compared side-by-side. In the heat exchanger schematic drawing seen in Fig. 3-1a, the temperature difference between a hot and cold fluid is the driving potential for heat transfer. The resistance to a heat flow per unit area is the reciprocal of the overall heat transfer coefficient, U. In the osmotic mass exchanger seen in Fig. 3-1b, the osmotic pressure difference between a concentrated and a dilute stream, draw and feed, is the driving potential for mass transfer. The resistance to mass transfer per unit membrane area for an ideal membrane is the reciprocal of the water permeability coefficient, A. For PRO systems, the driving potential, and thus the amount of mass transfer, is retarded by the hydraulic pressure difference, $P_{\mathrm{d}} - P_{\mathrm{f}}$, which is greater than zero and less than the maximum osmotic pressure difference in the exchanger. For FO systems, this hydraulic pressure difference is equal to zero.

For heat exchangers, the effectiveness-number of transfer units (ε-NTU) method developed by Kays and London [29] is a well-known design technique that determines the required surface area of a heat exchanger for a fixed effectiveness and inlet conditions. The method uses three dimensionless groups: the effectiveness, which is the ratio of actual heat transfer to the maximum heat exchange possible; a heat capacity ratio, which is the lower heat capacity divided by the higher heat capacity; and the number of transfer units, which is an effective size of the heat exchanger.

This chapter proposes an ε-MTU method for a PRO mass exchanger. The local transport equation for permeate flow in a zero-dimensional exchanger is combined

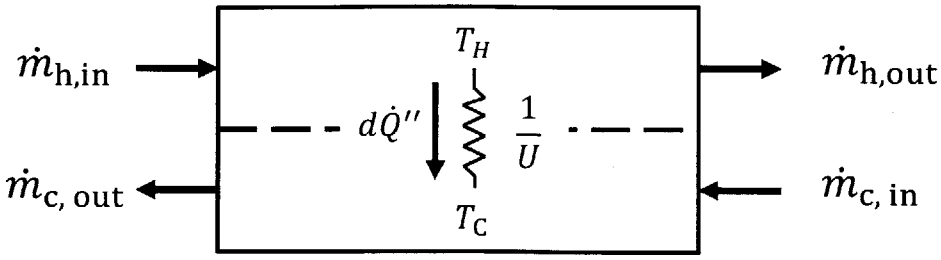

(a) Two-inlet stream heat exchanger

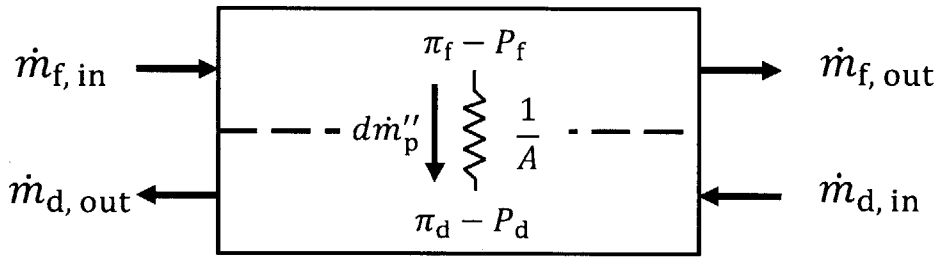

(b) Two-inlet stream osmotic mass exchanger

Figure 3-1: Schematic drawing of a two-inlet heat and osmotic mass exchanger.

with conservation of mass and a linearized equation for osmotic pressure to develop dimensionless expressions for parallel-flow and counterflow PRO exchangers. The expressions are closed-form solutions which relate dimensionless performance parameters of the exchanger to the effective size and input stream properties. The effectiveness of the PRO exchanger is defined as a novel performance parameter. The dimensionless groups used in the closed form solutions are discussed, and an analogy to the heat exchanger groups is made. A numerical model which uses a nonlinear osmotic pressure function is also implemented in order to assess the errors associated with linearizing the osmotic pressure function.

3.2 PRO mass exchanger model

Figure 3-2 is a schematic drawing of a membrane-based mass exchanger device. A feed solution with low salt concentration (low salinity) flows through a channel where one side of the channel has a semi-permeable membrane. On the other membrane side,

a draw solution with higher salt concentration flows in the same direction (Fig. 3-2a, parallel-flow configuration) or in the opposite direction (Fig. 3-2b, counterflow configuration). The inlet and outlet conditions of both feed and draw streams are given as the mass flow rate, osmotic pressure, and hydraulic pressure as indicated in Fig. 3-2. The membrane characteristics are given as the total membrane area (A_{m}) and water permeability coefficient (A) of the membrane material. The model makes the following assumptions:

- The water permeability coefficient (A) is constant.
- Concentration polarization effects are neglected, and the salt concentration near the membrane surface is equal to the bulk concentration of the flow stream.
- Pressure drop through the flow channel is negligible on both the feed and the draw side. Hence the hydraulic pressure difference between the draw side and feed side (ΔP) is fixed over the length of the exchanger.
- The salt rejection is 100% and only pure water diffuses through the membrane.
- Within the operating salinity range of the PRO exchanger, the osmotic pressure follows van 't Hoff's law so that it is linearly proportional to the stream salinity (see Appendix A). The constant of proportionality may vary under different operating conditions as shown in Appendix A.1.

3.2.1 Parallel-flow configuration PRO model

The differential permeate flow rate for an osmotic mass exchanger where the permeate flows from the feed to the draw stream is given by Eq. (3.1) [4]

$$d\dot{m}_{\mathrm{p}} = A \cdot (\Delta\pi - \Delta P)\, dA_{\mathrm{m}} \tag{3.1}$$

where

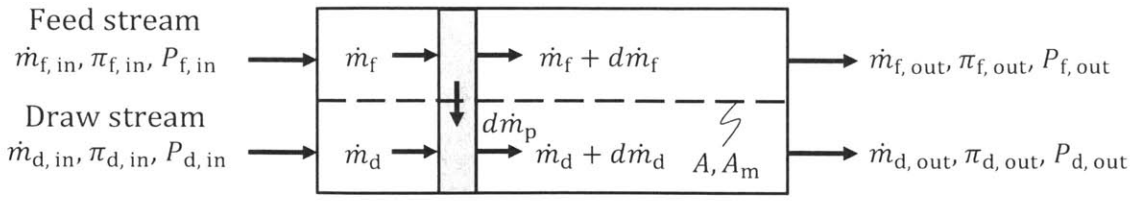

(a) Parallel-flow configuration

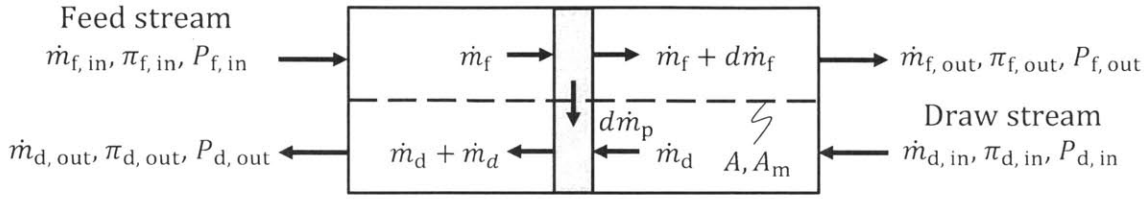

(b) Counterflow configuration

Figure 3-2: Schematic drawing of pressure retarded osmosis exchangers in parallel-flow and counterflow configurations.

- $d\dot{m}_p$, is the permeate mass flow rate through the membrane in kg/s,
- A, is the modified[2] water permeability coefficient of the membrane in kg/s-m^2-kPa,
- $\Delta\pi$ is the local osmotic pressure difference between the draw and feed (i.e., $\pi_d - \pi_f$) in kPa,
- ΔP is the hydraulic pressure difference between the draw and feed (i.e., $P_d - P_f$) in kPa, and
- A_m is the membrane surface area in m^2.

The osmotic pressure for a solution [30] is given by

$$\pi = \phi(RT\rho_{\text{solvent}}) \sum_{j=\text{solutes}} b_j \tag{3.2}$$

[2]It is important to note that the water permeability coefficient (A) is often given in units of m/s-bar or L/m^2-hr-bar [16], which is the permeate water volume flux per unit pressure difference; however, for the present model, we express this coefficient on a mass basis (equivalent to multiplying it by the density of pure water and some obvious SI conversion factors).

where ϕ is the osmotic coefficient, predominantly a function of temperature and salinity; R is the universal gas constant; T is the absolute temperature; ρ_{solvent} is the density of the solvent (pure water); and $\sum_{j=\text{solutes}} b_j$ is the sum of the molalities of each solute. A detailed derivation of the osmotic pressure for seawater is given in Appendix B.

Equation (3.2) shows that osmotic pressure is a nonlinear function of salinity. In order to facilitate our analysis, we use van 't Hoff's equation to linearize the osmotic pressure. In the second half of this chapter, this assumption will be checked for its validity by comparing results to a numerical model which uses the nonlinear osmotic pressure. Expressing the osmotic pressure as a linear function of salinity yields:

$$\Delta\pi = \pi_{\text{d}} - \pi_{\text{f}} = C(w_{\text{d}} - w_{\text{f}}) \tag{3.3}$$

where w is the salinity in g/kg and C is a modified van 't Hoff's coefficient. It follows that

$$d\dot{m}_{\text{p}} = A \cdot [C(w_{\text{d}} - w_{\text{f}}) - \Delta P]\, dA_{\text{m}} \tag{3.4}$$

Under the assumed condition of 100% salt rejection, only pure water permeates through the membrane; hence the salinity of the permeate is zero. Applying conservation of solutes to the feed stream between the inlet and any arbitrary location along the flow channel yields

$$\dot{m}_{\text{s, f}} = \dot{m}_{\text{f, in}} \times w_{\text{f, in}} = \dot{m}_{\text{f}} \times w_{\text{f}} \tag{3.5}$$

For the same arbitrary location, conservation of the solution requires that

$$\dot{m}_{\text{f, in}} = \dot{m}_{\text{f}} + \dot{m}_{\text{p}} \tag{3.6}$$

Substitution of Eq. (3.6) into Eq. (3.5) yields

$$w_{\mathrm{f}} = \frac{\dot{m}_{\mathrm{f,\,in}} \times w_{\mathrm{f,\,in}}}{\dot{m}_{\mathrm{f,\,in}} - \dot{m}_{\mathrm{p}}} \tag{3.7}$$

Similarly applying conservation of solutes and solution on the draw side for a parallel configuration yields

$$w_{\mathrm{d}} = \frac{\dot{m}_{\mathrm{d,\,in}} \times w_{\mathrm{d,\,in}}}{\dot{m}_{\mathrm{d,\,in}} + \dot{m}_{\mathrm{p}}} \tag{3.8}$$

Substituting Eqs. (3.7) and (3.8) into Eq. (3.4) yields

$$d\dot{m}_{\mathrm{p}} = A\left[C\left(\frac{\dot{m}_{\mathrm{d,\,in}} \times w_{\mathrm{d,\,in}}}{\dot{m}_{\mathrm{d,\,in}} + \dot{m}_{\mathrm{p}}} - \frac{\dot{m}_{\mathrm{f,\,in}} \times w_{\mathrm{f,\,in}}}{\dot{m}_{\mathrm{f,\,in}} - \dot{m}_{\mathrm{p}}}\right) - \Delta P\right] dA_{\mathrm{m}} \tag{3.9}$$

We now proceed to cast Eq. (3.9) in a dimensionless form. Four dimensionless parameters are introduced for this purpose, three of which are identical to those used to describe the RO exchanger behavior in Chapter 2.

3.2.2 Dimensionless parameters

Permeation ratio, PR

$$\mathrm{PR} \equiv \frac{\dot{m}_{\mathrm{p}}}{\dot{m}_{\mathrm{f,\,in}}} \tag{3.10}$$

The permeation ratio is a primary performance metric of the PRO mass exchanger as it represents the amount of pure water recovered from the feed stream. In so far as the inlet mass flow rate is greater than the maximum amount of permeate that can be recovered, the permeation ratio should not be confused with the effectiveness which will be described in the next section.

Mass flow rate ratio, MR

$$\mathrm{MR} \equiv \frac{\dot{m}_{\mathrm{d,\,in}}}{\dot{m}_{\mathrm{f,\,in}}} \tag{3.11}$$

The mass flow rate ratio is the ratio of the mass flow rate of the draw solution to that of the feed solution at the inlet of the PRO mass exchanger.

Osmotic pressure ratio, SR

For the draw side:

$$\mathrm{SR_d} \equiv \frac{\pi_{\mathrm{d,\,in}}}{\Delta P} \tag{3.12}$$

For the feed side:

$$\mathrm{SR_f} \equiv \frac{\pi_{\mathrm{f,\,in}}}{\Delta P} \tag{3.13}$$

The osmotic pressure ratio is the ratio of the osmotic pressure at the draw or feed inlet to the hydraulic pressure difference. For PRO exchanger operation, $\mathrm{SR_d}$ will always be greater than $\mathrm{SR_f}$.

Mass transfer units, MTU

$$\mathrm{MTU} \equiv \frac{A\,A_{\mathrm{m}}\,\Delta P}{\dot{m}_{\mathrm{f,\,in}}} \tag{3.14}$$

The number of *mass transfer units* (MTU) is a dimensionless parameter for a membrane mass exchanger similar to the *number of transfer units* (NTU) used in heat exchanger design. The total membrane area, A_{m}, is analogous to the total heat exchanger surface area and A is the overall water permeability coefficient which is analogous to the overall heat transfer coefficient in heat exchangers. Therefore, the MTU in the membrane-based mass exchanger will play the same role that NTU plays in ε-NTU analysis of heat exchangers.

Substituting Eqs. (3.10)–(3.14) into Eq. (3.9) yields

$$d\mathrm{PR} = \left(\frac{\mathrm{MR} \times \mathrm{SR_d}}{\mathrm{MR} + \mathrm{PR}} - \frac{\mathrm{SR_f}}{1 - \mathrm{PR}} - 1 \right) d\mathrm{MTU} \tag{3.15}$$

Equation (3.15) can be integrated as follows:

$$\int_0^{\mathrm{PR}} \left(\frac{\mathrm{MR} \times \mathrm{SR_d}}{\mathrm{MR} + \mathrm{PR}} - \frac{\mathrm{SR_f}}{1 - \mathrm{PR}} - 1 \right)^{-1} d\mathrm{PR} = \mathrm{MTU} \tag{3.16}$$

Equation (3.16) can be simplified into

$$\int_0^{\mathrm{PR}} \frac{(\mathrm{MR} + \mathrm{PR})(1 - \mathrm{PR})}{(\mathrm{PR} - \alpha)(\mathrm{PR} - \beta)} d\mathrm{PR} = \mathrm{MTU} \tag{3.17}$$

where

$$\begin{aligned} \alpha = {} & \frac{1}{2}(1 + \mathrm{MR}(\mathrm{SR_d} - 1) + \mathrm{SR_f}) \\ & - \frac{1}{2}\sqrt{(-1 - \mathrm{MR}(\mathrm{SR_d} - 1) - \mathrm{SR_f})^2 - 4\mathrm{MR}(\mathrm{SR_d} - \mathrm{SR_f} - 1)} \end{aligned} \tag{3.18}$$

$$\begin{aligned} \beta = {} & \frac{1}{2}(1 + \mathrm{MR}(\mathrm{SR_d} - 1) + \mathrm{SR_f}) \\ & + \frac{1}{2}\sqrt{(-1 - \mathrm{MR}(\mathrm{SR_d} - 1) - \mathrm{SR_f})^2 - 4\mathrm{MR}(\mathrm{SR_d} - \mathrm{SR_f} - 1)} \end{aligned} \tag{3.19}$$

Integration of Eq. (3.17) yields

$$\begin{aligned} \mathrm{MTU} = {} & \frac{(\beta - 1)(\mathrm{MR} + \beta)}{(\alpha - \beta)} \ln\left(\frac{\beta - \mathrm{PR}}{\beta} \right) \\ & - \frac{(\alpha - 1)(\mathrm{MR} + \alpha)}{(\alpha - \beta)} \ln\left(\frac{\alpha - \mathrm{PR}}{\alpha} \right) - \mathrm{PR} \end{aligned} \tag{3.20}$$

Therefore, Eq. (3.20) can be used in the design of a membrane mass exchanger where the required mass transfer units, effectively the membrane area, is given as an explicit relation.

An additional dimensionless parameter which may be useful to a designer is the concentration factor. The concentration factor is the ratio of the outlet salinity of a stream to the inlet salinity. If a designer is limited to output brine below certain salinity from the PRO exchanger, the concentration factor can be useful in determining the maximum MTU allowable. By considering a pure permeate and applying conservation of solution and solutes to the draw and feed streams separately, the expressions for the draw and feed concentration factors can be determined, as given by Eqs. (3.21) and (3.22).

For the draw side:

$$\mathrm{CF_d} \equiv \frac{w_{\mathrm{d,\,out}}}{w_{\mathrm{d,\,in}}} = \frac{\mathrm{MR}}{\mathrm{MR} + \mathrm{PR}} \tag{3.21}$$

For the feed side:

$$\mathrm{CF_f} \equiv \frac{w_{\mathrm{f,\,out}}}{w_{\mathrm{f,\,in}}} = \frac{1}{1 - \mathrm{PR}} \tag{3.22}$$

Figures 3-3 and 3-4 show the variation of the permeation ratio (PR) and the concentration factor (CF) with the mass transfer units (MTU), respectively, at different mass flow rate ratios for the parallel-flow configuration.

3.2.3 Counterflow configuration PRO model

The transport model Eq. (3.1) and the van 't Hoff osmotic pressure model Eq. (3.3) will again be used to describe the permeate flow rate in the counterflow configuration shown in Fig. 3-2b. The differential permeate flow rate is given by Eq. (3.4) and the conservation of solution and solute for the feed side between the inlet and any arbitrary location along the flow channel leads to Eq. (3.7) for the feed salinity. Applying

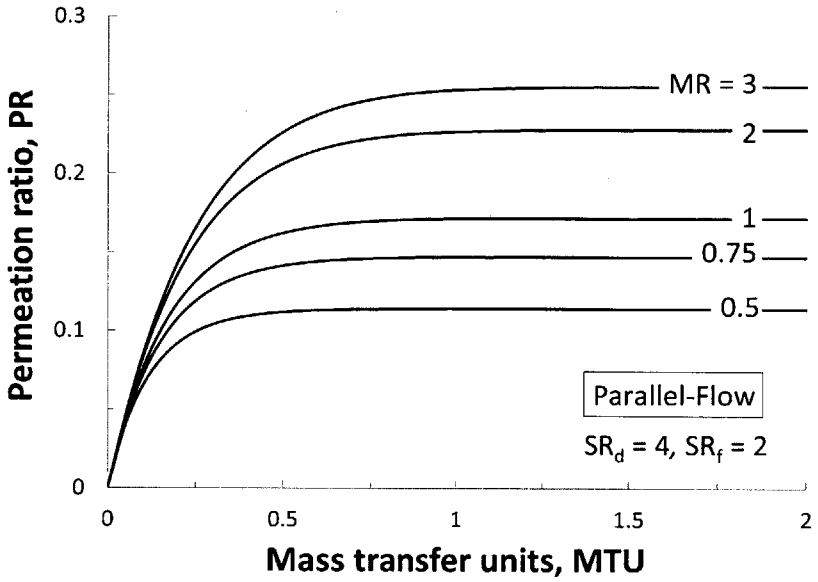

Figure 3-3: Permeation ratio vs. mass transfer units at different mass flow rate ratios for a parallel-flow configuration.

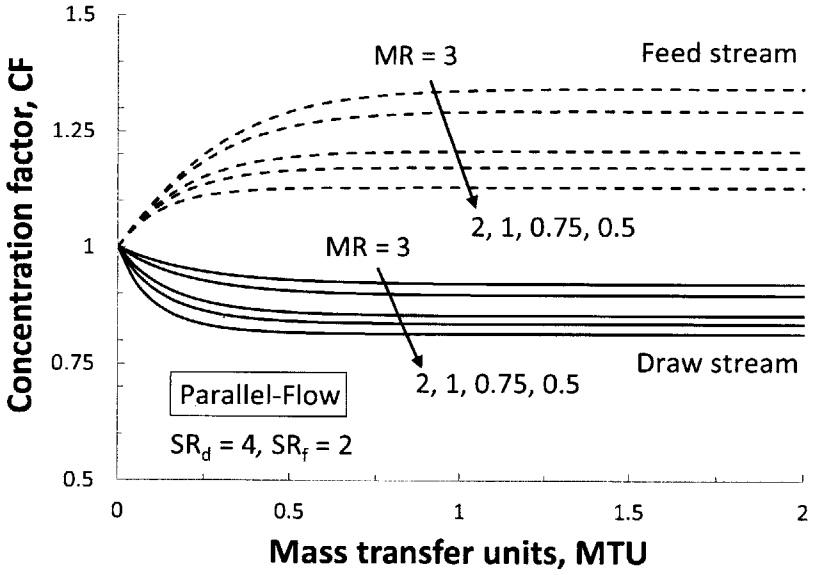

Figure 3-4: Concentration factor of the feed (dashed curves) and draw (solid curves) stream vs. mass transfer units at different mass flow rate ratios for a parallel-flow configuration.

a similar conservation of solution and solute on the draw side for the counterflow configuration at the same arbitrary location as taken for the feed stream gives a result that differs from Eq. (3.8) for the parallel-flow configuration.

$$w_{\mathrm{d}} = \frac{\dot{m}_{\mathrm{d,\,out}} \times w_{\mathrm{d,\,out}}}{\dot{m}_{\mathrm{d,\,out}} - \dot{m}_{\mathrm{p}}} \tag{3.23}$$

Substituting Eqs. (3.7) and (3.23) into Eq. (3.4) yields

$$d\dot{m}_{\mathrm{p}} = A\left[C\left(\frac{\dot{m}_{\mathrm{d,\,out}} \times w_{\mathrm{d,\,out}}}{\dot{m}_{\mathrm{d,\,out}} - \dot{m}_{\mathrm{p}}} - \frac{\dot{m}_{\mathrm{f,\,in}} \times w_{\mathrm{f,\,in}}}{\dot{m}_{\mathrm{f,\,in}} - \dot{m}_{\mathrm{p}}}\right) - \Delta P\right] dA_{\mathrm{m}} \tag{3.24}$$

Using the same dimensionless parameters as used for the parallel-flow configuration (i.e. PR, MR, $\mathrm{SR_d}$, $\mathrm{SR_f}$, and MTU), Eq. (3.24) can be rewritten in a dimensionless form. However, two additional dimensionless parameters are required; they are defined as follows.

Outlet mass flow rate ratio, $\mathrm{MR_o}$

$$\mathrm{MR_o} \equiv \frac{\dot{m}_{\mathrm{d,\,out}}}{\dot{m}_{\mathrm{f,\,in}}} \tag{3.25}$$

Osmotic pressure ratio at draw outlet, $\mathrm{SR_{d,\,o}}$

$$\mathrm{SR_{d,\,o}} \equiv \frac{\pi_{\mathrm{d,\,out}}}{\Delta P} \tag{3.26}$$

Since we are interested in expressing the permeation ratio (PR) as a function of the inlet flow conditions, we proceed to develop relations between the outlet dimensionless groups defined by Eqs. (3.25) and (3.25) and the inlet dimensionless groups defined by Eqs. (3.10)-(3.13).

The mass flow rate ratio defined in Eq. (3.11) can be written as a function of the outlet mass flow rate ratio defined by Eq. (3.25) and the permeation ratio defined by

Eq. (3.10).

$$\mathrm{MR} = \frac{\dot{m}_{\mathrm{d,\,in}}}{\dot{m}_{\mathrm{f,\,in}}} = \frac{\dot{m}_{\mathrm{d,\,out}} - \dot{m}_{\mathrm{p}}}{\dot{m}_{\mathrm{f,\,in}}} = \mathrm{MR_o} - \mathrm{PR} \tag{3.27}$$

Therefore,

$$\mathrm{MR_o} = \mathrm{MR} + \mathrm{PR} \tag{3.28}$$

Similarly, the osmotic pressure ratio of the outlet draw stream can be written as a function of the osmotic pressure ratio of the inlet draw stream, the mass flow rate ratio, and the permeation ratio.

$$\mathrm{SR_{d,\,o}} = \mathrm{SR_d}\frac{\mathrm{MR}}{\mathrm{MR} + \mathrm{PR}} \tag{3.29}$$

Using these dimensionless groups, Eq. (3.24) can be rewritten in a dimensionless form:

$$d\mathrm{PR} = \left(\frac{\mathrm{MR_o} \times \mathrm{SR_{d,\,o}}}{\mathrm{MR_o} - \mathrm{PR}} - \frac{\mathrm{SR_f}}{1 - \mathrm{PR}} - 1\right) d\mathrm{MTU} \tag{3.30}$$

Equation (3.30) can be integrated as follows:

$$\int_0^{\mathrm{PR}} \left(\frac{\mathrm{MR_o} \times \mathrm{SR_{d,\,out}}}{\mathrm{MR_o} - \mathrm{PR}} - \frac{\mathrm{SR_f}}{1 - \mathrm{PR}} - 1\right)^{-1} d\mathrm{PR} = \mathrm{MTU} \tag{3.31}$$

Equation (3.31) can be simplified into

$$\int_0^{\mathrm{PR}} \frac{(\mathrm{MR_o} - \mathrm{PR})(1 - \mathrm{PR})}{(\mathrm{PR} - \alpha')(\mathrm{PR} - \beta')} d\mathrm{PR} = \mathrm{MTU} \tag{3.32}$$

where

$$\alpha' = \frac{1}{2}(1 + \mathrm{MR_o}(1 - \mathrm{SR_{d,o}}) + \mathrm{SR_f}) - \frac{1}{2}\sqrt{(-1 + \mathrm{MR_o}(\mathrm{SR_{d,o}} - 1) - \mathrm{SR_f})^2 - 4\mathrm{MR_o}(1 - \mathrm{SR_{d,o}} + \mathrm{SR_f})} \quad (3.33)$$

$$\beta' = \frac{1}{2}(1 + \mathrm{MR_o}(1 - \mathrm{SR_{d,o}}) + \mathrm{SR_f}) + \frac{1}{2}\sqrt{(-1 + \mathrm{MR_o}(\mathrm{SR_{d,o}} - 1) - \mathrm{SR_f})^2 - 4\mathrm{MR_o}(1 - \mathrm{SR_{d,o}} + \mathrm{SR_f})} \quad (3.34)$$

Integration of Eq. (3.32) yields

$$\mathrm{MTU} = \frac{(\beta' - 1)(\beta' - \mathrm{MR_o})}{(\alpha' - \beta')} \ln\left(\frac{\beta' - \mathrm{PR}}{\beta'}\right) - \frac{(\alpha' - 1)(\alpha' - \mathrm{MR_o})}{(\alpha' - \beta')} \ln\left(\frac{\alpha' - \mathrm{PR}}{\alpha'}\right) - \mathrm{PR} \quad (3.35)$$

Therefore, Eq. (3.35) combined with Eqs. (3.25) and (3.26) can be used in the design of a membrane mass exchanger where the required mass transfer units, effectively the membrane area, is given as an explicit relation of the form

$$\mathrm{MTU} = \mathrm{fn}(\mathrm{PR},\ \mathrm{MR},\ \mathrm{SR_f},\ \mathrm{SR_d}) \quad (3.36)$$

Figures 3-5 and 3-6 show the variation of the permeation ratio (PR) and the concentration factor (CF) with the mass transfer units (MTU), respectively, at different mass flow rate ratios (MR) for the counterflow configuration. The concentration factors for the feed and draw stream as defined in Eqs. (3.21) and (3.21) are applicable to the counterflow configuration as well.

It can be seen by comparing Figs. 3-3 and 3-5 that, for each contour of MR, the permeation ratio is higher for the counterflow case than that of the parallel-flow case. This is an expected result which is found in PRO literature [42, 43, 46] and is analogous to similar results for heat exchangers.

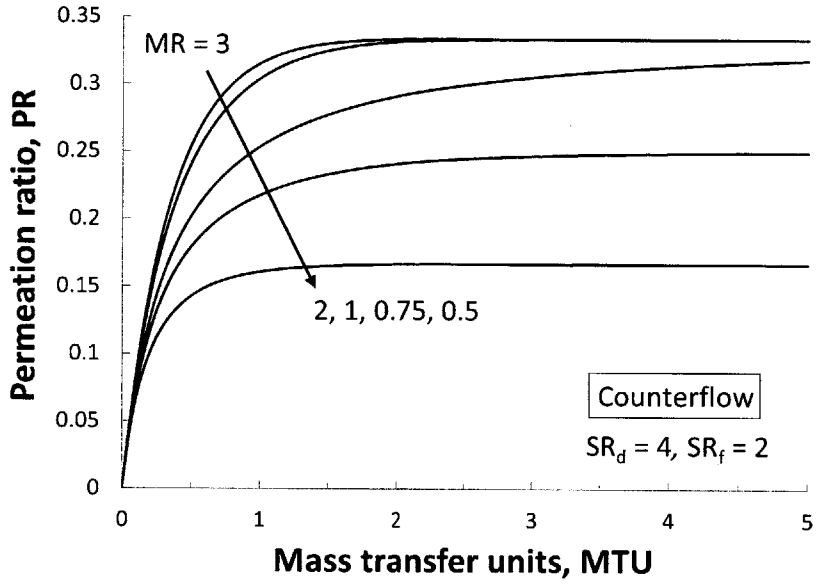

Figure 3-5: Permeation ratio vs. mass transfer units at different mass flow rate ratios for a counterflow configuration.

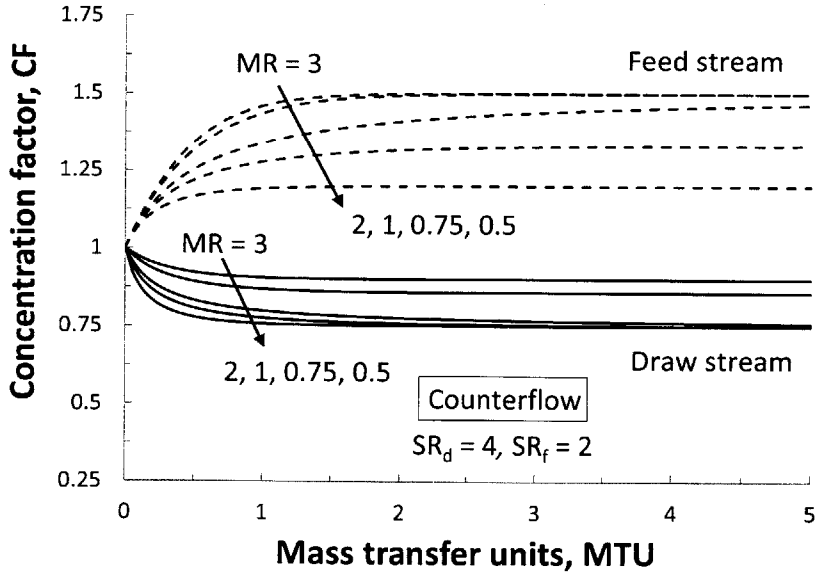

Figure 3-6: Concentration factor of the feed (dashed curves) and draw (solid curves) stream vs. mass transfer units at different mass flow rate ratios for a counterflow configuration.

3.3 PRO effectiveness (ε-MTU model)

The effectiveness of the PRO system can be defined as the ratio of the permeate flow rate to the maximum permeate flow rate, which occurs when MTU is increased to infinity. The effectiveness can also be defined as the permeation ratio divided by the maximum permeation ratio. Note that the maximum permeate flow rate is not the inlet feed flow rate. The maximum accumulated permeated water occurs when the net driving pressure ($\Delta\pi - \Delta P$) to draw water from the feed stream has decreased to zero at one end of the mass exchanger. The following is a derivation of the maximum permeation flow rate and, hence, of the effectiveness of the PRO exchanger.

3.3.1 Parallel-flow PRO effectiveness

Using Eq. (3.1), the maximum permeate in the case of parallel-flow configuration will occur when the hydraulic pressure difference is equal to the osmotic pressure difference at the outlet.

$$\Delta\pi_{\text{out}} = \pi_{\text{d, out}} - \pi_{\text{f, out}} = \Delta P \tag{3.37}$$

Using the van 't Hoff model

$$C(w_{\text{d, out}} - w_{\text{f, out}}) = \Delta P \tag{3.38}$$

Applying conservation of solutes and solution on the draw side, one can find that

$$w_{\text{d, out}} = \frac{\text{MR}}{\text{MR} + \text{PR}} w_{\text{d, in}} \tag{3.39}$$

Similarly on the feed side, one can find that

$$w_{\text{f, out}} = \frac{1}{1 - \text{PR}} w_{\text{f, in}} \tag{3.40}$$

Substituting Eqs. (3.39) and (3.40) into Eq. (3.38) and using the dimensionless groups defined earlier yields

$$\frac{\mathrm{MR} \times \mathrm{SR_d}}{\mathrm{MR} + \mathrm{PR}} - \frac{\mathrm{SR_f}}{1 - \mathrm{PR}} = 1 \tag{3.41}$$

Solving Eq. (3.41) to find the maximum permeation ratio, one can find that there are two solutions

$$\mathrm{PR}_{\mathrm{max},\,1} = \alpha \tag{3.42a}$$

$$\mathrm{PR}_{\mathrm{max},\,2} = \beta \tag{3.42b}$$

where α and β are given by Eqs. (3.18) and (3.19), respectively. We notice from Eqs. (3.18) and (3.19) that α is always less than 1 and β is always greater than 1. The permeation ratio must be less than one. Therefore, the maximum permeation ratio is equal to α. Now the effectiveness is defined as

$$\varepsilon = \frac{\mathrm{PR}}{\mathrm{PR}_{\mathrm{max}}} \tag{3.43}$$

Hence,

$$\mathrm{PR} = \varepsilon \mathrm{PR}_{\mathrm{max}} = \varepsilon\alpha \tag{3.44}$$

By substituting Eq. (3.44) into Eq. (3.20), an expression for MTU as a function of the effectiveness can be obtained:

$$\mathrm{MTU} = \frac{(\beta - 1)(\mathrm{MR} + \beta)}{(\alpha - \beta)} \ln\left(\frac{\beta - \varepsilon\alpha}{\beta}\right) - \frac{(\alpha - 1)(\mathrm{MR} + \alpha)}{(\alpha - \beta)} \ln(1 - \varepsilon) - \varepsilon\alpha \tag{3.45}$$

Figure 3-7 shows the effectiveness changing with the mass transfer units for varying mixing ratios.

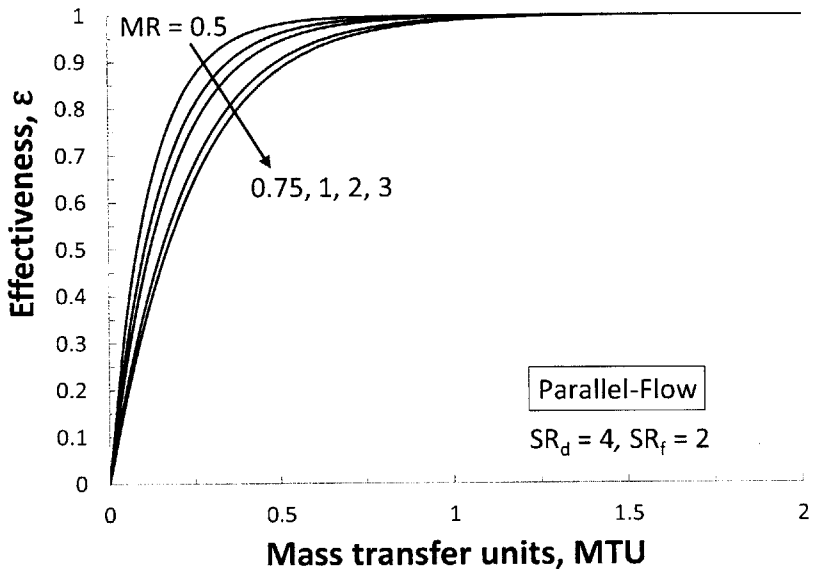

Figure 3-7: Effectiveness vs. mass transfer units at different mass flow rate ratios for a parallel-flow configuration.

3.3.2 Counterflow PRO effectiveness

Using Eq. (3.1), the maximum permeate in the case of counterflow configuration will occur when the hydraulic pressure difference is equal to the osmotic pressure difference at the right side or the left side of the exchanger schematic shown in Fig. 3-2b. Therefore, there are two conditions at which the driving force for permeate flow will vanish.

$$\pi_{\mathrm{d,\,out}} - \pi_{\mathrm{f,\,in}} = \Delta P \tag{3.46}$$

Using the van 't Hoff model and applying conservation of solution and solute, this condition will lead to

$$\mathrm{PR}_{\mathrm{max},\,1} = \frac{\mathrm{MR} \times \mathrm{SR_d}}{1 + \mathrm{SR_f}} - \mathrm{MR} \tag{3.47}$$

The other condition will lead to

$$\pi_{\mathrm{d,\,in}} - \pi_{\mathrm{f,\,out}} = \Delta P \tag{3.48}$$

and

$$\mathrm{PR}_{\mathrm{max},\,2} = 1 - \frac{\mathrm{SR_f}}{\mathrm{SR_d} - 1} \tag{3.49}$$

Since there are two solutions for the maximum permeation ratio, we should take the minimum value, hence:

$$\mathrm{PR_{max}} = \min\left\langle \mathrm{PR}_{\mathrm{max},\,1}, \mathrm{PR}_{\mathrm{max},\,2} \right\rangle \tag{3.50}$$

The effectiveness defined by Eq. (3.43) and the permeation ratio can be written in terms of the effectiveness and maximum permeation ratio as given by the first equality of Eq. (3.44). Substituting Eq. (3.44) into Eq. (3.35), an expression for MTU as a function of the effectiveness is obtained:

$$\begin{aligned}\mathrm{MTU} = {} & \frac{(\beta' - 1)(\beta' - \mathrm{MR_o})}{(\alpha' - \beta')} \ln\left(\frac{\beta' - \varepsilon \mathrm{PR_{max}}}{\beta'}\right) \\ & - \frac{(\alpha' - 1)(\alpha' - \mathrm{MR_o})}{(\alpha' - \beta')} \ln\left(\frac{\alpha' - \varepsilon \mathrm{PR_{max}}}{\alpha'}\right) - \varepsilon \mathrm{PR_{max}}\end{aligned} \tag{3.51}$$

Figure 3-8 shows the effectiveness changing with the mass transfer units for varying mass flow rate ratios.

It should be noted that by varying the modified van 't Hoff coefficient of each stream, the closed-form solutions given in the above sections allow for the two streams entering the PRO exchanger to have different compositions, such as seawater and ammonia-carbon dioxide, sodium chloride and pure water, or flowback water and ammonia-carbon dioxide.

3.4 Numerical PRO mass exchanger model

The closed form solutions derived in the previous sections required the assumption that osmotic pressure is a linear function of salinity. While this assumption is valid for

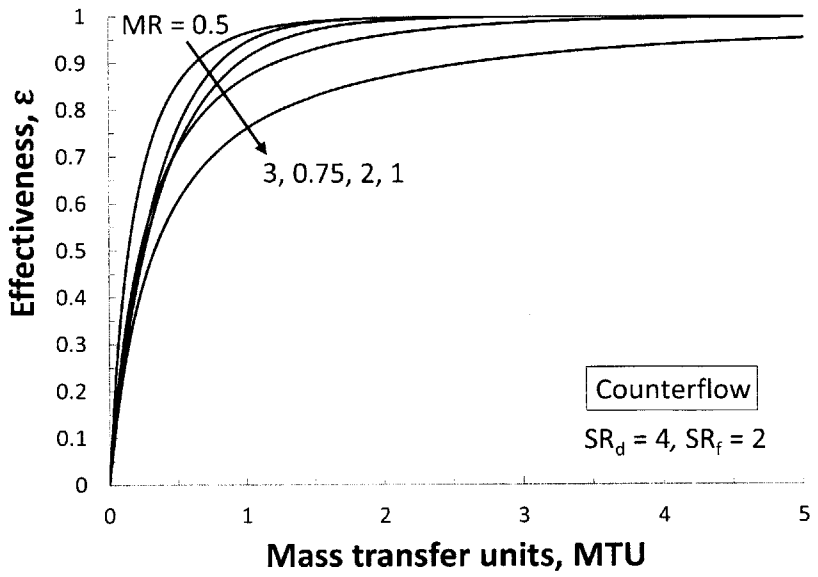

Figure 3-8: Effectiveness vs. mass transfer units at different mass flow rate ratios for a counterflow configuration

relatively dilute solutions, the variation becomes increasingly nonlinear as the mixture salinity increases. In this section, a numerical model of a one-dimensional PRO mass exchanger is developed using a nonlinear function for the osmotic pressure of seawater, so as to determine the accuracy of the approximate analytical results given earlier. The model applies a discretized version of the transport equation, Eq. (3.1), and conservation of solution and solutes to N membrane elements in series. The number of elements was increased to 50 at which point the results were grid independent. The total amount of permeate is calculated by numerically integrating the permeate mass flow rate produced by all elements. The equations comprised by the numerical model were solved using Engineering Equation Solver [48], a simultaneous equation solver which iterates to find a solution to sets of coupled nonlinear algebraic equations. The details of the nonlinear osmotic pressure function and the modified van 't Hoff coefficient used in this numerical model are given in Appendix B and Appendix A.1.

The numerical model is used to estimate the error in the analytical solutions that

Table 3.1: Data input for PRO numerical model

Input	Symbol	Value/Range
Ambient temperature	T_0	25 °C
Modified water permeability coefficient	A	3.07×10^{-6} kg/s-m^2-kPa
Feed mass flow rate	$\dot{m}_{\mathrm{f,in}}$	1 kg/s
Inlet draw salinity	$w_{\mathrm{d,in}}$	70 g/kg and 35 g/kg
Inlet feed salinity	$w_{\mathrm{f,in}}$	35 g/kg and 1.5 g/kg
Trans-membrane pressure difference	ΔP	1.24–1.47 MPa
Membrane area	A_{m}	0–9.45$\times 10^5$ m^2

results from using a linearized osmotic pressure function (the van 't Hoff equation). All other assumptions made for the analytical model are also made for the numerical model. An additional assumption is that the PRO membranes can withstand arbitrary net driving pressures. Two representative uses of a PRO system are for power production at a river delta [49] and for recovering the chemical energy which exists between the rejected brine of a desalination system and available seawater [28, 50, 51]. Therefore, two numerical cases are considered: (1) a power production case with seawater and river water, $w_{\mathrm{d,\,in}} = 35$ g/kg and $w_{\mathrm{f,\,in}} = 1.5$ g/kg; (2) and an energy recovery case with brine and seawater, $w_{\mathrm{d,\,in}} = 70$ g/kg and $w_{\mathrm{f,\,in}} = 1.5$ g/kg. The inputs for the numerical model are given in Table 3.1. The water permeability coefficient used is representative of a typical spiral wound forward osmosis membrane [52].

The percent error of the analytical model is given by Eq. (3.52)

$$\text{error} = \left|1 - \frac{\text{analytical}}{\text{numerical}}\right| \times 100\% \tag{3.52}$$

The inlet salinities given in Table 3.1 are used to calculate the inlet osmotic pressures using the nonlinear osmotic pressure function and the modified van 't Hoff coefficient. For both cases, the hydraulic pressure difference is set to equal one-half of the maximum osmotic pressure difference. This assumption requires that

Table 3.2: Modified van 't Hoff coefficients over three ranges for determining osmotic pressure as a function of salinity at $T = 25°C$.

C [kPa-kg/g]	Range [g/kg]	R^2
73.07	0 – 35	0.9997
76.76	35 – 70	0.9926
82.65	70 – 105	0.9691

$SR_d - SR_f = 2$. To improve the accuracy of the linear case, we use different values of the modified van 't Hoff coefficient to cover ranges of interest (see Appendix A.1 for details). Table 3.2 lists modified van 't Hoff coefficients for three ranges with the coefficient of determination given in the third column. The first and second value of C from Table 3.2 will be used in the linear model to compare the two numerical cases.

We first consider the seawater-river water stream combination with a counterflow exchanger configuration. Figure 3-9 shows the permeation ratio versus mass transfer units for contours of the mass flow rate ratio, MR, and for fixed inlet draw and feed salinities. The inlet salinities are used to calculate the nonlinear and linear osmotic pressure for the draw and feed stream and the hydraulic pressure difference is determined by assuming that $SR_d - SR_f = 2$ as described in the previous section. It can be seen in Fig. 3-9 that the errors associated with linearization are highest for low mass flow rate ratios and for high values of MTU. For MR = 0.5 and for MTU greater than 2, the largest error associated with linearization of the osmotic pressure function is 4.62%. Figures 3-10 and 3-11 show the concentration factor and effectiveness plotted versus MTU for the same contours of mass flow rate ratio and inlet salinity. The maximum error for the draw and feed stream concentration factors is 2.12% and 20.3%, respectively. The relatively high error of 20.3% results from the contour of MR = 1 and corresponds to an outlet salinity difference between the numerical model and the analytical solution of about 1.9 g/kg. The errors are

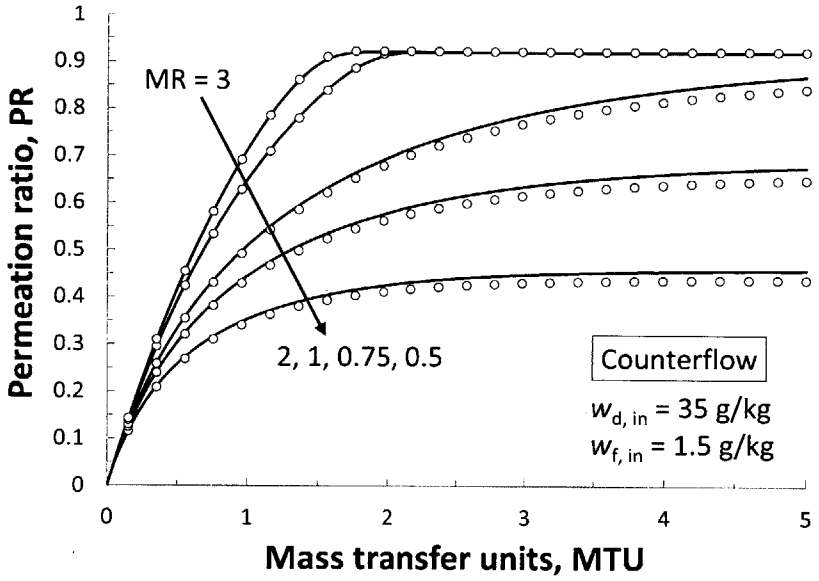

Figure 3-9: Permeation ratio vs. mass transfer units for varying mass flow rate ratios, counterflow configuration, and fixed inlet salinities representative of seawater and river water. Lines are from analytical Eq. (3.35), and the points are the results of a numerical model using a nonlinear osmotic pressure function.

higher for the feed stream concentration factor because the feed stream salinities are lower, which lends to a smaller denominator in the error calculation even though the overall difference in outlet feed salinities may be low. The maximum error for the effectiveness is 4.41%.

Figures 3-12 – 3-14 display the same dimensionless groups as Figs. 3-9 – 3-11 except that the inlet salinities are now representative of brine and seawater as defined by the energy recovery case 2. The maximum error between models for the permeation ratio versus MTU of Fig. 3-12 is 5.37% and corresponds to the lowest mass flow rate ratio of MR = 0.5 at MTU = 0.5. For the case 2 concentration factor and effectiveness versus MTU shown in Figs. 3-13 and 3-14, the maximum error is less than 2% and 5%, respectively. Table 3.3 summarizes the maximum error incurred for each dimensionless variable and for each case and configuration.

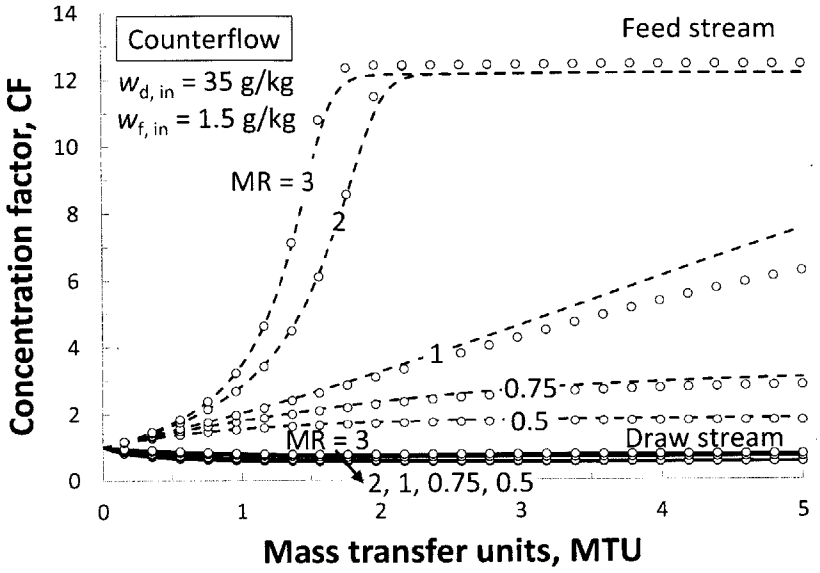

Figure 3-10: Concentration factor vs. mass transfer units for varying mass flow rate ratios, counterflow configuration, and fixed inlet salinities representative of seawater and river water. Solid and dashed lines are from analytical Eqs. (3.21) and (3.22), respectively, and the points are the results of a numerical model using a nonlinear osmotic pressure function.

Table 3.3: Maximum errors resulting from linearized osmotic pressure.

Case 1: Seawater & River Water	PR	CF_d	CF_f	ε
Parallel-flow	3.69%	1.61%	3.41%	3.36%
Counterflow	4.62%	2.12%	20.03%	4.41%
Case 2: Brine & Seawater	PR	CF_d	CF_f	ε
Parallel-flow	2.34%	0.43%	0.45%	1.71%
Counterflow	5.37%	1.26%	1.68%	4.95%

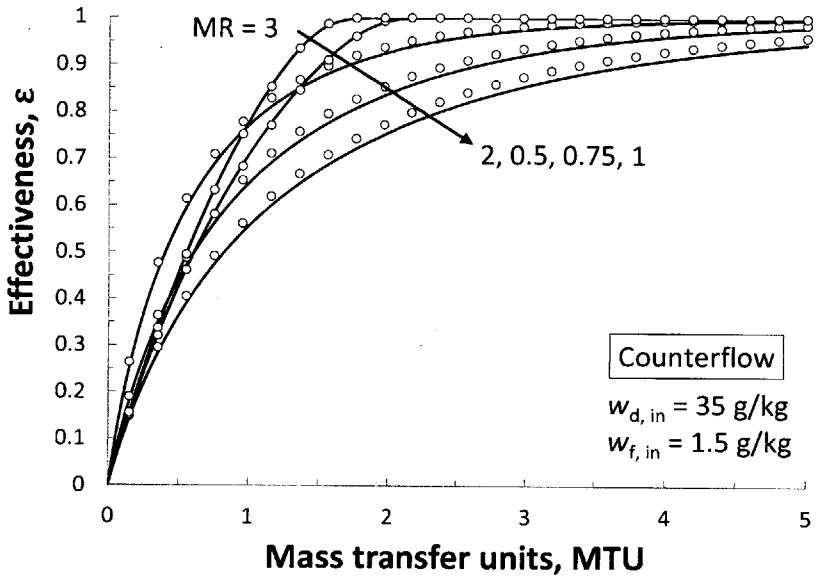

Figure 3-11: Effectiveness vs. mass transfer units for varying mass flow rate ratios, counterflow configuration, and fixed inlet salinities representative of seawater and river water. Lines are from analytical Eq. (3.51), and the points are the results of a numerical model using a nonlinear osmotic pressure function.

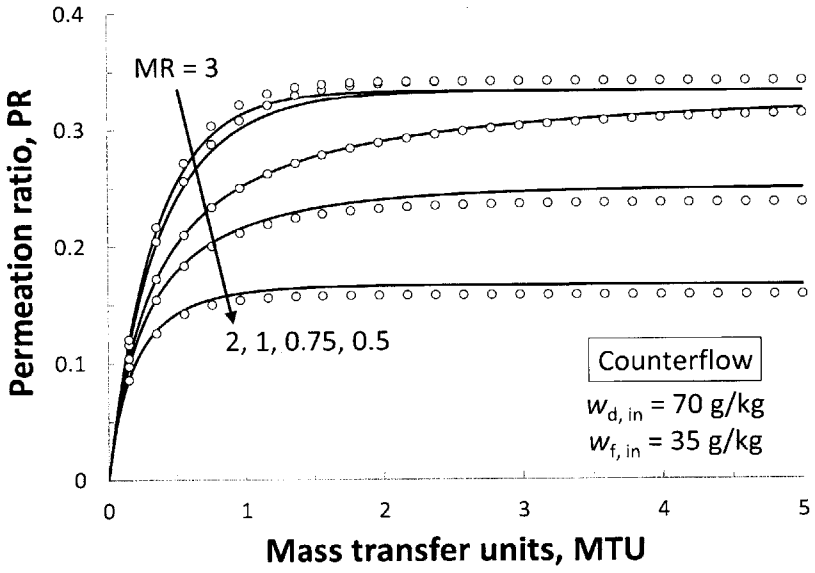

Figure 3-12: Permeation ratio vs. mass transfer units for varying mass flow rate ratios, counterflow configuration, and fixed inlet salinities representative of brine and seawater. Lines are from analytical Eq. (3.35), and the points are the results of a numerical model using a nonlinear osmotic pressure function.

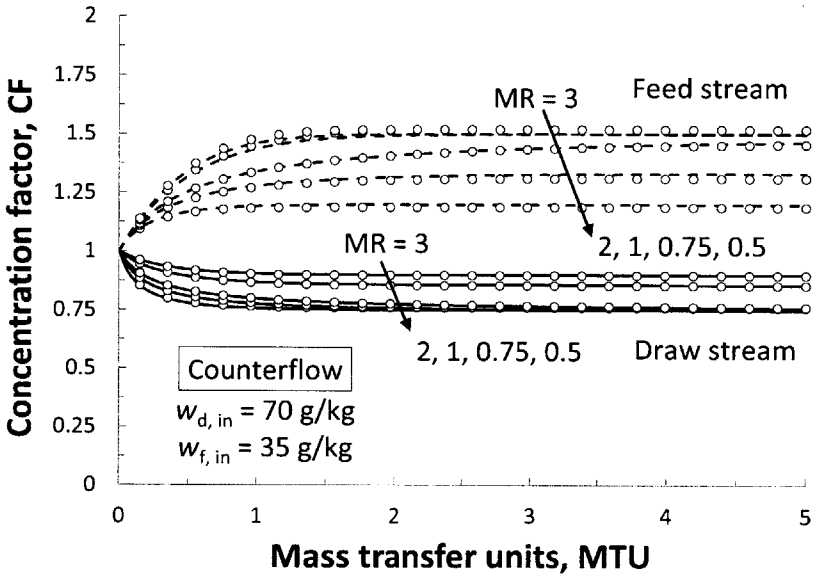

Figure 3-13: Concentration factor vs. mass transfer units for varying mass flow rate ratios, counterflow configuration, and fixed inlet salinities representative of brine and seawater. Solid and dashed lines are from analytical Eqs. (3.21) and (3.22), respectively, and the points are the results of a numerical model using a nonlinear osmotic pressure function.

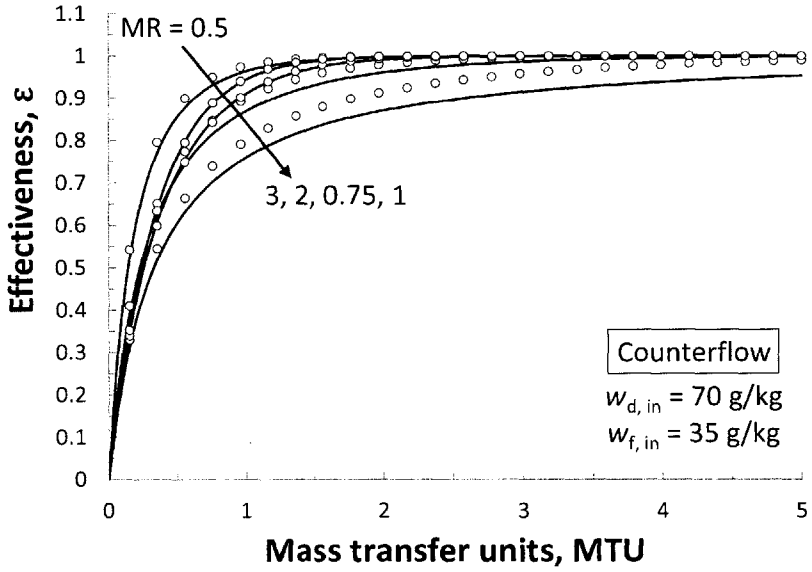

Figure 3-14: Effectiveness vs. mass transfer units for varying mass flow rate ratios, counterflow configuration, and fixed inlet salinities representative of brine and seawater. Lines are from analytical Eq. (3.51), and the points are the results of a numerical model using a nonlinear osmotic pressure function.

3.5 Conclusions

The major conclusions of this chapter are as follow:

1. Closed form analytical solutions for a one-dimensional pressure retarded osmosis mass exchanger using an ideal membrane were developed. The equations express the permeation ratio of the membrane as a function of the configuration of the membrane and four dimensionless groups: two osmotic pressure ratios, a mass flow rate ratio, and the number of mass transfer units.

2. A robust analogy exists between heat exchangers and osmotic mass exchangers in which the effectiveness can be expressed by four dimensionless groups. The new ε-MTU model developed for the osmotic mass exchanger can be used as a design tool for PRO systems using a linearized osmotic pressure function and ideal membrane characteristics. Combinations of stream compositions can be analyzed by selecting the appropriate modified van 't Hoff coefficient to be used in the dimensionless osmotic pressure ratio.

3. In order to develop closed-form analytical solutions of the PRO exchanger performance, osmotic pressure must be approximated as a linear function of salinity. Modest errors are incurred in doing so. Two cases were modeled to determine the errors associated with linearization: a power production case with inlet seawater and river water, and a desalination energy recovery case with inlet brine and seawater. For both cases the hydraulic pressure was set to equal half of the maximum osmotic pressure difference. Also for each case, the modified van 't Hoff coefficient is varied to more closely approximate the nonlinear osmotic pressure for the range of salinity. For the power production case, the maximum error is less than 5% for the permeation ratio and effectiveness of a counterflow PRO exchanger. For the energy recovery case, the maximum error is less than 5.5%.

Chapter 4

Limits of Flux and Power for a One-Dimensional Ideal FO and PRO Membrane

Chapter abstract

Pressure retarded osmosis (PRO) is a method of producing energy from two streams of a different salinity using a membrane-based mass exchanger. In practice, this technology uses seawater and river water, which converge at a river delta, to produce power. PRO technology can also be used to recover chemical energy from a reverse osmosis system by combining the rejected brine stream with the feed water source or available wastewater. In previous chapters of this work, it has been demonstrated that by making a few idealizations, closed-form expressions can be derived for the flux performance of one-dimensional RO and PRO membrane-based mass exchangers. These expressions are functions of several dimensionless parameters which relate the permeate flux, membrane area, hydraulic and osmotic pressure, and mass flow rates. These expressions are analogous to effectiveness vs. number of transfer unit relations that characterize heat exchanger performance. This chapter modifies the PRO closed-form expressions in order to more easily analyze the maximum flux attainable during direct forward osmosis operation and the power performance under PRO operation. For the PRO power production case, the optimal hydraulic pressure is found which produces the maximum power for a given membrane area and inlet stream salinities. The global maximum power attainable for given stream salinities is also found. Additionally, a reversible salinity gradient engine is studied to deter-

mine the maximum reversible power attainable by two streams of a different salinity. The reversible model is used as a benchmark for the one-dimensional PRO exchanger performance.

4.1 Introduction

When two streams of a different salinity are separated by a semipermeable membrane, the natural process of osmosis causes water to diffuse from the dilute to the concentrated stream. If the concentrated stream is pressurized to a hydraulic pressure greater than that of the dilute stream before entering into a PRO exchanger, then the permeate which enters into the concentrated stream via osmosis becomes pressurized. This permeate can be depressurized with the original concentrate through a turbine to create more electrical work than the concentrate alone would have provided. This method of power production is called pressure retarded osmosis (PRO) in the literature. Typically, seawater and river water are used as the concentrate, or draw, and dilute, or feed, streams, respectively. The process is 'pressure retarded' because the osmotic driving potential is deliberately reduced by increasing the hydraulic pressure of the draw stream relative to the feed stream in order to produce the maximum power.

In 1954, Pattle introduced a method for extraction of power from salinity gradients via a hydroelectric pile, now known as the Reverse Electrodialysis (RED) method [53]. The PRO method was introduced by Loeb two decades later [34]. A seminal paper in the PRO field was authored by Lee et al. in 1981 [4]. In addition to experimental results and an early characterization of concentration polarization in real membranes, Lee et al. present the commonly cited expression for the maximum power achievable for a zero-dimensional, ideal, and semi-permeable PRO membrane [54–57]. By considering the flux or power achievable from a zero-dimensional membrane, however, it is assumed that the streams do vary in concentration throughout the exchanger.

This assumption may be valid for small, coupon-sized membranes in a laboratory experiment, but for an FO desalination process or PRO power plant the membrane areas are greater and the change in salinity throughout the exchanger must usually be considered.

This chapter will apply dimensionless expressions for determining the flux through a one-dimensional FO or PRO membrane mass exchanger in order to provide a more realistic estimate of the performance of these exchangers. Because this chapter does not consider the effect of concentration polarization within the exchanger, and because that phenomenon effectively increases the resistance to mass transfer within the exchangers, the flux and power performance of both the FO and PRO exchangers by this analysis are considered to be an upper bound.

For a more detailed explanation of forward and pressure retarded osmosis exchanger operation, refer to Sec. 3.1.

4.2 Alternative PRO mass exchanger model

In this section, we will re-derive the PRO mass exchanger model from the previous chapter in order to facilitate analysis of the limits of permeation in direct forward osmosis (FO) operation and of power production in PRO operation. Modifications of the previous chapters' dimensionless parameters will be presented along with a new dimensionless parameter which balances the hydraulic to osmotic driving potential within the exchanger. One reason for these modifications is that in direct FO operation, the hydraulic pressure difference across the membrane is equal to zero. This results in osmotic pressure ratios (see Sec. 3.2.2) which approach infinity and a mass transfer units, MTU, value equal to zero independent of membrane area. Thus, it is important to separate the effect of the hydraulic pressure difference, ΔP, from these dimensionless parameters in order to properly analyze the performance of a one-

dimensional direct forward osmosis exchanger. In the case of PRO power production, we wish to find the optimal hydraulic pressure difference at which to operate the system to provide maximum power. Therefore, the MTU dependence on the pressure difference must be altered because we wish to vary ΔP while maintaining a fixed membrane area.

After developing the modified PRO closed-form expressions, the limits of direct forward osmosis performance will be presented followed by an analysis of the power attainable by mixing two streams reversibly with a salinity gradient engine. Finally, the modified expressions are used to determine the maximum power attainable and at which hydraulic pressure difference this power can be attained.

4.2.1 Parallel-flow configuration PRO model

For the details of the PRO closed-form expressions, refer to Sec. 3.2. Derivation of the modified closed-form expressions will begin with Eq. (3.9) for the PRO exchanger in a parallel-flow configuration and is reproduced here as Eq. (4.1).

$$d\dot{m}_{\mathrm{p}} = A\left[C\left(\frac{\dot{m}_{\mathrm{d,\,in}} \times w_{\mathrm{d,\,in}}}{\dot{m}_{\mathrm{d,\,in}} + \dot{m}_{\mathrm{p}}} - \frac{\dot{m}_{\mathrm{f,\,in}} \times w_{\mathrm{f,\,in}}}{\dot{m}_{\mathrm{f,\,in}} - \dot{m}_{\mathrm{p}}}\right) - \Delta P\right] dA_{\mathrm{m}} \qquad (4.1)$$

Some of the important assumptions inherent in this equation are that the water permeability coefficient is constant, concentration polarization effects are neglected, the pressure drop through the flow channel is negligible, the membrane is ideal and rejects 100% of solutes, and the osmotic pressure is a linear function of salinity.

Four dimensionless parameters are used to cast Eq. (4.1) in a dimensionless form. Two of these dimensionless parameters are identical to those used in Chapter 3.

4.2.2 Dimensionless parameters

Permeation ratio, PR

$$\mathrm{PR} \equiv \frac{\dot{m}_{\mathrm{p}}}{\dot{m}_{\mathrm{f,\,in}}} \tag{4.2}$$

The permeation ratio is identical to the parameter described in Chapter 3. It is the ratio of permeate to feed mass flow rate and it should not be confused with the effectiveness which will be described in a later section.

Mass flow rate ratio, MR

$$\mathrm{MR} \equiv \frac{\dot{m}_{\mathrm{d,\,in}}}{\dot{m}_{\mathrm{f,\,in}}} \tag{4.3}$$

The mass flow rate ratio is the mass flow rate of the draw solution divided by the feed solution at the inlet of the PRO mass exchanger. It is also the same parameter as described in Chapter 3.

Modified osmotic pressure ratio, θ

For the draw side:

$$\theta_{\mathrm{d}} \equiv \frac{\pi_{\mathrm{d,\,in}}}{\Delta\pi_{\mathrm{max}}} \tag{4.4}$$

For the feed side:

$$\theta_{\mathrm{f}} \equiv \frac{\pi_{\mathrm{f,\,in}}}{\Delta\pi_{\mathrm{max}}} \tag{4.5}$$

where

$$\Delta\pi_{\mathrm{max}} = \pi_{\mathrm{d,\,in}} - \pi_{\mathrm{f,\,in}} \tag{4.6}$$

The modified osmotic pressure ratio is the ratio of the osmotic pressure at the draw or feed inlet to the maximum osmotic pressure difference. The maximum osmotic pressure difference is simply equal to the difference of the inlet draw and feed solution osmotic pressures. For FO and PRO operation, θ_{d} will always be greater than θ_{f}.

Modified mass transfer units, MTU_π

$$\mathrm{MTU}_\pi \equiv \frac{A\, A_\mathrm{m}\, \Delta\pi_\mathrm{max}}{\dot{m}_\mathrm{f,\,in}} \tag{4.7}$$

As seen before, the number of *mass transfer units* (MTU) is a dimensionless parameter for a membrane mass exchanger similar to the *number of transfer units* (NTU) used in heat exchanger design. In this chapter, however, the mass transfer units is dependent on the maximum osmotic pressure difference, $\Delta\pi_\mathrm{max}$, from Eq. (4.6). The number of mass transfer units based on the hydraulic pressure difference, ΔP, which constitutes the RO and PRO solution in the previous chapters, could presently be denoted as MTU_P. This parameter is related to MTU_π by the equality $\mathrm{MTU}_P = \mathrm{MTU}_\pi \times P^*$ where P^* is the pressure ratio to be introduced in the following subsection.

Pressure ratio, P^*

$$P^* \equiv \frac{\Delta P}{\Delta\pi_\mathrm{max}} \tag{4.8}$$

The pressure ratio is equivalent to the hydraulic pressure difference divided by the maximum osmotic pressure difference. For FO and PRO operation where the permeate flows in the direction of the more concentrated solution, P^* is a number between zero and unity. When $P^* = 1$, the trans-membrane hydraulic pressure difference is equal to the maximum osmotic pressure difference and there is no flux through the exchanger, per Eq. (3.1), regardless of orientation. At the other limit when $P^* = 0$, the exchanger operates in the direct forward osmosis regime and the maximum amount of flux permeates through the membrane.

Dividing Eq. (4.1) by $\dot{m}_\mathrm{f,\,in}$, multiplying the right hand side by $\Delta\pi_\mathrm{max}/\Delta\pi_\mathrm{max}$, and substituting Eqs. (4.2)–(4.8) into Eq. (4.1) yields,

$$d\mathrm{PR} = \left(\frac{\mathrm{MR} \times \theta_\mathrm{d}}{\mathrm{MR} + \mathrm{PR}} - \frac{\theta_\mathrm{f}}{1 - \mathrm{PR}} - P^* \right) d\mathrm{MTU}_\pi \tag{4.9}$$

Equation (4.9) can be integrated as follows:

$$\int_0^{\mathrm{PR}} \left(\frac{\mathrm{MR} \times \theta_\mathrm{d}}{\mathrm{MR} + \mathrm{PR}} - \frac{\theta_\mathrm{f}}{1 - \mathrm{PR}} - P^* \right)^{-1} d\mathrm{PR} = \mathrm{MTU}_\pi \tag{4.10}$$

Equation (4.10) can be simplified into

$$\int_0^{\mathrm{PR}} \frac{(\mathrm{MR} + \mathrm{PR})(1 - \mathrm{PR})}{P^*(\mathrm{PR} - \kappa)(\mathrm{PR} - \lambda)} d\mathrm{PR} = \mathrm{MTU}_\pi \tag{4.11}$$

where

$$\begin{aligned} \kappa = {} & \frac{1}{2P^*}(P^* + \mathrm{MR}(\theta_\mathrm{d} - P^*) + \theta_\mathrm{f}) \\ & - \frac{1}{2P^*}\sqrt{(P^* + \mathrm{MR}(\theta_\mathrm{d} - P^*) + \theta_\mathrm{f})^2 - 4\mathrm{MR}\,P^*(\theta_\mathrm{d} - \theta_\mathrm{f} - P^*)} \end{aligned} \tag{4.12}$$

$$\begin{aligned} \lambda = {} & \frac{1}{2P^*}(P^* + \mathrm{MR}(\theta_\mathrm{d} - P^*) + \theta_\mathrm{f}) \\ & + \frac{1}{2P^*}\sqrt{(P^* + \mathrm{MR}(\theta_\mathrm{d} - P^*) + \theta_\mathrm{f})^2 - 4\mathrm{MR}\,P^*(\theta_\mathrm{d} - \theta_\mathrm{f} - P^*)} \end{aligned} \tag{4.13}$$

Therefore the integration of Eq. (4.11) will be

$$\begin{aligned} \mathrm{MTU}_\pi \times P^* = {} & \frac{(\lambda - 1)(\mathrm{MR} + \lambda)}{(\kappa - \lambda)} \ln\left(\frac{\lambda - \mathrm{PR}}{\lambda}\right) \\ & - \frac{(\kappa - 1)(\mathrm{MR} + \kappa)}{(\kappa - \lambda)} \ln\left(\frac{\kappa - \mathrm{PR}}{\kappa}\right) - \mathrm{PR} \end{aligned} \tag{4.14}$$

Equation (4.14) can be used in the design of a membrane mass exchanger where the required mass transfer units, effectively the membrane area, is given as an explicit relation.

As seen in the previous chapter, by considering a pure permeate and applying conservation of solution and solutes to the draw and feed streams separately, the expressions for the draw and feed concentration factors can be determined, as given by Eqs. (4.15) and (4.16)

For the draw side:

$$\mathrm{CF_d} \equiv \frac{w_{\mathrm{d,\,out}}}{w_{\mathrm{d,\,in}}} = \frac{\mathrm{MR}}{\mathrm{MR} + \mathrm{PR}} \tag{4.15}$$

For the feed side:

$$\mathrm{CF_f} \equiv \frac{w_{\mathrm{f,\,out}}}{w_{\mathrm{f,\,in}}} = \frac{1}{1 - \mathrm{PR}} \tag{4.16}$$

4.2.3 Counterflow configuration PRO model

For the PRO exchanger in a counterflow configuration, the derivation of the modified closed-form expressions will begin with Eq. (3.9) and is reproduced here as Eq. (4.17).

$$d\dot{m}_{\mathrm{p}} = A\left[C\left(\frac{\dot{m}_{\mathrm{d,\,out}} \times w_{\mathrm{d,\,out}}}{\dot{m}_{\mathrm{d,\,out}} - \dot{m}_{\mathrm{p}}} - \frac{\dot{m}_{\mathrm{f,\,in}} \times w_{\mathrm{f,\,in}}}{\dot{m}_{\mathrm{f,\,in}} - \dot{m}_{\mathrm{p}}}\right) - \Delta P\right] dA_{\mathrm{m}} \tag{4.17}$$

Using dimensionless parameters similar to those used for the parallel configuration (i.e. PR, MR, θ_{f}, P^*, and MTU_π), Eq. (4.17) can be rewritten in a dimensionless form. However, two additional dimensionless parameters are required and are defined as follows.

Outlet mass flow rate ratio, $\mathrm{MR_o}$

$$\mathrm{MR_o} \equiv \frac{\dot{m}_{\mathrm{d,\,out}}}{\dot{m}_{\mathrm{f,\,in}}} \tag{4.18}$$

Modified osmotic pressure ratio at draw outlet, $\theta_{\mathrm{d,\,o}}$

$$\theta_{\mathrm{d,\,o}} \equiv \frac{\pi_{\mathrm{d,\,out}}}{\Delta\pi_{\max}} \tag{4.19}$$

Since we are interested in expressing the permeation ratio as a function of the inlet parameters, the following are relations between the outlet dimensionless groups defined by Eqs. (4.18) and (4.19) and three inlet dimensionless groups.

The mass flow rate ratio defined in Eq. (4.3) can be written as a function of the outlet mass flow rate ratio defined by Eq. (4.18).

$$\mathrm{MR} = \frac{\dot{m}_{\mathrm{d,\,in}}}{\dot{m}_{\mathrm{f,\,in}}} = \frac{\dot{m}_{\mathrm{d,\,out}} - \dot{m}_{\mathrm{p}}}{\dot{m}_{\mathrm{f,\,in}}} = \mathrm{MR_o} - \mathrm{PR} \tag{4.20}$$

Therefore,

$$\mathrm{MR_o} = \mathrm{MR} + \mathrm{PR} \tag{4.21}$$

Similarly, the modified osmotic pressure ratio of the outlet draw stream can be written as a function of the modified osmotic pressure ratio of the inlet draw stream, the mass flow rate ratio, and the permeation ratio as follows:

$$\theta_{\mathrm{d,\,o}} = \theta_{\mathrm{d}} \frac{\mathrm{MR}}{\mathrm{MR} + \mathrm{PR}} \tag{4.22}$$

Using these dimensionless groups, Eq. (4.17) can be rewritten in a dimensionless form as follows:

$$d\mathrm{PR} = \left(\frac{\mathrm{MR_o} \times \theta_{\mathrm{d,\,o}}}{\mathrm{MR_o} - \mathrm{PR}} - \frac{\theta_{\mathrm{f}}}{1 - \mathrm{PR}} - P^* \right) d\mathrm{MTU}_{\pi} \tag{4.23}$$

Equation (4.23) can be integrated as follows:

$$\int_0^{\mathrm{PR}} \left(\frac{\mathrm{MR_o} \times \theta_{\mathrm{d,\,out}}}{\mathrm{MR_o} - \mathrm{PR}} - \frac{\theta_{\mathrm{f}}}{1 - \mathrm{PR}} - P^* \right)^{-1} d\mathrm{PR} = \mathrm{MTU}_{\pi} \tag{4.24}$$

Equation (4.24) can be simplified into

$$\int_0^{\mathrm{PR}} \frac{(\mathrm{MR_o} - \mathrm{PR})(1 - \mathrm{PR})}{P^*(\mathrm{PR} - \kappa')(\mathrm{PR} - \lambda')} d\mathrm{PR} = \mathrm{MTU}_{\pi} \tag{4.25}$$

where

$$\kappa' = \frac{1}{2P^*}(P^* + \mathrm{MR_o}(P^* - \theta_{\mathrm{d,\,o}}) + \theta_\mathrm{f}) - \frac{1}{2P^*}\sqrt{(P^* + \mathrm{MR_o}(P^* - \theta_{\mathrm{d,\,o}}) + \theta_\mathrm{f})^2 + 4P^*\mathrm{MR_o}(-P^* + \theta_{\mathrm{d,\,o}} - \theta_\mathrm{f})} \quad (4.26)$$

$$\lambda' = \frac{1}{2P^*}(P^* + \mathrm{MR_o}(P^* - \theta_{\mathrm{d,\,o}}) + \theta_\mathrm{f}) + \frac{1}{2P^*}\sqrt{(P^* + \mathrm{MR_o}(P^* - \theta_{\mathrm{d,\,o}}) + \theta_\mathrm{f})^2 + 4P^*\mathrm{MR_o}(-P^* + \theta_{\mathrm{d,\,o}} - \theta_\mathrm{f})} \quad (4.27)$$

Integration of Eq. (4.25) yields

$$\mathrm{MTU}_\pi \times P^* = \frac{(\lambda' - 1)(\lambda' - \mathrm{MR_o})}{(\kappa' - \lambda')} \ln\left(\frac{\lambda' - \mathrm{PR}}{\lambda'}\right) - \frac{(\kappa' - 1)(\kappa' - \mathrm{MR_o})}{(\kappa' - \lambda')} \ln\left(\frac{\kappa' - \mathrm{PR}}{\kappa'}\right) - \mathrm{PR} \quad (4.28)$$

Hence, Eq. (4.28) combined with Eqs. (4.21) and (4.22) can be used in the design of a PRO membrane mass exchanger where the required mass transfer units, effectively the membrane area, is given as an explicit relation of the form

$$\mathrm{MTU}_\pi = \mathrm{fn}(\mathrm{PR},\ \mathrm{MR},\ \theta_\mathrm{f},\ \theta_\mathrm{d},\ P^*) \quad (4.29)$$

4.3 Alternative PRO effectiveness (ε-MTU_π model)

As seen in Sec. 3.3, the effectiveness of a PRO exchanger is equivalent to the actual amount of permeate divided by the maximum possible amount of permeate. The maximum possible amount of permeate is achieved when the membrane area is large enough to allow the hydraulic and osmotic driving potentials to become equal. In this section, the effectiveness-MTU model is altered to account for the modified dimensionless parameters. The effectiveness is reproduced from the previous chapter

as Eq. (4.30).

$$\varepsilon \equiv \frac{\mathrm{PR}}{\mathrm{PR}_{\max}} \tag{4.30}$$

The derivation of the alternative effectiveness of a PRO mass exchanger operating in parallel or counterflow configuration is nearly identical to the steps shown in Sec. 3.3. Therefore, this derivation will be omitted and the final results displayed below.

4.3.1 Parallel-flow PRO effectiveness

For a parallel-flow PRO mass exchanger, the maximum permeation ratio, Eq. (4.1) is found to be one of the roots to the PR-MTU_π solution, κ, as given in Eq. (4.12). Therefore,

$$\mathrm{PR} = \varepsilon \mathrm{PR}_{\max} = \varepsilon\kappa \tag{4.31}$$

Substituting Eq. (4.31) into Eq. (4.14) yields an expression, Eq. (4.32), relating MTU_π, the effectiveness, and other dimensionless parameters.

$$\begin{aligned} \mathrm{MTU}_\pi \times P^* = {} & \frac{(\lambda-1)(\mathrm{MR}+\lambda)}{(\kappa-\lambda)} \ln\left(\frac{\lambda-\varepsilon\kappa}{\lambda}\right) \\ & - \frac{(\kappa-1)(\mathrm{MR}+\kappa)}{(\kappa-\lambda)} \ln(1-\varepsilon) - \varepsilon\kappa \end{aligned} \tag{4.32}$$

4.3.2 Counterflow PRO effectiveness

For a counterflow PRO mass exchanger, there are two local maximum permeation ratios which are found depending on which side of the exchanger first reaches a zero net driving potential. Equations (4.33) and (4.34) display these two local maxima.

$$\mathrm{PR}_{\max,\,1} = \frac{\mathrm{MR}\,\theta_\mathrm{d}}{P^* + \theta_\mathrm{f}} - \mathrm{MR} \tag{4.33}$$

$$\mathrm{PR}_{\max,\,1} = 1 - \frac{\theta_\mathrm{f}}{\theta_\mathrm{d} - P^*} \tag{4.34}$$

The lesser of these local maximum permeation ratios is the global maximum as given by Eq. (4.35).

$$\mathrm{PR}_{\max} = \min\left\langle \mathrm{PR}_{\max,\,1}, \mathrm{PR}_{\max,\,2} \right\rangle \tag{4.35}$$

Substituting Eq. (4.30) into Eq. (4.28) yields an expression for MTU_{π} as a function of effectiveness as given by Eq. (4.36).

$$\begin{aligned} \mathrm{MTU}_{\pi} \times P^{*} = {} & \frac{(\lambda' - 1)(\lambda' - \mathrm{MR}_{\mathrm{o}})}{(\kappa' - \lambda')} \ln\left(\frac{\lambda' - \varepsilon \mathrm{PR}_{\max}}{\lambda'}\right) \\ & - \frac{(\kappa' - 1)(\kappa' - \mathrm{MR}_{\mathrm{o}})}{(\kappa' - \lambda')} \ln\left(\frac{\kappa' - \varepsilon \mathrm{PR}_{\max}}{\kappa'}\right) - \varepsilon \mathrm{PR}_{\max} \end{aligned} \tag{4.36}$$

4.4 Forward osmosis mass exchanger model

The PR-MTU_{π} model Eqs. (4.14) and (4.28) and the ε-MTU_{π} model Eqs. (4.32) and (4.36) are closed-form solutions for the performance of a one-dimensional PRO exchanger with different inlet conditions and orientation. The equations are valid for a P^{*} value between zero and one. As previously mentioned, when $P^{*} = 0$, the maximum amount of permeate is achieved and the exchanger is said to operate in the direct FO, or FO, regime. Finding a solution for this regime is important because some desalination processes use FO as a means for separating water from a saline source using a concentrated draw solution. A back-end process, such as a distillation column, can then be used to recover the permeate and regenerate the draw solution. This section will derive equations which relate the permeation ratio and effectiveness with MTU_{π} for FO processes where $P^{*} = 0$.

4.4.1 Parallel-flow FO permeation ratio and effectiveness

One way to achieve the permeation ratio and effectiveness for the FO case is to perform numerical calculations that approach the limit of $P^{*} \rightarrow 0$ using computer

software. To derive a closed-form solution for the FO case, however, we must return to Eq. (4.10) and set $P^* = 0$ as shown in Eq. (4.37) in a simplified form.

$$\int_0^{\mathrm{PR}} \frac{(\mathrm{MR}+\mathrm{PR})(1-\mathrm{PR})}{\mathrm{MR}\,\theta_\mathrm{d}(1-\mathrm{PR})-\theta_\mathrm{f}(\mathrm{MR}+\mathrm{PR})} d\mathrm{PR} = \mathrm{MTU}_\pi \tag{4.37}$$

Integrating Eq. (4.37) yields,

$$\begin{aligned}\mathrm{MTU}_\pi = {} & \frac{\mathrm{MR}}{b}\ln\left|\frac{X}{a}\right| + (1-\mathrm{MR})\left(\frac{\mathrm{PR}}{b}+\frac{a}{b^2}\ln\left|\frac{a}{X}\right|\right) \\ & + \frac{1}{b^3}\left[a^2\left(\ln\left|\frac{a}{X}\right|-\frac{3}{2}\right)+2aX-\frac{X^2}{2}\right]\end{aligned} \tag{4.38}$$

where

$$a = \mathrm{MR}\,(\theta_\mathrm{d}-\theta_\mathrm{f}) \tag{4.39}$$

$$b = -\left(\mathrm{MR}\,\theta_\mathrm{d}+\theta_\mathrm{f}\right) \tag{4.40}$$

$$X = a + b\times\mathrm{PR} \tag{4.41}$$

Figures 4-1 and 4-2 show the variation of the permeation ratio (PR) and the concentration factor (CF) with the mass transfer units (MTU_π) at different mass flow rate ratios for the parallel-flow configuration. An inlet draw stream salinity of twice the inlet feed stream salinity is considered.

To find the maximum permeation ratio of the parallel-flow case, we equate the osmotic driving potential to zero instead of equating it to the hydraulic pressure difference, ΔP, as was done in the previous chapter.

$$\Delta\pi_\mathrm{out} = \pi_{\mathrm{d,\,out}} - \pi_{\mathrm{f,\,out}} = C\left(w_{\mathrm{d,\,out}} - w_{\mathrm{f,\,out}}\right) = 0 \tag{4.42}$$

Substituting conservation of solution and solutes for the draw and feed streams, as done in the previous chapter in Eqs. (3.39) and (3.40), to express the outlet salinities

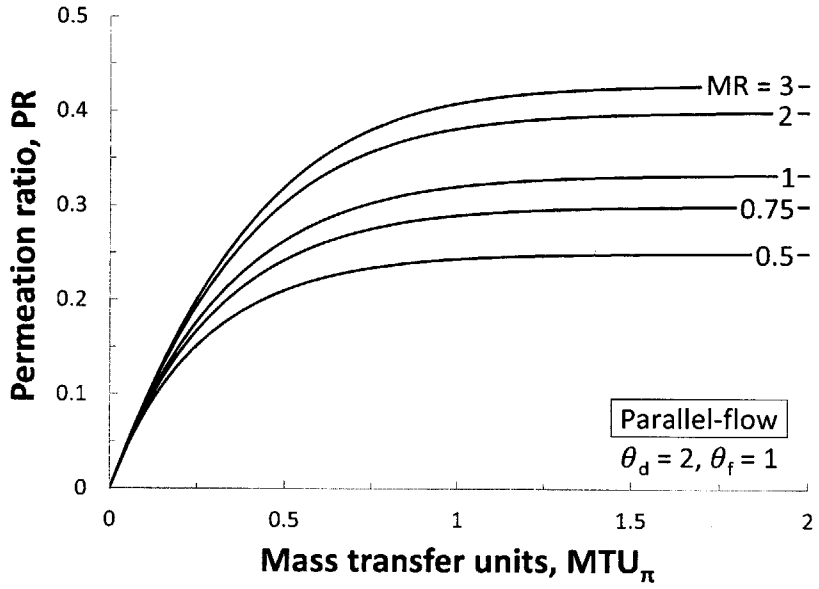

Figure 4-1: Permeation ratio vs. mass transfer units with contours of mass flow rate ratio for a parallel-flow configuration in FO operation.

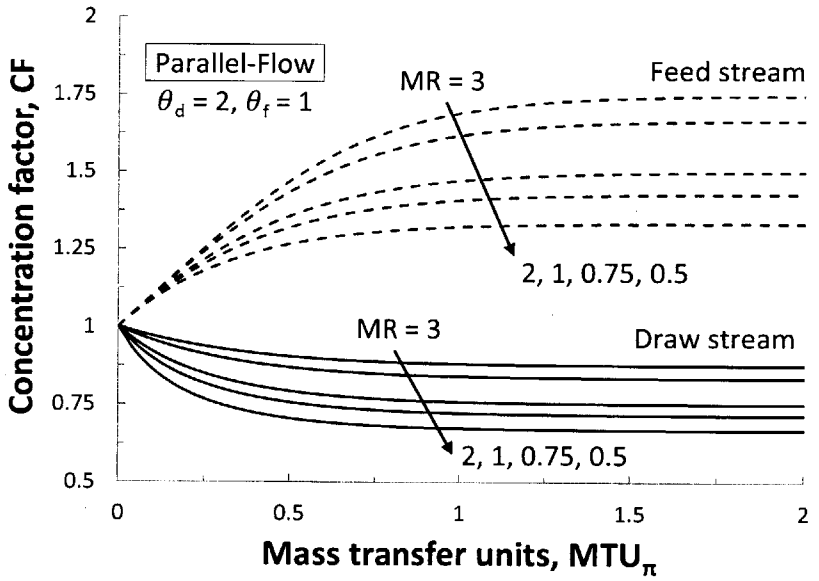

Figure 4-2: Concentration factor vs. mass transfer units with contours of mass flow rate ratio for a parallel-flow configuration in FO operation.

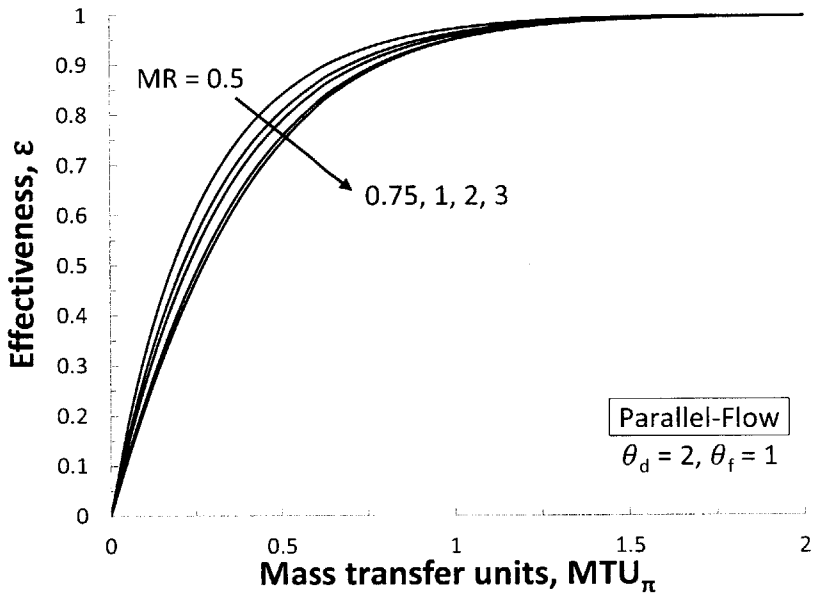

Figure 4-3: Effectiveness vs. mass transfer units with contours of mass flow rate ratio for a parallel-flow configuration in FO operation.

in terms of the inlet salinities and other dimensionless variables, and dividing by $\Delta\pi_{\max}$, yields the following expression,

$$\frac{\theta_{\mathrm{d}}\,\mathrm{MR}}{\mathrm{MR}+\mathrm{PR}_{\max}}-\frac{\theta_{\mathrm{f}}}{1-\mathrm{PR}_{\max}}=0 \tag{4.43}$$

Solving for $\mathrm{PR}_{\max}$ yields,

$$\mathrm{PR}_{\max}=\frac{\mathrm{MR}\,(\theta_{\mathrm{d}}-\theta_{\mathrm{f}})}{\theta_{\mathrm{d}}\,\mathrm{MR}+\theta_{\mathrm{f}}} \tag{4.44}$$

Again, the effectiveness is defined by Eq. (4.30) and is plotted versus MTU_{π} for the parallel-flow configuration in Fig. 4-3.

4.4.2 Counterflow FO permeation ratio and effectiveness

Again, Eqs. (4.26)–(4.28) and Eqs. (4.33)–(4.36) can be solved numerically as P^* approaches zero in order to solve for the limit of FO operation. To arrive at a closed form solution, however, Eq. (4.24) must be integrated where $P^* = 0$ as shown in

Eq. (4.45) in a simplified form.

$$\int_0^{\mathrm{PR}} \frac{(\mathrm{MR_o} - \mathrm{PR})(1 - \mathrm{PR})}{\mathrm{MR_o}\,\theta_{\mathrm{d,\,o}}\,(1 - \mathrm{PR}) - \theta_{\mathrm{f}}\,(\mathrm{MR_o} - \mathrm{PR})} d\mathrm{PR} = \mathrm{MTU}_\pi \tag{4.45}$$

Performing this integral yields the following result:

$$\begin{aligned}\mathrm{MTU}_\pi = {} & \frac{\mathrm{MR_o}}{d} \ln\left|\frac{Y}{c}\right| + (1 + \mathrm{MR_o})\left(\frac{\mathrm{PR}}{d} + \frac{c}{d^2} \ln\left|\frac{Y}{c}\right|\right) \\ & + \frac{1}{d^3}\left[c^2\left(\ln\left|\frac{Y}{c}\right| + \frac{3}{2}\right) + \frac{Y^2}{2} - 2cY\right]\end{aligned} \tag{4.46}$$

where

$$c = \mathrm{MR_o}\,(\theta_{\mathrm{d,\,o}} - \theta_{\mathrm{f}}) \tag{4.47}$$

$$d = \theta_{\mathrm{f}} - \mathrm{MR_o}\,\theta_{\mathrm{d,\,o}} \tag{4.48}$$

$$Y = c + d \times \mathrm{PR} \tag{4.49}$$

Figures 4-4 and 4-5 show the variation of the permeation ratio (PR) and the concentration factor (CF) with the mass transfer units (MTU_π) at different mass flow rate ratios for the counterflow configuration. A draw stream salinity of twice the feed stream salinity is considered.

To find the effectiveness, the osmotic driving potential is set to zero on both sides of the exchanger.

$$\pi_{\mathrm{d,\,out}} - \pi_{\mathrm{f,\,in}} = 0 \tag{4.50}$$

Using the van 't Hoff model and applying conservation of solution and solutes, this condition will lead to

$$\mathrm{PR}_{\mathrm{max,\,1}} = \mathrm{MR}\left(\frac{\theta_{\mathrm{d}}}{\theta_{\mathrm{f}}} - 1\right) \tag{4.51}$$

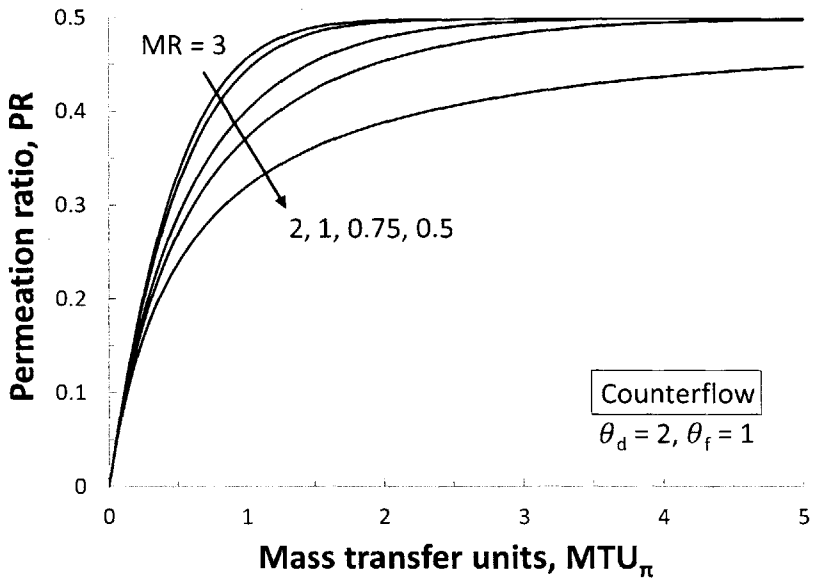

Figure 4-4: Permeation ratio vs. mass transfer units with contours of mass flow rate ratio for a counterflow configuration in FO operation.

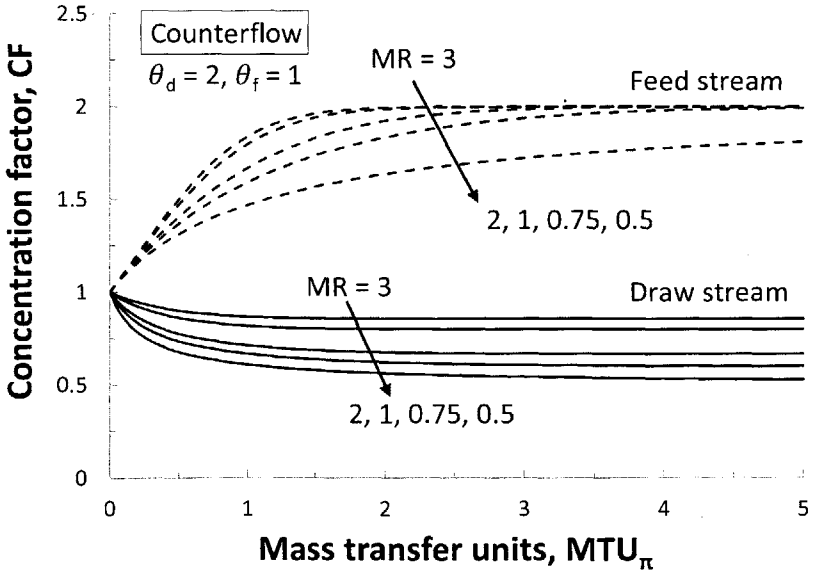

Figure 4-5: Concentration factor vs. mass transfer units with contours of mass flow rate ratio for a counterflow configuration in FO operation.

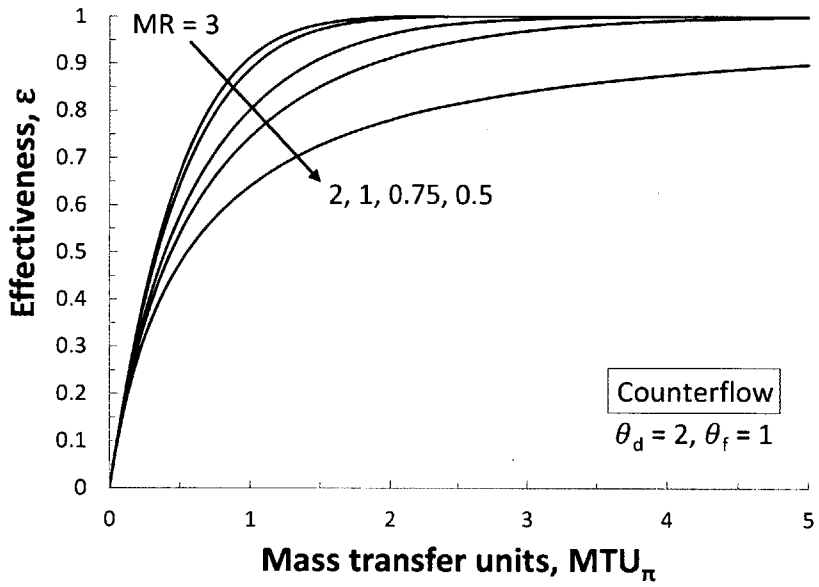

Figure 4-6: Effectiveness vs. mass transfer units with contours of mass flow rate ratio for a counterflow configuration in FO operation.

The other condition will lead to

$$\pi_{d,\,in} - \pi_{f,\,out} = 0 \tag{4.52}$$

and

$$PR_{max,\,2} = 1 - \frac{\theta_f}{\theta_d} \tag{4.53}$$

Since there are two solutions for the maximum permeation ratio, we should take the minimum value.

$$PR_{max} = \min \langle PR_{max,\,1}, PR_{max,\,2} \rangle \tag{4.54}$$

The effectiveness is defined as given by Eq. (4.30) and is plotted versus MTU_π for the counterflow configuration in Fig. 4-6.

4.4.3 Effect of concentration polarization on FO permeate flux

Again, it is important to note that the values shown in Figs. 4-1 – 4-6 will be altered once concentration polarization is included in the model. To gain an understanding of how significant the decrease in flux can become when concentration polarization is taken into account, a simple example of a zero-dimensional FO exchanger with and without concentration polarization is presented below.

The permeation flow rate per unit area through a zero-dimensional ideal membrane operating in the direct forward osmosis regime is given by

$$\dot{m}''_{\mathrm{p}} = A\left(\pi_{\mathrm{d}} - \pi_{\mathrm{f}}\right) \tag{4.55}$$

where A is the water permeability coefficient given in units of kg/s-m^2-kPa and the two osmotic pressure terms pertain to the draw and feed streams with units of kPa. The ideal membrane assumption implies no salt permeation and no concentration polarization effects.

Unlike ideal membranes, real membranes operated in the FO and PRO regime will experience a dual diffusion process allowing for salt permeation from the concentrate to the dilute stream. Real membranes also experience internal and external concentration polarization (ICP and ECP). ICP is due to concentration boundary layers that occur within the porous support layers of the membrane. The function of these support layers is to provide structural support to the active layer. ECP is due to external concentration boundary layers which form on both sides of the membrane. Collectively, salt permeation, ICP, and ECP reduce the net driving pressure across the membrane, thereby reducing the permeate flux for FO and PRO systems and the power produced in PRO systems.

The governing equation for the permeate flux in a zero-dimensional membrane

operating in the FO mode with ICP, the ECP on the feed side of the membrane, and no salt permeation is given by

$$\dot{m}''_{\mathrm{p}} = A\left[\pi_{\mathrm{d}}\ \exp\left(-\frac{\dot{m}''_{\mathrm{p}}K}{\rho_{\mathrm{p}}}\right) - \pi_{\mathrm{f}}\ \exp\left(\frac{\dot{m}''_{\mathrm{p}}}{\rho_{\mathrm{p}}k_{\mathrm{f}}}\right)\right] \tag{4.56}$$

where K is the solute resistance to diffusion within the support layer of the membrane with units of s/m, k_{f} is the mass transfer coefficient for the feed side with units of m/s, and ρ_{p} is the permeate density (considered to be pure water) with units of $\mathrm{kg/m^3}$ [52]. The osmotic pressure difference from Eq. (4.55) has now been replaced by the effective osmotic pressure difference which is the expression within the square brackets of Eq. (4.56). This expression includes the difference of the bulk osmotic pressures each multiplied by an exponential modulus which limits the amount of permeate per unit area of membrane due to concentration polarization effects. The first modulus represents the ICP, is a function of K, and reduces the draw side osmotic pressure when the term within the exponential brackets is less than zero. The second modulus represents the ECP, is a function of k_{f}, and increases the feed side osmotic pressure when the term in the exponential is greater than zero. The equation is implicit in the variable $\dot{m}''_{\mathrm{p}}$ and therefore requires a numerical method of solution.

The permeate mass flux through an ideal and real membrane is now compared. The inputs for the calculation are given in Table 4.1. The water permeability coefficient A, mass transfer coefficient k_{f}, and the solute resistance to diffusion K are given by McCutcheon and Elimelech [52]. The solutions are taken as having the same solute ratios as the solutes in seawater. The osmotic pressure model used for the solutions is discussed in Appendix B. A simultaneous equation solving software, Engineering Equation Solver (EES), is used to solve both functions [48]. The inlet salinities chosen are representative of a differential element of an FO exchanger used for desalinating seawater.

Table 4.1: Inputs for the calculation of flux through an ideal and real membrane

Input	Symbol	Value
Ambient temperature	T_0	25 °C
Draw salinity	$w_{\mathrm{d,in}}$	42 g/kg
Feed salinity	$w_{\mathrm{f,in}}$	35 g/kg
Permeate density	ρ_{p}	1000 kg/m^3
Water permeability coefficient	A	3.07×10^{-6} kg/s-m^2-kPa
Feed side mass transfer coefficient	k_{f}	1.74×10^{-5} m/s
Solute resistance to diffusion	K	2.67×10^{5} s/m

For the given stream salinities, the osmotic pressures are $\pi_{\mathrm{d}} = 31.4$ bar and $\pi_{\mathrm{f}} = 25.9$ bar and the rate of permeate mass flux through the ideal membrane is 1.70×10^{-3} kg/s-m^2. Including the exponential moduli for ICP and ECP decreases the flux to 4.35×10^{-4} kg/s-m^2. This result indicates that the amount of permeate flux through the real membrane is 25.7% of the flux through an ideal membrane for the inputs given.

By inspecting Eq. (4.56), one can see that there are ways to reduce the effects of concentration polarization and achieve more permeate from the real membrane. By reducing the solute resistance to diffusion, K, and increasing the mass transfer coefficient, k_{f}, the permeate flow rate can be increased. For example, by halving the value of K, the real membrane mass flux increases to 37.05% of the ideal membrane flux. This signifies an 11.4% increase in flux. By doubling k_{f}, however, the real flux is 27.4% of the ideal flux, which results in a mere flux increase of 1.7%. Comparing both of these examples, it is clear that reducing K has a stronger effect than increasing k_{f}. This is because FO is dominated by internal concentration polarization as has been documented in the literature [4, 35, 58].

In the limit that there is no support layer, then $K = 0$ and the real membrane mass flux increases to nearly 68% of the ideal membrane flux. In order to achieve a real membrane flux reduction of 10% compared to an ideal membrane, there must

be no support layer and k_f must be increased by a factor of 4.2 for the inputs given in Table 4.1. In theory, this could be achieved by designing a structurally stronger membrane active layer in order to do away with the support layer, reducing the channel spacing of the feed stream, and increasing the feed stream Reynolds number.

Due to the significance of concentration polarization in these osmotic mass exchanger systems, future work should focus on modifying the current equations to account for this phenomenon. The present model, however, can serve as a useful upper bound on performance for the ideal case where the mass transfer resistances due to concentration polarization are negligibly small compared to the resistance through the active layer of the membrane.

4.5 Reversible model for salinity gradient power production

Before determining the limits of power production for a PRO exchanger, a reversible model is first analyzed to provide the thermodynamic upper limit to the power available from two streams of a different salinity. In thermodynamics, a reversible heat engine produces power by exploiting a heat transfer from a high temperature reservoir to a low temperature reservoir. Here, we analyze a reversible salinity gradient engine (SGE) which produces power by exploiting the mixing of a high chemical potential stream with a low chemical potential stream. Thermodynamic analysis is performed on two black box models, shown in Fig. 4-7, to determine the maximum amount of power an SGE can produce by completely or incompletely mixing two streams of a different salinity. The systems are first introduced and the governing equations for determining the amount of power available are subsequently derived.

A control volume for a salinity gradient engine with three streams of water of varying salinity is denoted by the dashed box in Fig. 4-7a. The boundary of the

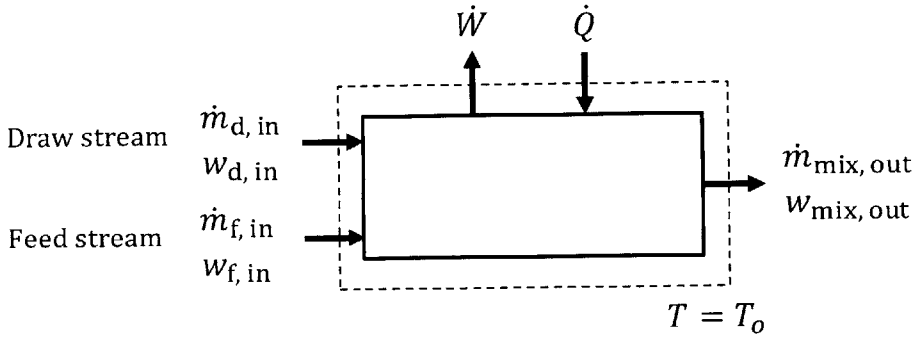

(a) Complete mixing engine

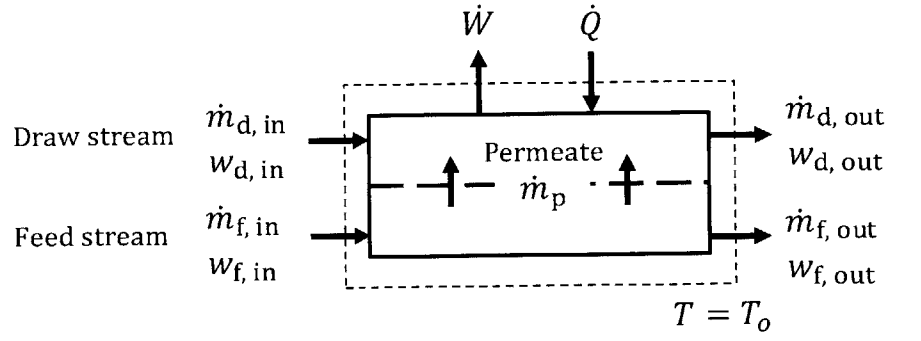

(b) Incomplete mixing engine

Figure 4-7: Schematic diagram of a reversible salinity gradient engine with (a) complete mixing and (b) incomplete mixing schemes.

control volume is drawn far away enough from the internal process so that all streams are at ambient pressure and temperature as defined by Mistry et al. [59]. The control volume itself is at ambient temperature. Within the control volume, a concentrated, or draw, stream of water is completely mixed with a dilute, or feed, stream which results in a solution with a salinity of w_{mix}. The maximum amount of power available from the two inlet streams of different salinity is produced during complete reversible mixing, and the value has been derived in the PRO literature [56, 60].

Figure 4-7b shows a more specific model that accounts for incomplete mixing through the use of four streams instead of three, as is the case in a PRO system, and is cited in literature [61]. Unlike the model considered in [61], however, salt diffusion from the draw to the feed stream is not considered due to the high salt rejection in membranes. For instance, salt rejection rates of greater than 99.7% are found in commercial seawater RO membranes [62]. In the incomplete mixing model, a draw and feed stream are brought together within a control volume and only water from the feed stream is allowed to mix with the draw stream. This water permeate, defined as $\dot{m}_{\text{p}} = \dot{m}_{\text{f, in}} - \dot{m}_{\text{f, out}}$, dilutes the incoming draw stream and concentrates the feed stream.

Also in the incomplete mixing model, as in the complete mixing model, the control volume is at ambient temperature and the boundary of the control volume is drawn such that all streams are at ambient pressure and temperature. The boundary, however, is not drawn so far as to allow the outlet streams to mix completely, where the salinity of the outlet streams are equal. This means that there is an amount of power that is lost due to incomplete mixing because the outlet streams could once again be brought together to produce more power. If the salinities of the outlet streams are equal ($w_{\text{d, out}} = w_{\text{f, out}}$), the power produced will limit to the maximum amount of available power given by the system in Fig. 4-7a.

4.5.1 Governing equations for a reversible mixing process

To quantify the amount of reversible power available from both systems, let us consider a generalized open, steady state, power-producing system with multiple streams of varying salinities entering and exiting the control volume. The system is in thermal equilibrium with the environment via a heat interaction, $\dot{Q}$, that enters the control volume at the temperature of the boundary which is equal to the ambient temperature, T_0. Neglecting changes in kinetic and gravitational energies of the streams, the First and Second Law of Thermodynamics for the system are given below:

$$0 = \dot{Q} - \dot{W} + \sum_{\text{in}} \dot{m}h - \sum_{\text{out}} \dot{m}h \tag{4.57}$$

$$0 = \frac{\dot{Q}}{T_0} + \sum_{\text{in}} \dot{m}s - \sum_{\text{out}} \dot{m}s + \dot{S}_{\text{gen}} \tag{4.58}$$

We multiply Eq. (4.58) by T_0 and subtract the result from Eq. (4.57) to attain an expression for the power of mixing, Eq. (4.59).

$$\dot{W}_{\text{mix}} = \sum_{\text{in-out}} \dot{m}h - T_0 \sum_{\text{in-out}} \dot{m}s + T_0 \dot{S}_{\text{gen}} \tag{4.59}$$

For a reversible system, $\dot{S}_{\text{gen}} = 0$, and Eq. (4.59) simplifies to Eq. (4.60).

$$\dot{W}^{\text{rev}}_{\text{mix}} = \sum_{\text{in-out}} \dot{m}h - T_0 \sum_{\text{in-out}} \dot{m}s \tag{4.60}$$

When the inlet and outlet streams are isothermal and at ambient temperature, we can substitute the definition for specific Gibbs free energy ($g \equiv h - Ts$) into Eq. (4.60) to give:

$$\dot{W}^{\text{rev}}_{\text{mix}} = \sum_{\text{in}} \dot{m}g - \sum_{\text{out}} \dot{m}g \tag{4.61}$$

If the value for the Gibbs free energy as a function of temperature, pressure, and salinity of each stream is available, the amount of reversible power by mixing can be calculated by inputting these values along with the flow rates of each stream into Eq. (4.61).

Two previously defined dimensionless parameters are used in this analysis. The mass flow rate ratio, MR from Eq. (4.3), and the permeation ratio, PR from Eq. (4.2). In this case, the permeation ratio controls how much of the feed stream is used for dilution of the draw stream.

Maximum reversible power by complete mixing

To find the maximum reversible power of mixing, Eq. (4.61) is applied to the complete mixing model of Fig. 4-7a. Several equations for mass conservation and Eq. (4.3) will also be used.

The mass conservation equations for solutions and solutes are given by

$$\dot{m}_{\mathrm{d,\,in}} + \dot{m}_{\mathrm{f,\,in}} = \dot{m}_{\mathrm{mix,\,out}} \tag{4.62}$$

$$\dot{m}_{\mathrm{d,\,in}} w_{\mathrm{d,\,in}} + \dot{m}_{\mathrm{f,\,in}} w_{\mathrm{f,\,in}} = \dot{m}_{\mathrm{mix,\,out}} w_{\mathrm{mix,\,out}} \tag{4.63}$$

The maximum reversible power by complete mixing is normalized by the feed stream mass flow rate to account for system size and is given by:

$$\frac{\dot{W}^{\mathrm{rev}}_{\mathrm{complete}}}{\dot{m}_{\mathrm{f,\,in}}} = \mathrm{MR}\, g_{\mathrm{d,\,in}} + g_{\mathrm{f,\,in}} - (1 + \mathrm{MR})\, g_{\mathrm{mix,\,out}} \tag{4.64}$$

Reversible power of incomplete mixing

To find the reversible power for a system with incomplete mixing, Eq. (4.61) is applied to the model in Fig. 4-7b along with several equations for mass conservation and use of Eqs. (4.3) and (4.2). For the mass conservation equations, the salinity of the

permeate must also be given.

The mass conservation equations for solutions and solutes are given by

$$\dot{m}_{\mathrm{d,\,in}} + \dot{m}_{\mathrm{f,\,in}} = \dot{m}_{\mathrm{d,\,out}} + \dot{m}_{\mathrm{f,\,out}} \tag{4.65}$$

$$\dot{m}_{\mathrm{f,\,in}} w_{\mathrm{f,\,in}} = \dot{m}_{\mathrm{p}} w_{\mathrm{p}} + \dot{m}_{\mathrm{f,\,out}} w_{\mathrm{f,\,out}} \tag{4.66}$$

$$\dot{m}_{\mathrm{d,\,in}} w_{\mathrm{d,\,in}} + \dot{m}_{\mathrm{p}} w_{\mathrm{p}} = \dot{m}_{\mathrm{d,\,out}} w_{\mathrm{d,\,out}} \tag{4.67}$$

The reversible power by incomplete mixing is normalized by the feed stream mass flow rate to account for system size and is given by:

$$\frac{\dot{W}^{\mathrm{rev}}_{\mathrm{incomplete}}}{\dot{m}_{\mathrm{f,\,in}}} = \mathrm{MR}\, g_{\mathrm{d,\,in}} + g_{\mathrm{f,\,in}} - (\mathrm{MR} - \mathrm{PR})\, g_{\mathrm{d,\,out}} - (1 + \mathrm{PR})\, g_{\mathrm{f,\,out}} \tag{4.68}$$

When the outlet salinities are equal in the incomplete mixing case, then the specific Gibbs free energy of the outlet streams become equal, $g_{\mathrm{d,\,out}} = g_{\mathrm{f,\,out}}$, and Eq. (4.68) reduces to Eq. (4.64).

4.5.2 Reversible model results and discussion

The reversible power derived for the complete and incomplete mixing cases is plotted against the variation of relevant parameters and the trends are discussed. The specific Gibbs free energy of each stream as a function of temperature, pressure, and salinity is evaluated using a seawater package developed by Sharqawy et al. [63].

Complete mixing case

Figure 4-8 shows the specific maximum reversible power of complete mixing, Eq. (4.64), plotted against the mass flow rate ratio at $T_0 = 25°\mathrm{C}$, $P_0 = 1$ bar, and fixed inlet salinities representative of seawater, $w_{\mathrm{d,\,in}} = 35$ g/kg, and river water, $w_{\mathrm{f,\,in}} = 1.5$ g/kg.

The figure shows that as the mass flow rate ratio is increased, the power rather quickly approaches an asymptotic value. As MR approaches infinity, this value reaches

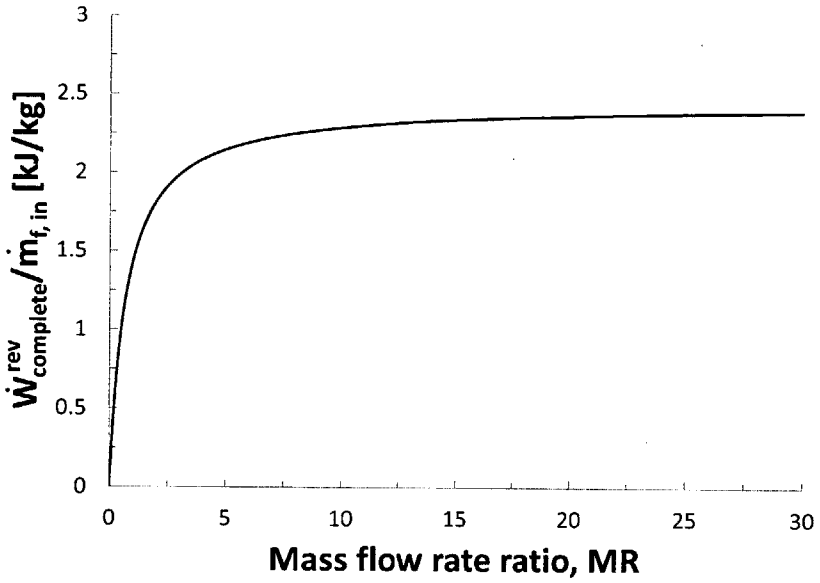

Figure 4-8: Specific maximum reversible power of complete mixing versus the mass flow rate ratio for fixed inlet salinities.

roughly 2.44 kJ per kilogram of feed for the given inlet salinities and represents the absolute maximum amount of power available by mixing two streams.

Incomplete mixing case

The specific power of incomplete mixing, Eq. (4.68), is plotted in Figure 4-9 as a function of the permeation ratio for various mass flow rate ratios.

As the permeation ratio increases, each MR contour approaches the maximum specific power where the salinities of both streams are equal. Note that Fig. 4-8 is reproducible by plotting Eq. (4.68) with equal outlet salinities ($w_{\mathrm{d,\,out}} = w_{\mathrm{f,\,out}}$).

4.6 Irreversible model for PRO power production

The previous section investigated the limits of reversible power production from two streams of a different salinity. This section will use equations derived earlier in this

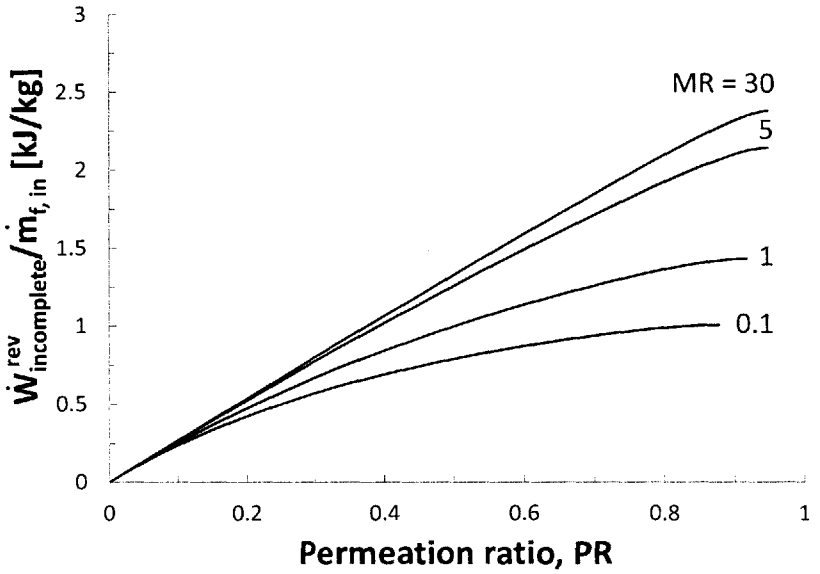

Figure 4-9: Reversible power of incomplete mixing versus permeation ratio for varying mass flow rate ratios and fixed inlet salinities.

chapter for the flux performance through a one-dimensional PRO mass exchanger to determine the maximum power achievable in a process more representative of an actual system.

For a zero-dimensional PRO exchanger, the governing equation for the mass flow rate of permeate is given by the integral form of Eq. (3.1):

$$\dot{m}_{\mathrm{p}} = A \cdot (\Delta\pi - \Delta P)\, A_{\mathrm{m}} \tag{4.69}$$

Figure 4-10 shows a PRO system that takes in a draw and feed stream, or seawater and fresh water, respectively [54]. The draw and feed solutions are brought into the system at atmospheric pressure and pumped to a slightly higher pressure via two low pressure pumps. The draw solution is then pressurized to a variable top pressure by entering a pressure exchanger. The pressurized feed and the draw streams enter a counterflow PRO mass exchanger where an amount of permeate is forced through a

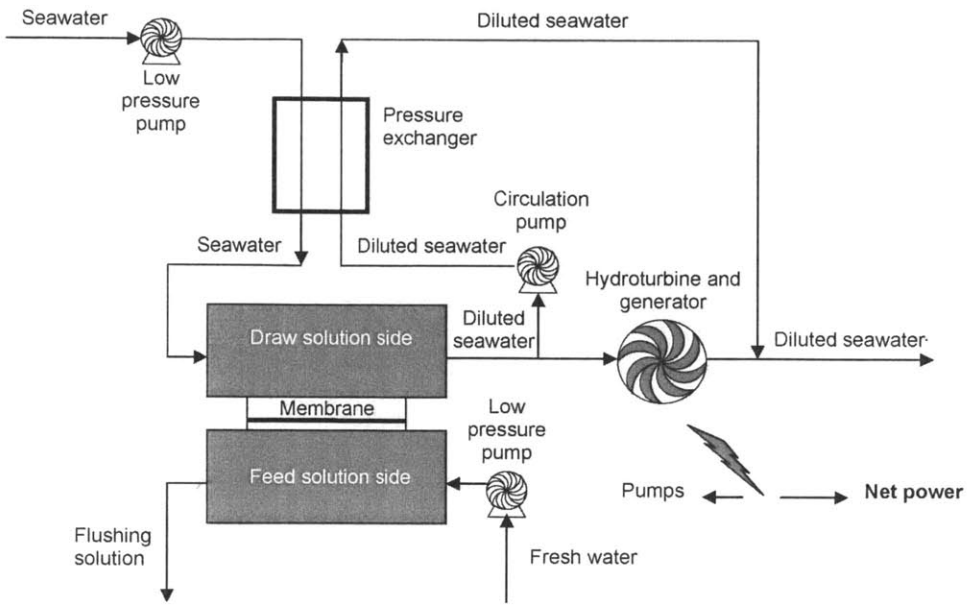

Figure 4-10: Schematic diagram of a PRO power generation system from Achilli et al. [54]. The permeate is depressurized through the hydroturbine to produce useful power.

semi-permeable membrane. The permeate is depressurized through a Pelton wheel or hydroturbine while the remaining outlet draw solution, which is now diluted, is used to pre-pressurize the inlet draw solution via a circulation pump and a pressure exchanger. A portion of the power from the hydroturbine is used to operate the pumps and the remainder is useful power.

We can determine the amount of useful power achievable from the permeate depressurization by applying the First Law of Thermodynamics to the hydroturbine. Equation (4.70) assumes that the system is open, at steady state, and adiabatic where changes in kinetic and gravitational energy are neglected.

$$\dot{W}_{\text{actual}} = \dot{m}_{\text{p}} \left(h_{\text{in}} - h_{\text{out}}\right)_{\text{actual}} \tag{4.70}$$

The enthalpy difference is given by integrating the definition of enthalpy between the

inlet and outlet states, as shown in Eq. (4.71).

$$h_{\text{in}} - h_{\text{out}} = \int_{\text{out}}^{\text{in}} \left(T\,ds + \frac{1}{\rho}\,dP \right) \tag{4.71}$$

We will first calculate the isentropic power and then correct for the actual power by using a turbine efficiency. For an isentropic process, the change in specific entropy is zero ($ds = 0$). Furthermore, the incompressible fluid model (ρ = constant) is used so that the density of the stream can be taken outside of the integral, yielding Eq. (4.72). The density in this equation is equal to the density of the diluted outlet draw stream which in Fig. 4-10 is labeled as diluted seawater.

$$(h_{\text{in}} - h_{\text{out}})_{\text{rev}} = \frac{1}{\rho}\,(P_{\text{in}} - P_{\text{out}}) \tag{4.72}$$

The definition of the isentropic efficiency is used to relate the reversible and actual enthalpy differences as shown in Eq. (4.73).

$$\eta = \frac{(h_{\text{in}} - h_{\text{out}})_{\text{actual}}}{(h_{\text{in}} - h_{\text{out}})_{\text{rev}}} \tag{4.73}$$

Equations (4.72) and (4.73) are substituted into Eq. (4.70) to give an expression for the actual power produced by the hydroturbine. The inlet hydraulic pressure to the hydroturbine is taken to be the draw stream pressure and the outlet is taken to be the feed stream pressure which is slightly above atmospheric. Therefore, the change in pressures for the hydroturbine is equal to the PRO trans-membrane hydraulic pressure, ΔP.

$$\dot{W}_{\text{actual}} = \eta \times \frac{\dot{m}_{\text{p}}}{\rho} \Delta P \tag{4.74}$$

By substituting Eq. (4.69) into Eq. (4.74) and differentiating with respect to ΔP, it can be shown that the maximum power occurs when $\Delta P = \Delta\pi/2$. This result was

first shown by Lee et al. [4] and is valid for a zero-dimensional membrane where the salinity, and consequently the osmotic pressure, does not vary throughout the length of the exchanger. This result corresponds to an optimal pressure ratio of $P^*_{\text{opt}} \equiv \Delta P/\Delta\pi = 1/2$ for the zero dimensional case. For a zero-dimensional exchanger, $\Delta\pi = \Delta\pi_{\text{max}}$, and it can be shown that the maximum power per unit mass flow rate of the feed stream, is given by Eq. (4.75)

$$\frac{\dot{W}_{\text{max, 0-D}}}{\dot{m}_{\text{f, in}}} = \frac{\eta}{\dot{m}_{\text{f, in}}} \frac{A_{\text{m}} A}{\rho} \frac{\Delta\pi^2}{4} \tag{4.75}$$

where ρ is the density of the outlet draw stream, A_{m} is the membrane area, and A is the water permeability coefficient.

To find the actual power for a one-dimensional exchanger, we make use of the equations developed in the first half of this chapter for determining the flux performance of the membranes. Returning to Eq. (4.74), and dividing by $\dot{m}_{\text{f, in}}$ and multiplying the right hand side by $\Delta\pi_{\text{max}}/\Delta\pi_{\text{max}}$, yields the following expression for the specific power of a one-dimensional exchanger relative to an inlet feed stream of one kilogram per second:

$$\frac{\dot{W}_{\text{1-D}}}{\dot{m}_{\text{f, in}}} = \frac{\eta\,\Delta\pi_{\text{max}}}{\rho} \text{PR} \cdot P^* \tag{4.76}$$

As previously mentioned, the limits for P^* are between zero and one for PRO operation. When $P^* = 0$, the maximum permeation ratio is achievable for a fixed value of MTU_π but there is no hydraulic pressure difference and therefore no power is produced. When $P^* = 1$, there is a maximum amount of hydraulic pressure difference, but zero permeation ratio and therefore no power is produced. In the following power analysis we will only consider a counterflow PRO exchanger.

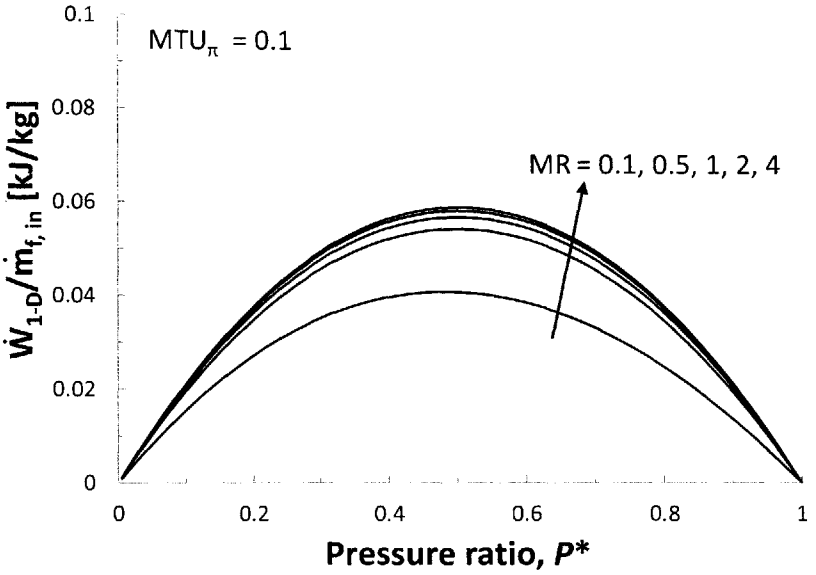

Figure 4-11: Specific power vs. pressure ratio at $\mathrm{MTU}_\pi = 0.1$ with contours of MR for a one-dimensional, counterflow PRO membrane.

4.6.1 Irreversible model results and discussion

Using Eqs. (4.26)–(4.28) and (4.76), the specific power output achievable can be plotted versus the full range of the pressure ratio for a given value of MTU_π and contours of MR varying between 0.1 and 4 as shown in Figs. 4-11 – 4-13. The inlet salinities considered in this analysis are $w_{\mathrm{d,\,in}} = 35$ g/kg and $w_{\mathrm{f,\,in}} = 1.5$ g/kg, which are representative of seawater and river water. The isentropic turbine efficiency, η, is considered to be unity to determine the maximum power for the given inputs.

It can be seen from these plots that for a given mass flow rate ratio, a maximum power results for a given value of the pressure ratio. Therefore, these plots can be used to better approximate the design hydraulic pressure to use in a PRO system for optimum performance. These plots can also be used to give an upper bound for the maximum power achievable from a one-dimensional PRO membrane. This upper bound is more realistic than the one given by Eq. (4.75) because the salinity of each stream is allowed to change throughout the length of the exchanger.

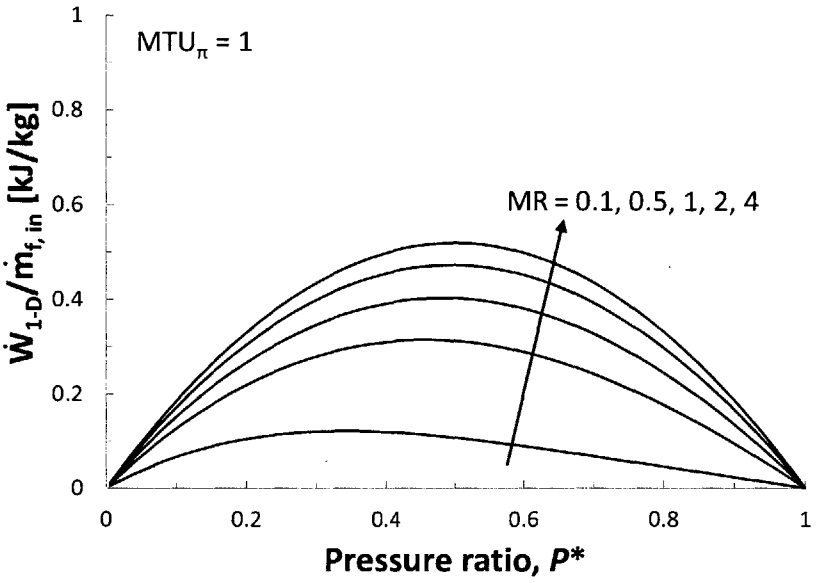

Figure 4-12: Specific power vs. pressure ratio at $\mathrm{MTU}_\pi = 1$ with contours of MR for a one-dimensional, counterflow PRO membrane.

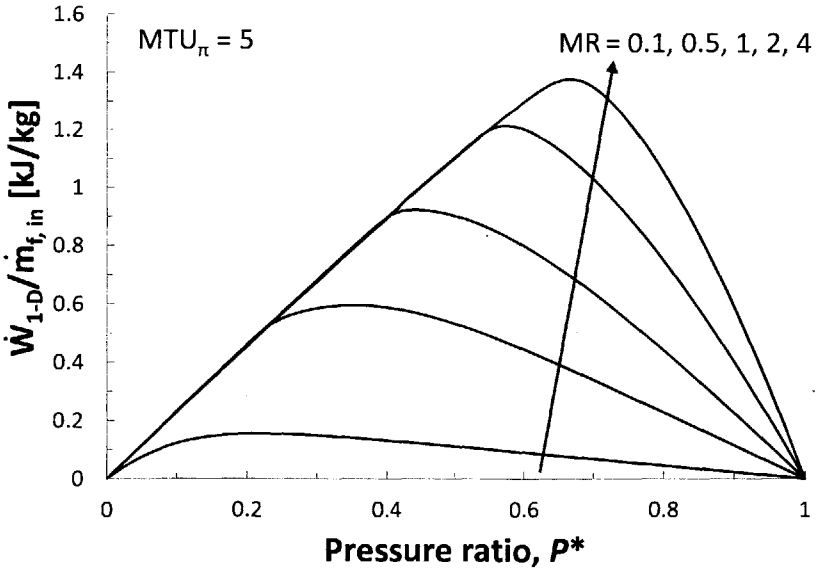

Figure 4-13: Specific power vs. pressure ratio at $\mathrm{MTU}_\pi = 5$ with contours of MR for a one-dimensional, counterflow PRO membrane.

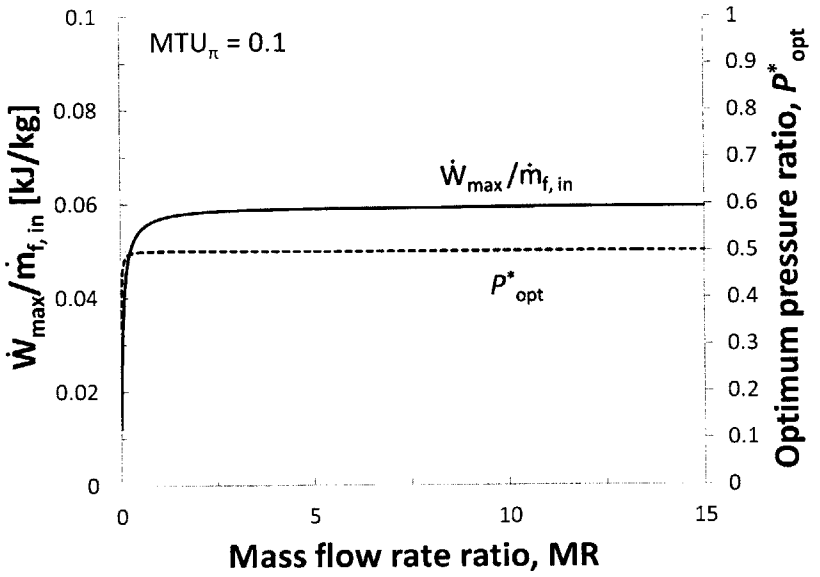

Figure 4-14: Specific maximum power (solid line) and optimum pressure ratio (dashed line) vs. MR at$\text{MTU}_\pi = 0.1$ for a one-dimensional, counterflow PRO membrane.

The optimum pressure ratio, P^*_{opt}, is found by using the quadratic approximations numerical optimization method in Engineering Equation Solver [48]. By substituting the optimum pressure ratio into Eq. (4.76), the maximum specific power, $\dot{W}_{\text{max}}/\dot{m}_{\text{f, in}}$, can be determined. Figures 4-14 through 4-16 show the maximum specific power rising to an asymptotic value as MR increases from 0.1 to 15. These figures also show the optimum pressure ratio deviating from the zero-dimensional limit of one-half as MR varies. The deviation from the zero-dimensional limit increases as MTU_π increases.

The global maximum specific power achievable for a combination of seawater and river water is found when MR approaches infinity and MTU_π is increased to where the effectiveness of the exchanger is unity. This global maximum specific power is determined to be 1.57 kJ/kg, which is not much greater than what is shown in Fig. 4-16. Dividing the global maximum specific power by the maximum reversible power of complete mixing, $\dot{W}^{\text{rev}}_{\text{complete}}/\dot{m}_{\text{f, in}} = 2.44$ kJ/kg, yields a Second Law efficiency of 64.48%. This is a high value because the one-dimensional power values achieved in

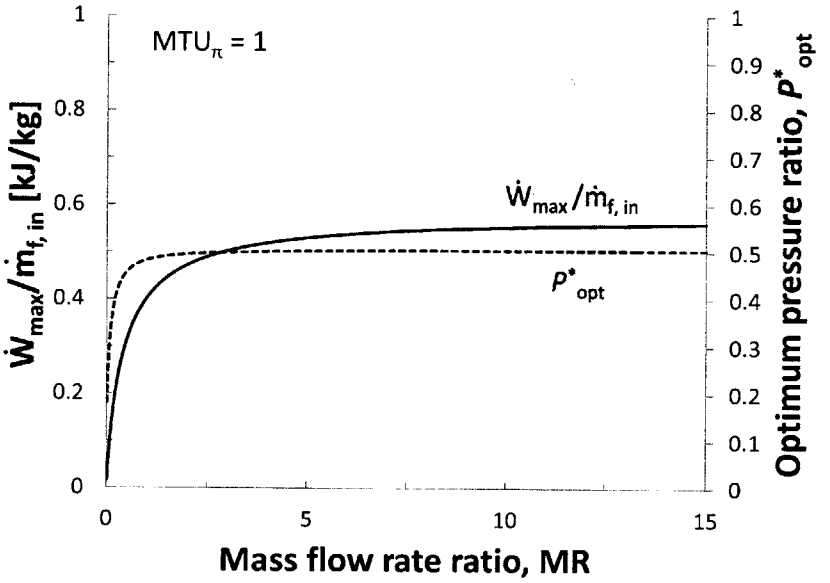

Figure 4-15: Specific maximum power (solid line) and optimum pressure ratio (dashed line) vs. MR at $\text{MTU}_\pi = 1$ for a one-dimensional, counterflow PRO membrane.

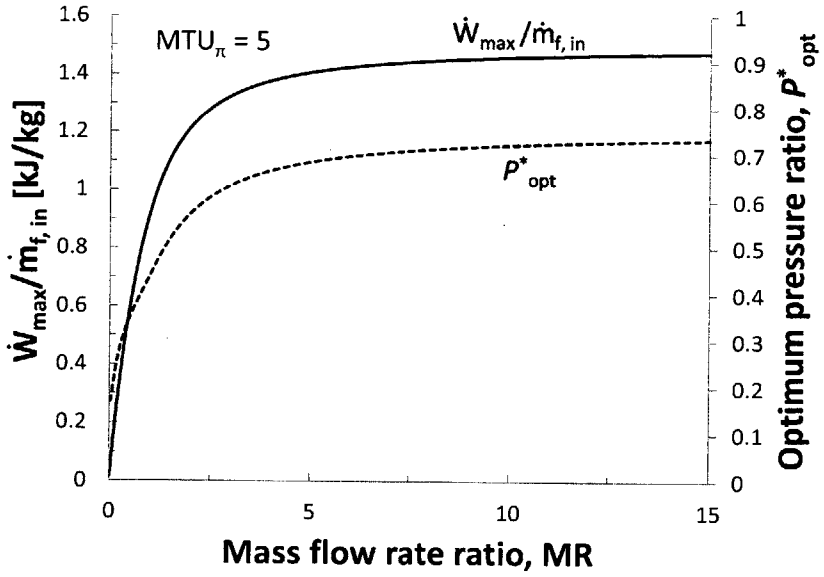

Figure 4-16: Specific maximum power (solid line) and optimum pressure ratio (dashed line) vs. MR at $\text{MTU}_\pi = 5$ for a one-dimensional, counterflow PRO membrane.

this section assume an ideal membrane with no concentration polarization and no salt permeation. The addition of concentration polarization and salt permeation into the transport model will effectively add resistances to mass transfer. To first order, the effect of concentration polarization can significantly decrease the amount of permeate flux achievable, and therefore the power which can be produced. This analysis is still useful, however, in that the values determined here provide important upper limits for power performance.

4.7 Conclusions

The important conclusions from this chapter are as follow:

1. The analogy between osmotic mass exchangers and heat exchangers allows for effectiveness versus mass transfer units expressions to be developed. These expressions function in a similar way to the ε-NTU expressions used to size and rate heat exchangers. The expressions, developed in the previous chapter of this work, can be modified to facilitate the analysis of the upper limits of flux and power performance for FO and PRO membrane mass exchangers.

2. A new dimensionless group, the pressure ratio P^*, is presented which represents a balance of trans-membrane hydraulic to osmotic driving potentials. This dimensionless group conveniently varies between zero and unity which spans the range of operation for a PRO exchanger.

3. The maximum reversible power available to a salinity gradient engine occurs during complete mixing of streams and limits to 2.44 kJ/kg of feed for representative seawater and river water salinities of 35 and 1.5 g/kg. An incomplete mixing case was also investigated for the reversible salinity gradient engine.

4. For a one-dimensional osmotic mass exchanger used in a PRO system, the zero-

dimensional theory that the maximum power available occurs at a hydraulic pressure difference equal to exactly one-half of the osmotic pressure difference is shown to be an idealization which is only valid for membranes with a small MTU_π, effectively small membrane areas. As the size of the membrane increases, significant deviations from this one-half value result and are quantified in this chapter.

5. A global maximum power per unit of feed flow rate exists for a one-dimensional PRO system given the salinities of the two inlet streams. This value is found where the MTU_π increases until the effectiveness of the exchanger is equal to unity and the mass flow rate ratio increases to infinity. For a combination of seawater and river water, this value is 1.57 kJ/kg. Dividing this value by the reversible power of complete mixing, a Second Law efficiency of nearly 64.5% is realized. This is an optimistic upper bound which will decrease as a result of concentration polarization, salt permeation, and pressure drop.

Chapter 5

Use of PRO Membranes as Energy Recovery Devices

Chapter abstract

Thermodynamic analysis is applied to assess the energy efficiency of hybrid desalination cycles that are driven by simultaneous mixed inputs, including heat, electrical power, and chemical energy. A seawater desalination cycle using power and a chemical input stream is analyzed using seawater properties. Two system models, a reversible separator and an irreversible component based model, are developed to find the least power required to operate the system with and without osmotic recovery. The component based model represents a proposed desalination system which uses a reverse osmosis membrane for solute separation, a pressure exchanger for recovering a fraction of the mechanical energy associated with the pressurized discharge brine, and a pressure retarded osmosis (PRO) module for recovering some of the chemical energy contained within the concentrated discharge brine. The energy attained by the addition of the chemical input stream serves to lower the amount of electrical power required for operation. For this analysis, a wastewater stream of varying solute concentration, ranging from feed to brackish water salinity, is considered as the chemical stream. Unlike other models available in the literature, the PRO exchanger is numerically simulated as a mass exchanger of given size which accounts for changing stream concentration, and consequently, stream-wise variations of osmotic pressure throughout the length of the unit. A parametric study is performed on the models by varying input conditions. For the reversible case it is found that significant power reductions can be made through the use of an energy recovery device when the inlet wastewater salinity used is less than the feed salinity of 35 g/kg. For the irreversible case with

a typical recovery ratio and feed salinity, significant power reductions are only noted for wastewater inlet salinities of less than 20 g/kg due to pumping power losses. In the irreversible case, the use of a numerical model to simulate the PRO exchanger results in a maximum power reduction when the pressure difference between streams was around one half of the osmotic pressure difference as opposed to the precise value of one half found in zero-dimensional exchanger models.

5.1 Introduction

As fresh water resources are strained, the world is increasingly turning to saline water sources to meet water demands. Both membrane and thermal technologies are commercially available for desalinating saline water sources, but a concern surrounding their implementation is the high energy cost associated with separation. As a result of a variety of technological improvements, such as the development of the pressure exchanger and falling membrane costs, reverse osmosis (RO) separation is currently the most widely used method for desalination [3]. In an effort to make RO more viable, an energy recovery device (ERD) has been proposed [64] to reduce the amount of electrical power required for operation.

All desalination systems discharge a concentrated brine with a higher salinity than the feed stream. By virtue of its composition, the brine stream has a higher Gibbs free energy than the feed and can be used to recover chemical energy if it is not immediately rejected to the environment. The proposed energy recovery device is a type of forward osmosis exchanger (FO), called a pressure retarded osmosis (PRO) mass exchanger, integrated with a pressure exchanger. The device can be used when a chemical stream with a lower total dissolved solids than the discharge brine is available. The chemical stream could be the feed stream water or another source such as wastewater. In certain cases, it may be more advantageous to simply purify and treat the wastewater source instead of desalinating the more saline stream. This study, however, assumes that the wastewater is only used to recover energy for the

desalination process. This might represent a case where policy does not allow for the human consumption of treated wastewater.

Current literature in the area of FO is generally between studies of desalination [64–68] and studies of power production [4, 28, 34, 47, 49, 54, 56–58, 69–71]. Forward osmosis based power production is often referred to as pressure retarded osmosis (PRO) and it is currently receiving significant attention in the literature.

This chapter explores two perspectives of the ERD. First, we will use control volume thermodynamic analysis on two reversible separators, one with and the other without energy recovery, in order to determine the theoretical least power required for operation. Second, we use thermodynamic analysis to determine the power required for a model of two systems with irreversible components. The first irreversible system is a single pass RO system with a pressure exchanger and the second is the same plant integrated with a PRO-based ERD.

For the reversible case it is found that significant power reductions can be made through the use of an ERD when the inlet wastewater salinity used is lower than the feed salinity of 35 g/kg. For the irreversible case, early results suggested a wastewater turbine is a necessary component for maximum power recovery. For the irreversible case with a recovery ratio of 0.5 and a feed salinity of 35 g/kg, significant power reductions were only noted for a wastewater inlet of less than 20 g/kg due to pumping power losses. In the irreversible case, the use of a numerical model to simulate the PRO exchanger resulted in a maximum power reduction when the pressure difference between streams was around one half of the osmotic pressure difference as opposed to the precise value of one half found in zero-dimensional exchanger models [4, 28, 54, 71].

5.2 Thermodynamic analysis of reversible separation

Two reversible separators are shown in Fig. 5-1. Both systems represent black box processes that reversibly separate an incoming feed stream of saline water into a product stream of low salinity and a concentrated brine stream. The mass flow rates, denoted by $\dot{m}$, are in units of kilogram of solution per second. The control volume displayed in Fig. 5-1a, the reversible separator without recovery, was studied by [59] and represents a typical desalination process. This system is referred to as system A. As shown, system A rejects a concentrated brine stream which contains a higher salt concentration, and thus has a higher Gibbs free energy, than the feed stream. The difference in Gibbs energy is related to a difference in osmotic pressure and can be used to drive a mass flux of water from the less saline to the more saline stream when the streams are separated by a semi-permeable membrane. This additional mass flow can be converted into useful power using a turbine or used to create power transfer in a pressure exchanger. The difference in Gibbs energy is also related to a difference in chemical energy which could be converted into useful power by using a reverse electro-dialysis process [57].

The control volume displayed in Fig. 5-1b, referred to as system B, uses system A to separate the feed stream into a product and brine stream, and then uses a reversible energy recovery device to recover power. The reversible energy recovery device considered here is identical to the salinity gradient engine considered in Section 4.5. System B recovers power by taking in a chemical stream and rejecting a diluted brine stream. In the cases considered in this chapter, the chemical stream is a low salinity water stream, such as might result from wastewater after secondary treatment. The wastewater stream enters the reversible ERD at a certain salinity, transfers an amount of water into the brine stream, and exits at an increased con-

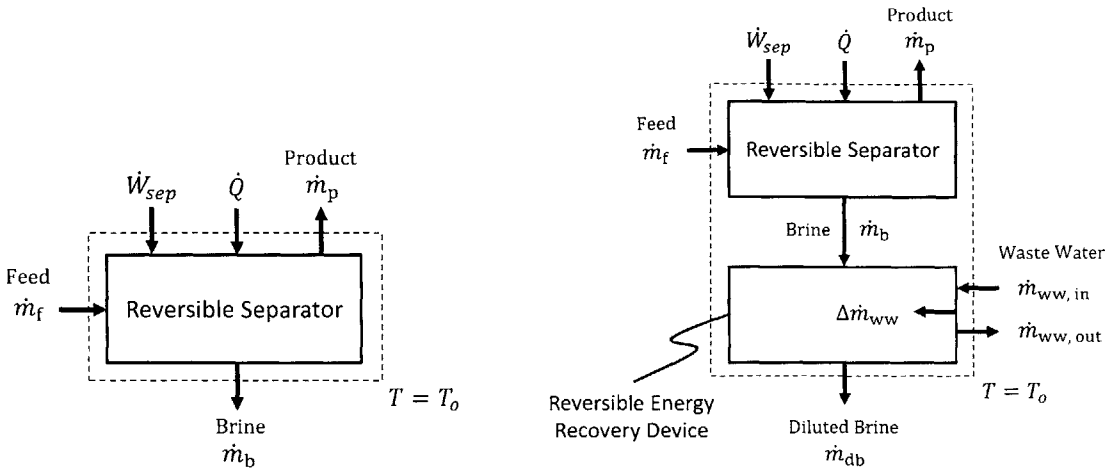

(a) System A (b) System B

Figure 5-1: Schematic diagram of a reversible separator without and with a reversible energy recovery device.

centration. The wastewater inlet stream must have a salinity less than the salinity of the brine stream if power is to be recovered. This chapter will only consider the case where the wastewater that exits the ERD has the total mass flow rate of salts as the incoming wastewater. This means that the wastewater which dilutes the brine stream is pure water with zero salinity which implies perfect salt rejection by the PRO module.

5.2.1 Governing equations

To find the maximum reduction of power that can be attained by the reversible energy recovery device, a control volume analysis is performed on systems A and B.

Least power formulation

The First and Second Laws of Thermodynamics are given in Eqs. (5.1) and (5.2) for an open, steady state, power-consuming system in thermal equilibrium with its environment where changes in the kinetic and gravitational potential energy of each stream

are neglected. The heat transfer into each system is at the ambient temperature.

$$0 = \dot{Q} + \dot{W}_{\text{sep}} + \sum_{\text{in}} \dot{m}h - \sum_{\text{out}} \dot{m}h \tag{5.1}$$

$$0 = \frac{\dot{Q}}{T_0} + \sum_{\text{in}} \dot{m}s - \sum_{\text{out}} \dot{m}s + \dot{S}_{\text{gen}} \tag{5.2}$$

We multiply Eq. (5.2) by T_0 and subtract it from Eq. (5.1) to attain an expression for the power of separation, Eq. (5.3).

$$\dot{W}_{\text{sep}} = \sum_{\text{out-in}} \dot{m}h - T_0 \sum_{\text{out-in}} \dot{m}s + T_0 \dot{S}_{\text{gen}} \tag{5.3}$$

For a reversible system, $\dot{S}_{\text{gen}} = 0$, and Eq. (5.3) becomes Eq. (5.4).

$$\dot{W}_{\text{least}} \equiv \dot{W}_{\text{sep}}^{\text{rev}} = \sum_{\text{out-in}} \dot{m}h - T_0 \sum_{\text{out-in}} \dot{m}s \tag{5.4}$$

If we assume for simplicity that all streams entering and exiting the control volume are isothermal at the environment temperature, then the energy balance given in Eq. (5.4) becomes a Gibbs free energy ($g \equiv h - Ts$) balance as given in Eq. (5.5).

$$\dot{W}_{\text{least}} = \sum_{\text{out}} \dot{m}g - \sum_{\text{in}} \dot{m}g \tag{5.5}$$

Conservation of mass

For both separator models, conservation of mass must be satisfied. Solution and salt balances for system A are given in Eqs. (5.6) and (5.7). Here we define w as the mass fraction of salt in units of grams of solute per kilogram of solution (parts per thousand).

$$\dot{m}_{\text{f}} = \dot{m}_{\text{p}} + \dot{m}_{\text{b}} \tag{5.6}$$

$$\dot{m}_{\text{f}} w_{\text{f}} = \dot{m}_{\text{p}} w_{\text{p}} + \dot{m}_{\text{b}} w_{\text{b}} \tag{5.7}$$

Equations (5.6) and (5.7) still apply for system B along with additional balance expressions for the streams interacting with the control volume around the reversible energy recovery device given in Eqs. (5.8)–(5.10).

$$\dot{m}_{\mathrm{b}} + \dot{m}_{\mathrm{ww,\,in}} = \dot{m}_{\mathrm{db}} + \dot{m}_{\mathrm{ww,\,out}} \tag{5.8}$$

Two salt balances are required for the brine and the wastewater streams because the salt is conserved in both streams.

$$\dot{m}_{\mathrm{b}} w_{\mathrm{b}} = \dot{m}_{\mathrm{db}} w_{\mathrm{db}} \tag{5.9}$$

$$\dot{m}_{\mathrm{ww,\,in}} w_{\mathrm{ww,\,in}} = \dot{m}_{\mathrm{ww,\,out}} w_{\mathrm{ww,\,out}} \tag{5.10}$$

Dimensionless parameters

Equations (5.11)–(5.13) present three dimensionless parameters used for analysis: recovery ratio, RR; permeation ratio, PR; and a mass flow rate ratio, MR. These parameters were introduced and used in earlier chapters, but will be reintroduced here. The first dimensionless parameter, recovery ratio, is defined for the reversible separator as the ratio of product mass flow rate to that of the feed.

$$\mathrm{RR} \equiv \frac{\dot{m}_{\mathrm{p}}}{\dot{m}_{\mathrm{f}}} \tag{5.11}$$

This parameter is greater than zero, and limited to some value less than one to avoid scaling or precipitation in the RO unit.

The second dimensionless parameter, permeation ratio, is defined for the ERD as the ratio of the permeate wastewater to the inlet wastewater stream mass flow rate.

$$\mathrm{PR} \equiv \frac{\dot{m}_{\mathrm{ww,\,in}} - \dot{m}_{\mathrm{ww,\,out}}}{\dot{m}_{\mathrm{ww,\,in}}} = \frac{\Delta \dot{m}_{\mathrm{ww}}}{\dot{m}_{\mathrm{ww,\,in}}} \tag{5.12}$$

Where $\Delta \dot{m}_{\mathrm{ww}}$ is the water from the inlet wastewater which dilutes the brine stream.

The permeation ratio is greater than or equal to zero. It will be less than one to avoid salt precipitation in the PRO unit.

The final parameter, MR, represents the ratio of brine entering the ERD to the inlet wastewater mass flow rate.

$$\mathrm{MR} \equiv \frac{\dot{m}_{\mathrm{b}}}{\dot{m}_{\mathrm{ww,\,in}}} \tag{5.13}$$

5.2.2 Expressions for least power

Following Eq. (5.5) and using the solution balances from Eqs. (5.6) and (5.8), we may now express the least amount of power per unit of product water for both systems in terms of the dimensionless parameters RR, PR, and MR. For system A,

$$\frac{\dot{W}_{\mathrm{least,\,A}}}{\dot{m}_{\mathrm{p}}} = \left(\frac{1}{\mathrm{RR}} - 1\right) g_{\mathrm{b}} + g_{\mathrm{p}} - \frac{1}{\mathrm{RR}}\, g_{\mathrm{f}} \tag{5.14}$$

For system B,

$$\begin{aligned}\frac{\dot{W}_{\mathrm{least,\,B}}}{\dot{m}_{\mathrm{p}}} = {} & \frac{1}{\mathrm{MR}}\left(\frac{1}{\mathrm{RR}} - 1\right)\left[(1-\mathrm{PR})(g_{\mathrm{ww,\,out}} - g_{\mathrm{db}}) + g_{\mathrm{db}} - g_{\mathrm{ww,\,in}}\right] \\ & + \left(\frac{1}{\mathrm{RR}} - 1\right) g_{\mathrm{db}} + g_{\mathrm{p}} - \frac{1}{\mathrm{RR}}\, g_{\mathrm{f}}\end{aligned} \tag{5.15}$$

We define the reversible recovered power as the difference between the least power for system A and system B in Eq. (5.16).

$$\frac{\Delta \dot{W}_{\mathrm{rev}}}{\dot{m}_{\mathrm{p}}} = \frac{\dot{W}_{\mathrm{least,\,A}}}{\dot{m}_{\mathrm{p}}} - \frac{\dot{W}_{\mathrm{least,\,B}}}{\dot{m}_{\mathrm{p}}} \tag{5.16}$$

A reversible recovered power of greater than zero means that the ERD is advantageous for power recovery. If the reversible recovered power is greater than the least power of system A, this means that system B is producing excess power than what is required

to separate the feed stream into product and brine.

Limits of permeation ratio

We now briefly discuss the limits of PR and their effect on the least power of separation with recovery. In the limit of PR equals to zero, system B functions exactly as system A because no wastewater is being used to dilute the brine stream. This can be shown mathematically by substituting PR = 0 into Eq. (5.15) and recognizing that $g_{\mathrm{ww,\,in}} = g_{\mathrm{ww,\,out}}$ and $g_{\mathrm{db}} = g_{\mathrm{b}}$ when PR = 0.

In the other limit, PR can only equal one when the salinity of the incoming wastewater is zero. When saline wastewater is used, PR cannot equal one because of the constraint that the leaving waste stream should not be so concentrated that salt precipitation could occur. It is for this reason that we do not consider a specific maximum PR in our analysis.

Reversible model inputs

For simulation of the reversible model, we consider a system with a recovery ratio of 0.5. This will allow for a clear comparison of power with the irreversible system which is also operated at a recovery ratio of 0.5. The specific Gibbs free energy of each stream is evaluated using a seawater property package developed by Sharqawy et al. [63]. The seawater package allows for thermophysical properties of a stream to be evaluated as a function of temperature and salinity and is applicable for temperatures of 0–120°C and salinities of 0–120 g/kg.

5.2.3 Reversible model results and discussion

We now plot Eq. (5.16) with the inputs listed in Table 5.1. Each plot in Figs. 5-2a – 5-2d shows the reversible recovered power per kilogram of product water as a function of PR and several values of MR. Four plots are given for wastewater salinities ranging

Table 5.1: Reversible model inputs

Input	Symbol	Value / Range
Ambient temperature	T_0	25 °C
Ambient pressure	P_0	1 bar
Feed mass flow rate	$\dot{m}_f$	1 kg/s
Feed salinity	w_f	35 g/kg
Product salinity	w_p	0 g/kg
Recovery ratio	RR	0.5
Mass flow rate ratio	MR	0.2, 0.4, ..., 4.0
Permeation ratio	PR	$0 \rightarrow$ max
Inlet wastewater salinity	$w_{ww,\,in}$	$35 \rightarrow 1.5$ g/kg

from 1.5 to 35 g/kg. For a recovery ratio of 0.5, the specific least power of system A alone is 3.93 kJ per kilogram of product water.

The reversible recovered power plots show that in the reversible case, considerable reductions in the power required can be achieved for the range of MR plotted. Each successive figure allows for higher permeation ratios to be used because for lower salinities of inlet wastewater, the permeation ratio can approach one. The maximum PR displayed corresponds to a wastewater outlet salinity of nearly 120 g/kg which is the salinity limit for a stream in the seawater property package used.

Several conclusions can be drawn by comparing the figures. As expected, a lower inlet wastewater salinity will allow for larger reductions in least power. We can also note that reversible recovered power increases for decreasing MR. As PR decreases to zero, the reversible recovered power approaches zero; meaning that the system B power is equal to the system A power as less water is extracted from the wastewater stream. An optimum permeation ratio exists for each MR contour. This is because a there is a trade-off between diluting the brine stream coming into the reversible ERD at the expense of rejecting a more highly concentrated wastewater stream. The optimum permeation ratio appears to increase for decreasing inlet wastewater salinities. This is because at higher inlet wastewater salinities, a high PR will reject

a highly concentrated wastewater stream, penalizing the attainable power reduction.

It can also be seen in Figs. 5-2c and 5-2d that the reversible ERD in system B is capable of producing excess power than what is required to separate the feed stream for lower values of MR. This is evident by noting that certain contours of MR result in recovered reversible power values above 3.93 kJ/kg, the least power of separation for system A. For a wastewater salinity of 1.5 g/kg, the largest power recovery of 7.84 kJ/kg can be achieved at the local optimum permeation ratio of 0.88 and MR = 0.2. This means that system B produces $7.84 - 3.93 = 3.91$ kJ of power for each kilogram of product water separated from the feed source. For the case in which seawater is used as a wastewater energy recovery stream, Figure 5-2a shows that the maximum recovered power is 0.94 kJ/kg. This corresponds to a least power of 2.99 kJ/kg for system B, which is a 24% reduction in the reversible power of separation.

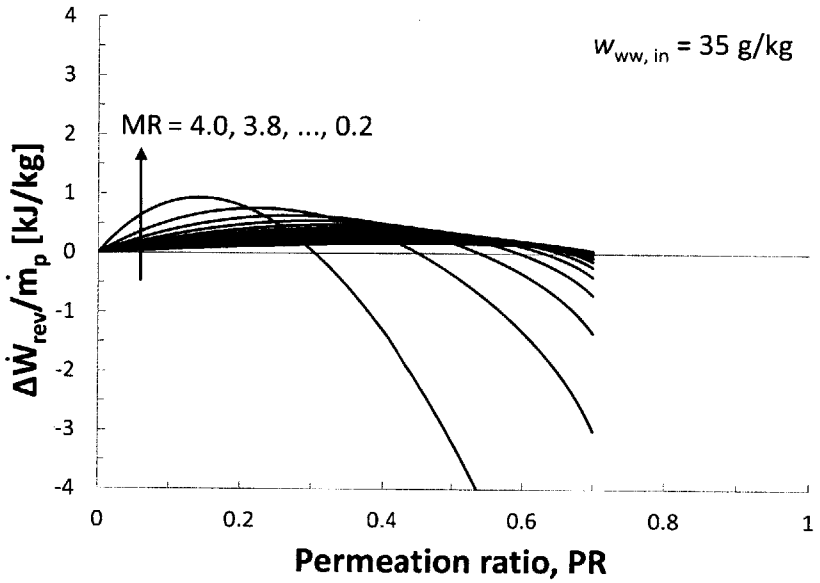

(a)

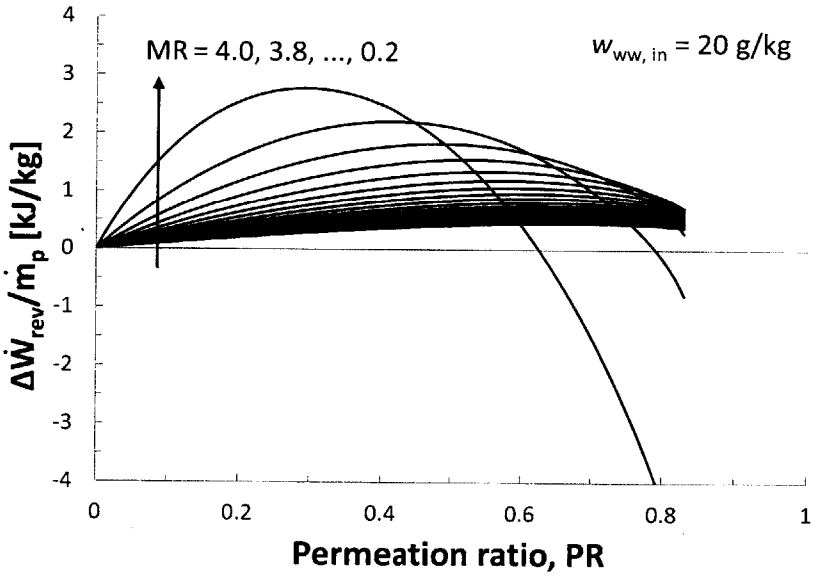

(b)

Figure 5-2: Reversible recovered power vs. permeation ratio for varying MR and wastewater salinity at a separation recovery ratio of 0.5.

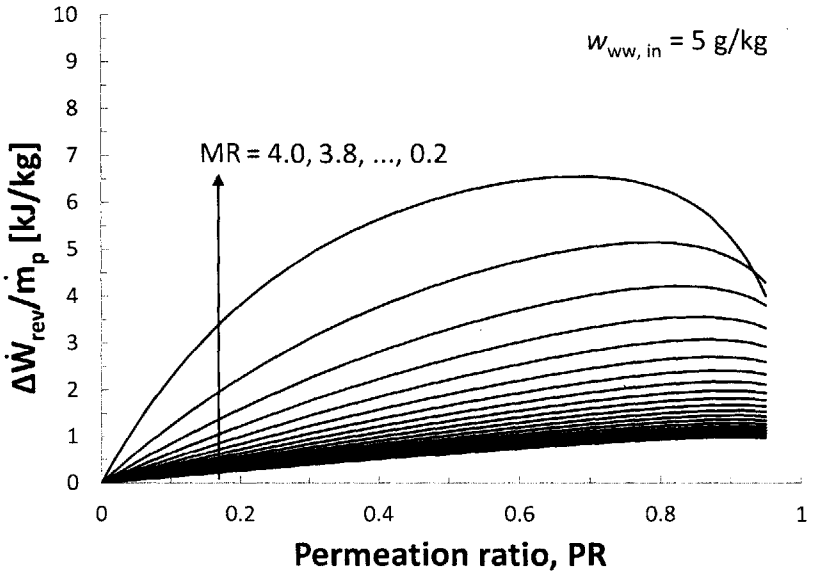

(c)

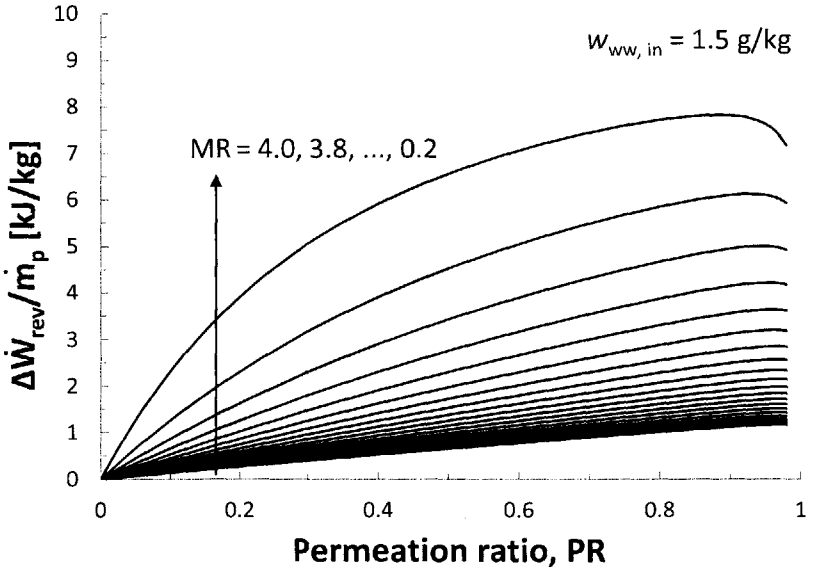

(d)

Figure 5-2: Reversible recovered power vs. permeation ratio for varying MR and wastewater salinity at a separation recovery ratio of 0.5.

5.3 Thermodynamic analysis of irreversible separation

To determine how much power is recovered through use of the ERD integrated with an RO system, we must first find the power required for the irreversible RO system without energy recovery. We then combine the system with an additional pump, a PRO-based mass exchanger for energy recovery, and a turbine to recover a fraction of the wastewater pumping losses. The RO system with a PRO mass exchanger and pump comprise a system proposed in literature [72]. A wastewater turbine was added to the present model after early analyses pointed to excessive, recoverable losses in the wastewater pump.

The governing equations used for analysis of the system performance are given after the system descriptions.

5.3.1 Reverse osmosis system with pressure exchanger

A typical single pass seawater RO system with a pressure exchanger (PX) is displayed in Fig. 5-3a. In this system, denoted as system A, a feed stream of seawater at a given salinity is initially pumped to a pressure of 2 bar by pump P1. The feed is then split into two streams. One stream is pre-pressurized by the PX and the other is sent to a high pressure pump, P2, where it is brought to the top pressure of 64.8 bar required for operation of the cross-flow RO exchanger. The stream exiting the PX is pressurized to an intermediate pressure of 60.5 bar and is pumped to 64.8 bar by pump P3 after which it joins the high pressure stream exiting pump P2. The full mass flow is now sent through the RO where a fraction permeates through the membrane to become product water at the environment pressure of 1 bar. The remaining mass exits the RO module at a higher salinity than the feed stream and at a slightly lower pressure, 63.5 bar, due to viscous losses within the exchanger. The full amount of pressurized

brine is finally sent through the PX before being rejected to the environment. The PX is designed to allow two streams with the same volume flow rate to enter and exit. Conditions selected for this model RO system are representative of an actual large scale RO plant [59, 73].

5.3.2 Modified system with PRO exchanger

A modified version of the schematic diagram of Fig. 5-3a is shown in Fig. 5-3b. This system now includes a PRO exchanger, a pump (P4), and a turbine (T1) for energy recovery. In this system configuration, the brine stream exiting the RO module enters the PRO module at a high salinity relative to the feed stream. On the opposite side of the PRO membrane, a wastewater stream is pumped to a variable pressure of P_{ww} by pump P4 and runs in a counterflow configuration to the brine stream. Along the length of the PRO exchanger, mass is exchanged. The mass exchanged is pure water which permeates from the wastewater stream through the semi-permeable membrane to the brine stream. The net driving pressure responsible for mass flux results from hydraulic and osmotic pressure differentials in the usual way. The remaining wastewater that exits the PRO unit is depressurized through a turbine, T1, in order to recover a fraction of the pumping power from pump P4. The PRO unit, pump, and turbine comprise the ERD and can potentially reduce the net power into the RO system by increasing the volumetric flow rate entering the PX. As the volumetric flow rate entering the PX increases, the amount of feed water that can be pre-pressurized by the PX increases, thereby reducing the amount of power required by the high pressure pump, P3.

Pressure retarded osmosis exchanger

The PRO exchanger was numerically modeled in Engineering Equation Solver [48] as a finite difference counterflow mass exchanger with N sections of unit width by

a differential length. By testing for the convergence of permeate flow rate through the PRO exchanger for each additional section added, N was determined to be fifty sections.

5.3.3 Governing equations

To evaluate the pumping power associated with pressurizing an incompressible fluid, Eq. (5.17) is used.

$$\dot{W}_{\text{pump}} = \frac{\dot{m}\,(P_{\text{out}} - P_{\text{in}})}{\rho\,\eta_{\text{pump}}} \tag{5.17}$$

The turbine power associated with depressurizing an incompressible fluid is given by Eq. (5.18).

$$\dot{W}_{\text{turb}} = \frac{\dot{m}\,(P_{\text{in}} - P_{\text{out}})\,\eta_{\text{turb}}}{\rho} \tag{5.18}$$

The pressure of the feed stream exiting the pressure exchanger is given by Eq. (5.19), which is derived by equating the power of pressurization of the feed stream to the depressurization of the diluted brine stream [59].

$$P_{\text{f, out}} = P_{\text{f, in}} + \eta_{\text{comp}}\eta_{\text{exp}}\left(\frac{\dot{m}_{\text{db}}\rho_{\text{f}}}{\rho_{\text{db}}\dot{m}_{\text{f}}}\right)(P_{\text{db, in}} - P_0) \tag{5.19}$$

The differential mass flow rate through each section of the exchanger is a function of four parameters: the water permeability coefficient, the differential area of each section, the local difference in osmotic pressure across the membrane, and the local difference in hydraulic pressure across the membrane:

$$d\dot{m}_i = A \times A_{\text{m},\,i}\,(\Delta\pi_i - \Delta P_i) \tag{5.20}$$

Here $A_{\text{m},\,i}$, in units of square meters, is the differential area of each membrane section and is given by the total membrane area of the exchanger, A_{m}, divided by N number of sections, $A_{\text{m},\,i} = A_{\text{m}}/N$. A is defined as the water permeability coefficient, is a

property of the membrane characteristics, and has units of kg/s-m^2-kPa. The local hydraulic and osmotic pressure differences are given by Eqs. (5.21a) and (5.21b):

$$\Delta\pi_i = \pi_{\mathrm{b},\,i} - \pi_{\mathrm{ww},\,i} \tag{5.21a}$$

$$\Delta P_i = P_{\mathrm{b},\,i} - P_{\mathrm{ww},\,i} \tag{5.21b}$$

The differences in osmotic and hydraulic pressures are equal to the brine value of the i^{th} section minus the wastewater value of the i^{th} section. Both differentials have units of pressure in kPa. Equation (5.20) denotes forward osmosis operation, meaning that the permeate flows in the direction of increasing salinity, and requires that $\Delta\pi_i > \Delta P_i$. For a direct FO unit, the hydraulic pressure difference ΔP_i is zero. For RO operation, $\Delta P_i > \Delta\pi_i$. The ERD is PRO-based because this system will operate at a hydraulic pressure difference between FO and RO operation.

The mass of the permeate for each section is calculated, added to the brine stream, and subtracted from the wastewater stream. The salinities for subsequent sections are calculated based on the new water flow rates which will alter the osmotic pressures in each stream. For simplicity, this model does not consider changes in hydraulic pressure along the PRO module.

The total permeate mass in the pressure retarded osmosis exchanger is equal to the sum of the differential mass flow rates through each section, Eq. (5.22).

$$\Delta\dot{m}_{\mathrm{ww}} = \sum_{i=1}^{N} d\dot{m}_i \tag{5.22}$$

Equations (5.23a) and (5.23b) define the net power consumed by the components shown in Figs. 5-3a and 5-3b. Equation (5.23c) presents the difference of the two net powers per kilogram of product water, or the specific recovered power, for assessment of plant performance.

$$\dot{W}_{\text{net, A}} = \dot{W}_{\text{P 1}} + \dot{W}_{\text{P 2}} + \dot{W}_{\text{P 3}} \tag{5.23a}$$

$$\dot{W}_{\text{net, B}} = \dot{W}_{\text{P 1}} + \dot{W}_{\text{P 2}} + \dot{W}_{\text{P 3}} + \dot{W}_{\text{P 4}} - \dot{W}_{\text{T 1}} \tag{5.23b}$$

$$\frac{\Delta \dot{W}}{\dot{m}_{\text{p}}} = \frac{\dot{W}_{\text{net, A}}}{\dot{m}_{\text{p}}} - \frac{\dot{W}_{\text{net, B}}}{\dot{m}_{\text{p}}} \tag{5.23c}$$

A specific recovered power, Eq. (5.23c), of greater than zero results in an advantageous use of the ERD.

Dimensionless parameters for irreversible case

In this section we describe dimensionless parameters that are useful for the irreversible system analysis. From the reversible case, we again use recovery ratio, Eq. (5.11), to govern the streams in the RO module. We also use the dimensionless flow rate of brine to wastewater stream, MR from Eq. (5.13), to define the flow rate of incoming wastewater in the irreversible case simulations.

The pressure ratio, P^*, Eq. (5.24), previously introduced in Sec. 4.2.2, is defined to set the limits of operation for pump 4 in system B as a value between zero and one.

$$P^* \equiv \frac{\Delta P}{\Delta \pi_{\text{max}}} = \frac{P_{\text{b, in}} - P_{\text{ww, in}}}{\pi_{\text{b, in}} - \pi_{\text{ww, in}}} \tag{5.24}$$

By Eq. (5.24), $\Delta P = 0$ when $P^* = 0$ which means that pump 4 pressurizes the wastewater to match the brine stream pressure at 63.5 bar (assuming no hydraulic pressure drop in the PRO module). According to Eq. (5.20) this will maximize the mass flow rate through the PRO exchanger. When $P^* = 1$, pump 4 pressurizes the wastewater stream to the lowest pressure allowable for maintaining forward osmosis operation. A balance between P^* and MR will be required for optimum system performance.

Irreversible model assumptions

In these model simulations we made several assumptions to reduce the problem space. We neglected hydraulic pressure drop in the PRO exchanger and also the presence of internal or external concentration polarization. According to Wilf [62], for typical spiral wound seawater RO membranes, salt rejection rates are about 99.8% with a water permeability coefficient of 1.0 L/hr-m^2-bar. We neglected salt permeation through the PRO membrane because of the high rejection rate. The total membrane area for the PRO exchanger is equivalent to the total RO membrane area required for a single pass seawater RO desalination plant with the same amount of product water, as given by Wilf [62]. Parameter values used for the simulation are listed in Table 5.2. It is also unclear whether current pressure retarded osmosis membranes can withstand the applied hydraulic pressures present in the current model [56]. For the recovery ratio chosen, the mass flow rate of the brine and product streams will be 0.5 kg/s. The density of each stream is evaluated as a function of temperature and salinity using seawater properties developed by Sharqawy et al. [63]. The osmotic pressure of each stream is evaluated using a seawater osmotic pressure model developed in Appendix B.

5.3.4 Irreversible model results and discussion

For the inputs shown in Table 5.2, the net power required for system A is a constant 7.50 kJ per kilogram of product water. The power recovered by the system with recovery, Eq. (5.23c), is plotted against P^* varying between zero and one for a range of MR values in Figs. 5-4a – 5-4d. Each figure corresponds to a value of the wastewater inlet salinity which varies between 35 and 1.5 g/kg.

Figure 5-4a shows that for a wastewater inlet salinity equal to that of the feed stream salinity, at any MR, the addition of the ERD to the RO system is not advantageous. This is because the power required by pump 4 is greater than the power saved

Table 5.2: Irreversible model inputs

Input	Symbol	Value / Range
Ambient temperature	T_0	25 °C
Ambient pressure	P_0	1 bar
Feed mass flow rate	$\dot{m}_f$	1 kg/s
Feed salinity	w_f	35 g/kg
Product salinity	w_p	0 g/kg
Recovery ratio	RR	0.5
Pump efficiency	η_{pump}	90%
Turbine efficiency	η_{turb}	90%
PX compression efficiency	η_{comp}	98%
PX expansion efficiency	η_{exp}	98%
Total PRO membrane area	A_m	128 m^2
Water permeability coefficient	A	2.67×10^{-6} kg/s-m^2-kPa
Mass flow rate ratio	MR	0.2, 0.4, ..., 4.0
Pressure ratio	P^*	$0 \rightarrow 1$
Inlet wastewater salinity	$w_{ww,\,in}$	$35 \rightarrow 1.5$ g/kg

by pumping less feed in pump 2. The conclusion is all the more convincing given that concentration polarization and pressure drop in the pressure retarded osmosis exchanger were not considered in this analysis.

For certain values of MR, the recovered power contours stop for low values of P^*. This end point is termed 'end of operation' and is due to an unacceptably high net driving pressure across the membrane which would result in more permeate flow than provided by the wastewater stream.

For a wastewater inlet salinity of 20 g/kg, in Fig. 5-4b, we begin to see a point at which the ERD is advantageous for P^* values of between 0.2 to 0.85. The concave shape of each MR contour is due to the trade-off associated with a high or low value of P^*. For low P^*, the pump 4 input power increases, but more permeate is allowed through the PRO exchanger. For high values of P^* the opposite is true.

Figure 5-4c clearly shows that for a wastewater salinity of 5 g/kg an optimal value of P^* exists for each MR contour. This optimum point shifts to higher values of

P^* for larger values of MR. Theoretically, as published in literature, the maximum power obtainable by a zero-dimensional (1 section) PRO exchanger used for power production is where $\Delta P = \Delta\pi/2$ [4, 28, 54, 71]. Although it is not entirely analogous (because the system considered in this chapter does not produce power), Fig. 5-4c shows that for a one-dimensional exchanger the optimal pressure is not at half of the maximum osmotic pressure gradient and that it also varies with MR for a fixed inlet wastewater salinity. The greatest recovered power shown in Fig. 5-4c is 1.34 kJ/kg and corresponds to MR = 1.2 and $P^* = 0.42$.

As expected, more power can be recovered for very low values of inlet wastewater salinity as shown in Fig. 5-4d. The greatest recovered power value of 1.71 kJ/kg, shown in the figure, corresponds to MR = 1.2 and also $P^* = 0.42$. This power recovered yields a total system B power of 5.8 kJ/kg and represents a power reduction of about 22.7% which can be significant for large scale plants. Values of MR less than 1.2 do not result in greater recovered power for the input conditions chosen. This highlights the trade-off associated with the choice of MR. For higher MR, the pump 4 power decreases but less permeate can be attained through the exchanger. The opposite is true for lower values of MR.

Figures 5-5a – 5-5d show the variation of recovered power with permeation ratio, as previously shown for the reversible case. In Fig. 5-5a it is once again apparent that for the case in which the inlet wastewater stream and feed stream salinities are 35 g/kg, any value of MR cannot contribute to a system A power reduction. The main reason for the overestimation of power reduction in the reversible case stems from the fact that there is no pump in the reversible case and there is no energy penalty for introducing a large mass flow rate of wastewater into the system. This pumping power penalty can also been seen by the fact that when PR is equal to zero, i.e., when zero wastewater permeates through the forward osmosis membrane, the recovered power does not equal zero as it did in the reversible case. This is because of

the energy penalty associated with pumping the wastewater through the ERD system regardless of whether permeate was attained. Similar to the reversible case, the other figures also exhibit the existence of an optimum PR which increases with decreasing wastewater inlet salinity.

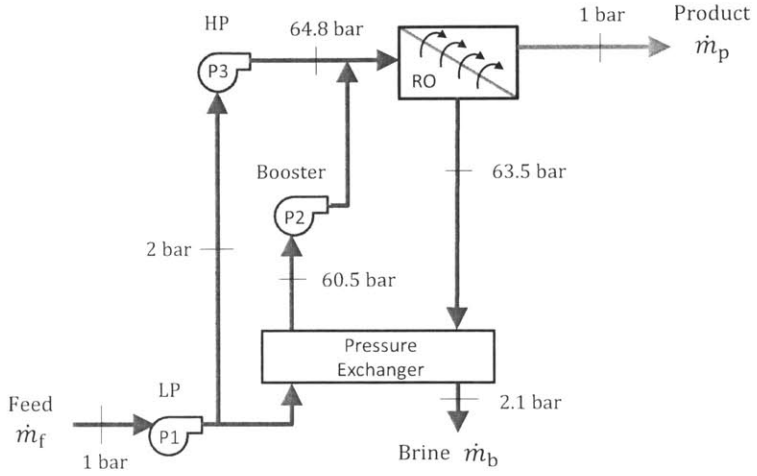

(a) System A

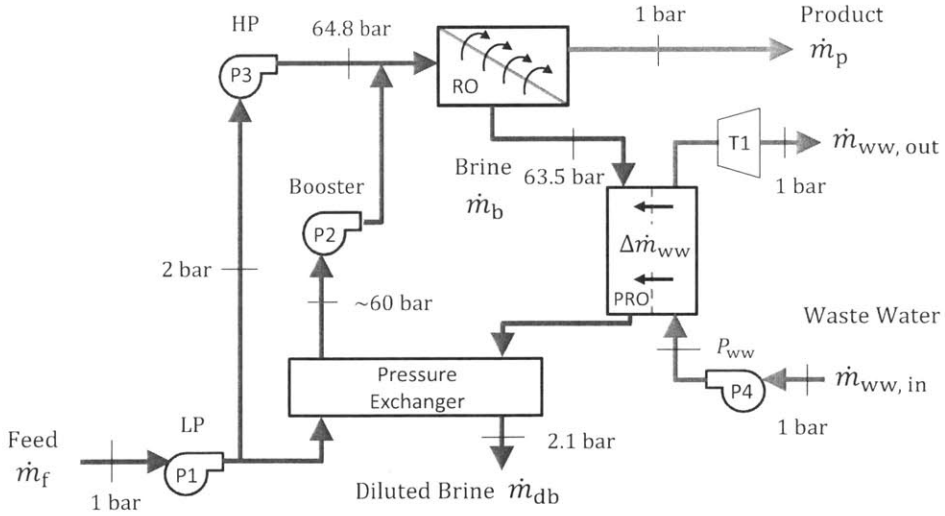

(b) System B

Figure 5-3: Schematic diagram of an irreversible separation system without and with a pressure retarded osmosis based energy recovery device.

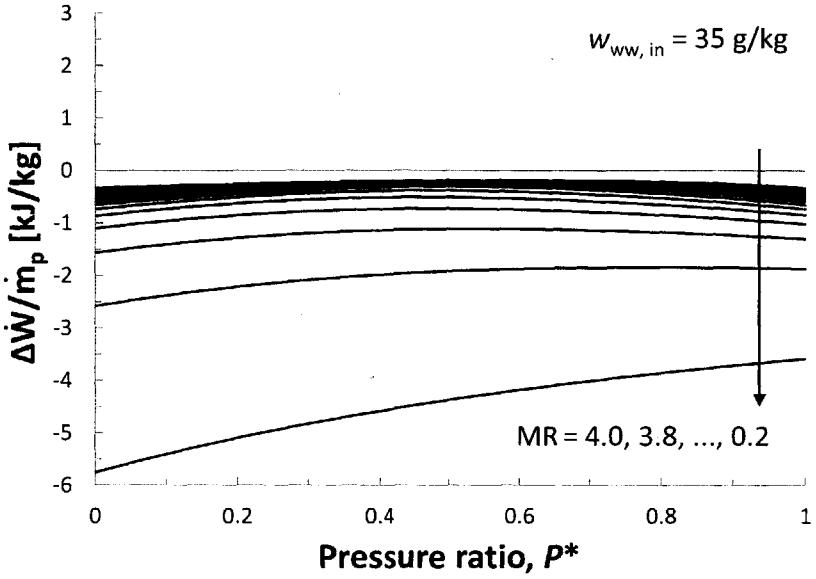

(a)

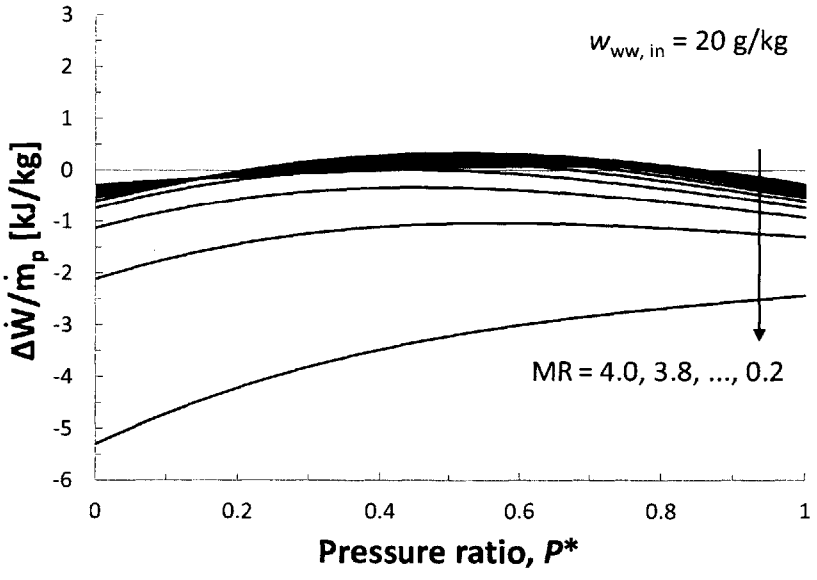

(b)

Figure 5-4: Specific recovered power vs. pressure ratio with contours of MR for a fixed brine inlet salinity and varying wastewater salinity.

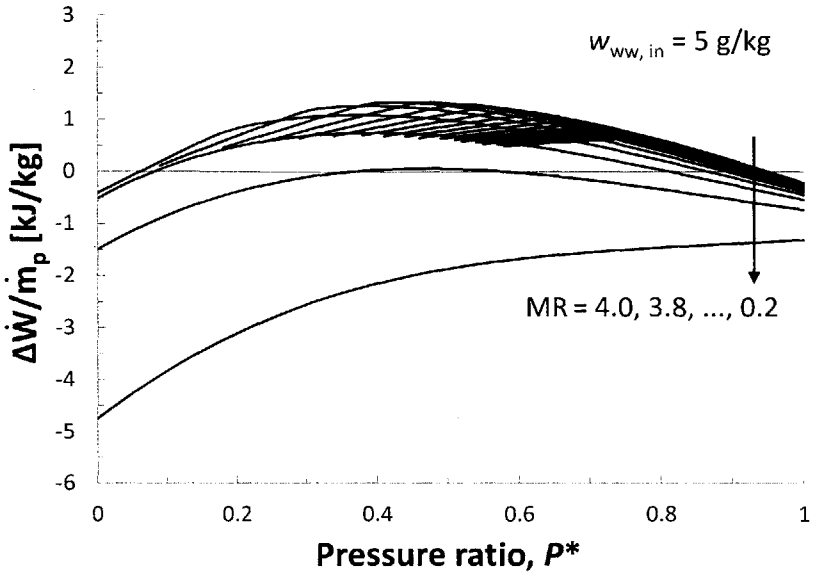

(c)

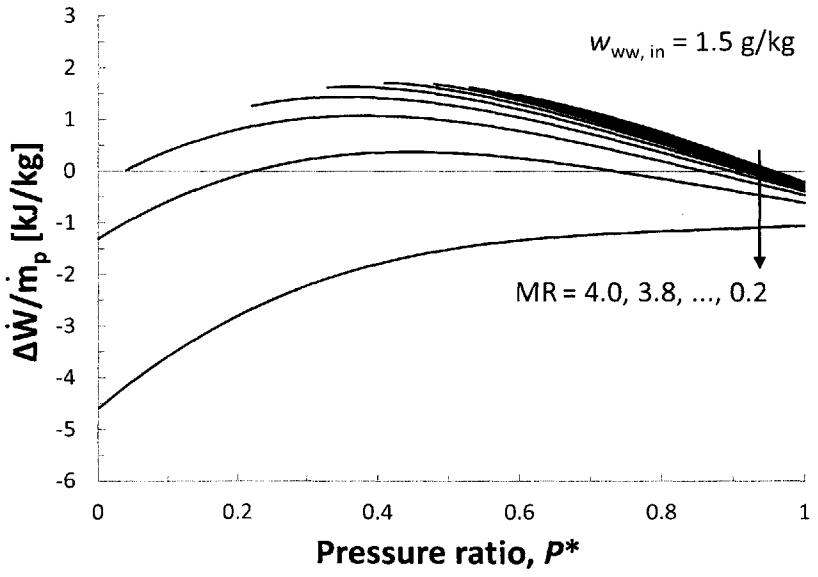

(d)

Figure 5-4: Specific recovered power vs. pressure ratio with contours of MR for a fixed brine inlet salinity and varying wastewater salinity.

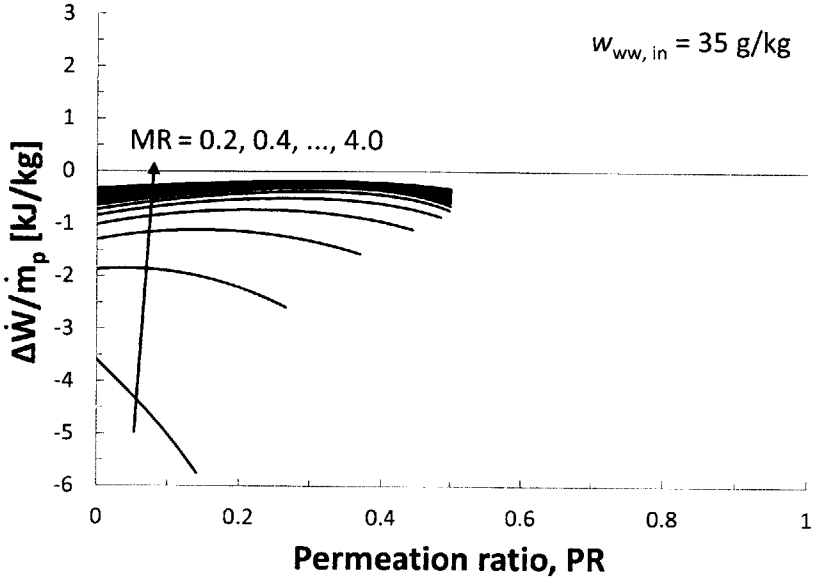

(a)

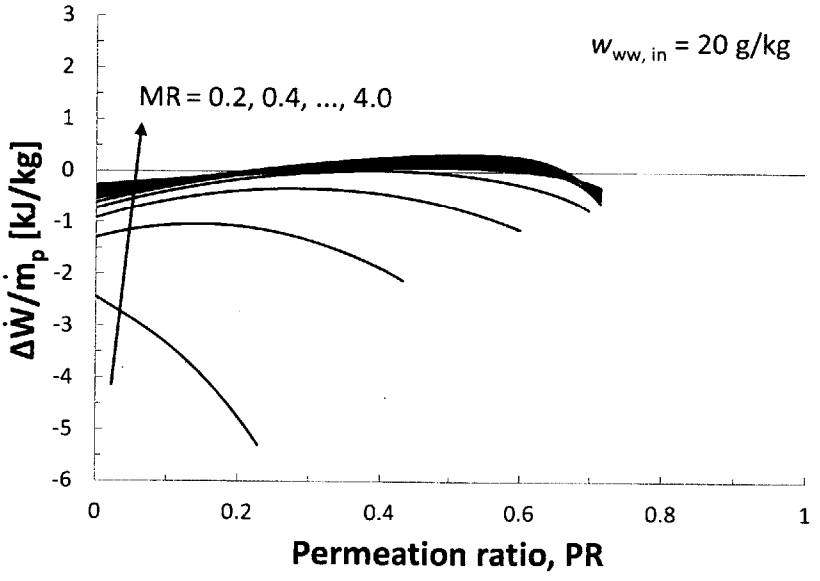

(b)

Figure 5-5: Specific recovered power vs. permeation ratio with contours of MR for a fixed brine inlet salinity and varying wastewater salinity.

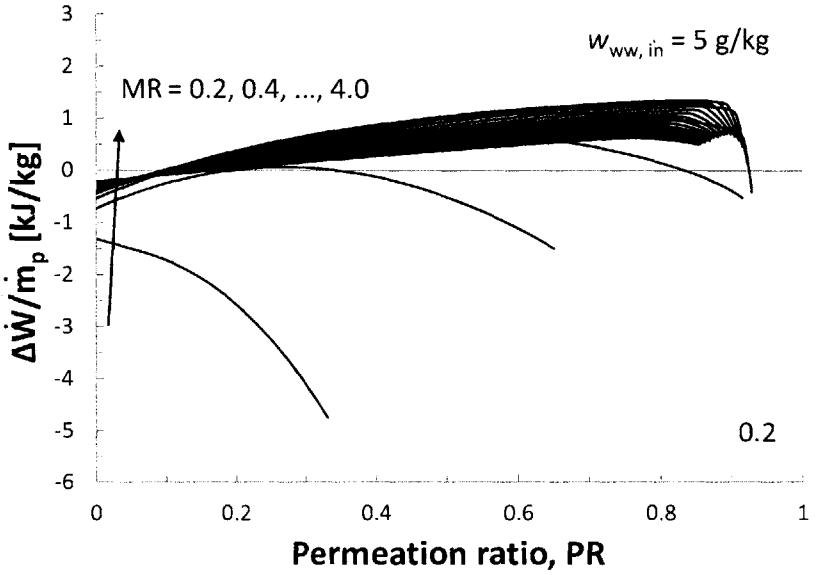

(c)

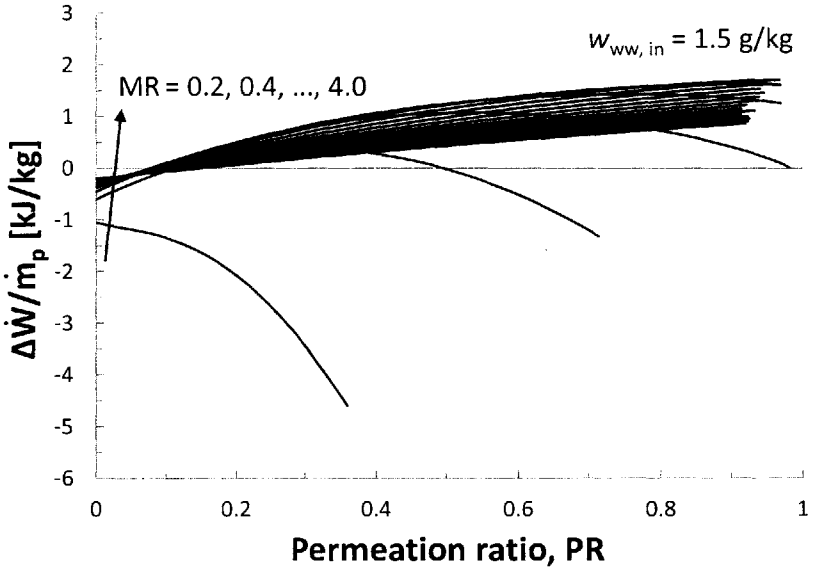

(d)

Figure 5-5: Specific recovered power vs. permeation ratio with contours of MR for a fixed brine inlet salinity and varying wastewater salinity.

5.4 Conclusions

Desalination systems reject a highly concentrated discharge brine which has a higher Gibbs free energy than the feed stream. With a pressure retarded osmosis mass exchanger, a portion of this energy can be recovered to reduce the system's net power of separation. This can be done if an available wastewater stream of a salinity less than that of the rejected brine stream is available.

Expressions were derived to describe the least power of separation for a system without and with a reversible energy recovery device. Along with the recovery ratio, two dimensionless parameters relating the mass flow rates in the reversible energy recovery device, MR, and permeation ratio, PR, were used to assess the performance of a system with energy recovery. In addition to investigating the thermodynamic limits of separation for a reversible system, a simple model of an irreversible component-based system with and without energy recovery was numerically simulated.

The major conclusions of this chapter are as follow:

1. Reversible results suggest that significant power reductions can be made with a salinity gradient engine used as an energy recovery device.

2. For maximum power recovery, a wastewater turbine is recommended to recover a fraction of the energy penalty incurred in pumping the wastewater into the PRO mass exchanger.

3. With reasonable assumptions made regarding the PRO membrane area and characteristics, the irreversible case shows that by using seawater as the feed stream and the wastewater stream, an energy recovery device is not advantageous. This conclusion is made more convincing by recognizing that concentration polarization and pressure drop in the pressure retarded osmosis membrane will further contribute to losses in the system.

4. A wastewater stream with a salinity of less than 20 g/kg is necessary to make the PRO-based energy recovery device advantageous.

5. An optimal hydraulic pressure difference and mass flow rate ratio between streams in the PRO exchanger exists for maximum power reduction. The optimal pressure, contrary to expressions found in the literature, was not found to equal exactly half of the maximum osmotic pressure difference between the streams.

THIS PAGE INTENTIONALLY LEFT BLANK

Appendix A

Modified van 't Hoff Coefficient

The van 't Hoff equation for osmotic pressure [30] applies to dilute, ideal solutions and is given as:

$$\pi \approx iRTc \tag{A.1}$$

where i is the van 't Hoff factor, R is the universal gas constant, T is the absolute temperature, and c is the molarity of the solution with units of mol/m^3. Molarity can be expressed as a function of salinity, the density of the solution, and the molecular weight of the solute in units of g/mol:

$$c = \frac{\rho_{\text{solution}} w}{M_{\text{solute}}} \tag{A.2}$$

Because the van 't Hoff equation assumes a dilute solution, the density in Eq. (A.2) is approximated as that of pure water. Substituting this expression for molarity into the van 't Hoff equation Eq. (A.1), we can now define a modified van 't Hoff coefficient, C, to linearize the osmotic pressure function:

$$\pi \approx \frac{iRT\rho_{\text{pure}}}{M_{\text{solute}}} w = Cw \tag{A.3}$$

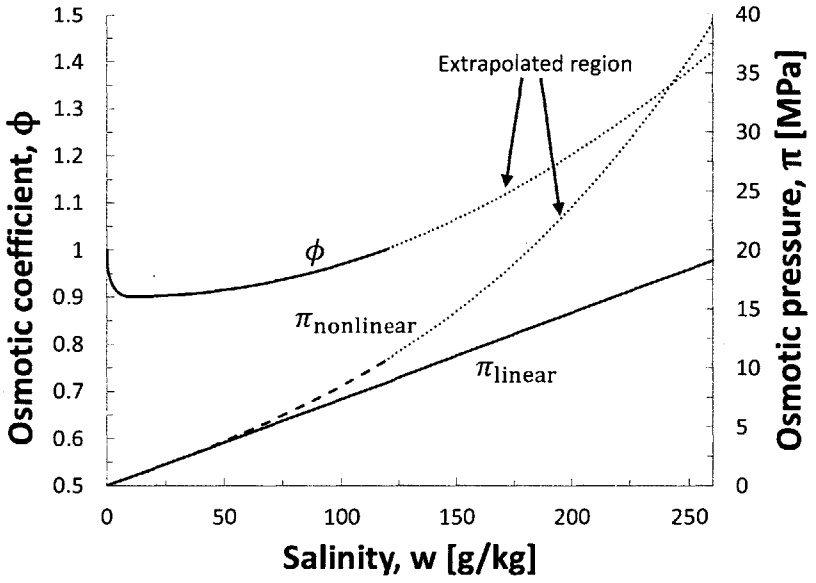

Figure A-1: Seawater osmotic coefficient and osmotic pressures versus salinity at $T = 25°C$ shown as solid and dashed curves. The osmotic coefficient curve and nonlinear osmotic pressure curves are extrapolated for salinities greater than 120 g/kg and these sections are shown as bold dashed lines. The linear osmotic pressure curve is denoted by a solid line.

Using a least squares method for salinities between 0 and 10 g/kg on Fig. A-1, the modified van 't Hoff coefficient (C) is determined to be 73.45 kPa-kg/g at a temperature of 25°C. This linear model represented by Eq. (A.3) can be used for a salinity range of 0 to 70 g/kg, which is the typical range for most desalination applications. For this range, the maximum deviation from the non-linear osmotic pressure function is 6.8%.

For processes in which the salinity of a stream exceeds 70 g/kg, large deviations between the nonlinear and linear osmotic pressure can lead to large errors in performance calculations. These deviations are especially prevalent in seawater reverse osmosis processes with very high recovery ratios as seen in Sec. 2.3.2.

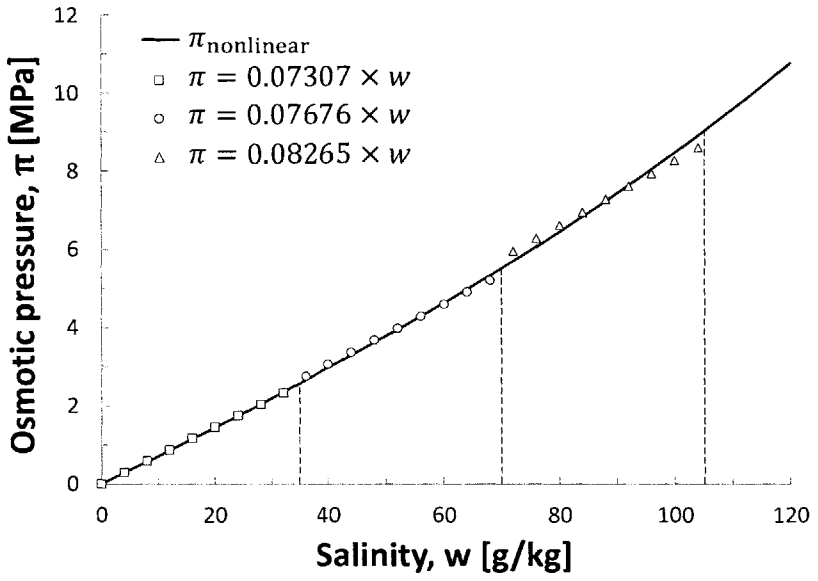

Figure A-2: Seawater osmotic pressure vs. salinity at $T = 25°C$ shown as a solid curve. The points indicate the linear osmotic pressure approximation using varying modified van 't Hoff coefficients.

A.1 van 't Hoff coefficients for various PRO operating conditions

A PRO process may use inlet stream salinities which differ according to the operation required. For power production, seawater and river water may be the PRO input streams, whereas for brine chemical energy recovery, a concentrated brine and seawater may be used. To reduce the errors associated with linearizing the nonlinear osmotic pressure function, salinity ranges of interest are approximated as linear.

The nonlinear osmotic pressure of seawater as a function of salinity in g/kg is shown in Fig. A-2. The modified van 't Hoff coefficient, C, can be determined as the slope of the nonlinear osmotic pressure between specific salinity ranges of interest. The osmotic pressure can be approximated as the product of the modified van 't Hoff coefficient and the salinity of the solution using Eq. (A.3).

Using a best-fit least squares method between the range of 0 and 35 g/kg, the modified van 't Hoff coefficient is determined to be 73.07 kPa-kg/g at a temperature of 25°C. This linear model represented by Eq. (A.3) can be used for a salinity range of 0 to 35 g/kg, which is the typical range for power production at a river delta with a PRO exchanger. For salinities between 35 and 70 g/kg, the modified van 't Hoff coefficient is determined to be 76.76 kPa-kg/g which is the typical range for power production using seawater and disposed brine from a seawater desalination plant. For salinities between 70 and 105 g/kg, the modified van 't Hoff coefficient is determined to be 82.65 kPa-kg/g.

Appendix B

Determination of the Osmotic Pressure Function

From Robinson and Stokes [30, chap. 2], the osmotic pressure for a solution composed of multiple solutes can be written as:

$$\pi = \phi(RT\rho_{\text{solvent}}) \sum_{j=\text{solutes}} b_j \tag{B.1}$$

where ϕ is the osmotic coefficient; R is the universal gas constant; T is the absolute temperature; ρ_{solvent} is the density of pure water; and b_j is the molality of the j^{th} solute in the solution. The molality of a solution with multiple solutes is equal to the sum of the molality of each solute. The molality of a solution written as a function of salinity is given by

$$\sum_{j=\text{solutes}} b_j = \frac{1}{(1000 - w)} \sum_j \frac{w_j}{M_j} \tag{B.2}$$

where w is the salinity of the solution, w_j is the salinity of the j^{th} solute, and M_j is the molecular weight of the j^{th} solute with units of kg/mol. A table of seawater constituents, which we will call a recipe, was found in Millero and Leung [74] where

the salinity for each solute of seawater, w_j, is given for a solution of a fixed salinity, w. To use the recipe, we note that w_j can be scaled with a solution of variable salinity, w, by the following expression:

$$w_j = \frac{w \cdot w_{j,\,\text{recipe}}}{\sum\limits_j w_{j,\,\text{recipe}}} \tag{B.3}$$

This scaling expression is substituted into Eq. (B.2) which can be rewritten as

$$\sum_{j=\text{solutes}} b_j = \frac{w}{(1000 - w)} \sum_j \frac{w_{j,\,\text{recipe}}}{M_j \sum\limits_j w_{j,\,\text{recipe}}} \tag{B.4}$$

Using the seawater recipe, the summed term on the right side of Eq. (B.4) results in a value of 31.841 mol/kg.

A correlation for the osmotic coefficient of seawater is given by Sharqawy et al. [63] and is valid between 0 and 200°C and for salinities between 10 and 120 g/kg. The osmotic coefficient for a mixture, as described by Debye-Hückel theory, approaches a value of 1 with decreasing salinity and does so independently of temperature. Literature values and correlations of the osmotic coefficient and osmotic pressure for diluted seawater with a salinity of 10 g/kg and below which adhere to this proper physical limit have been difficult to find. Therefore, an extension of the correlation provided by Sharqawy et al. is proposed by use of the theoretical expression for the osmotic coefficient given in Eq. (B.5), Brønsted's equation [75].

$$\phi = 1 - \beta b^{1/2} + \lambda b \tag{B.5}$$

This expression describes the osmotic coefficient as a function of molality and is dependent on two constants, β and λ. To find the value of these constants, Eq. (B.5) and the first derivative of Eq. (B.5) with respect to salinity form two equations with the two constants as unknowns. These equations are set to equal the value of ϕ

given by the correlation and its first derivative with respect to salinity at a salinity of 10 g/kg. For a temperature of 25°C, the two constants are found to be $\beta = 0.3484$ and $\lambda = 0.3076$. The final osmotic coefficient function is now set to be a piece-wise function with Eq. (B.5) forming the function for $0 \leq w < 10$ g/kg and the correlation forming the $10 \leq w \leq 120$ g/kg section. The extended osmotic coefficient function and the sum of molalities as a function of salinity, Eq. (B.4), are now implemented into Eq. (B.1) to determine the osmotic pressure of a stream at a given temperature and salinity. Figure A-1 shows the resultant seawater osmotic coefficient, osmotic pressure, and van 't Hoff approximation vary as functions of salinity at a fixed temperature of $T = 25°C$.

THIS PAGE INTENTIONALLY LEFT BLANK

Bibliography

[1] United Nations Development Program. *Human Development Report.* http://www.un.org/waterforlifedecade/scarcity.shtml, 2006.

[2] The Telegraph. Dirty water kills more people than war, UN says, March 2010.

[3] IDA. *Desalination Yearbook, Section 1. Market Profile.* International Desalination Association, 2011 - 2012.

[4] K.L. Lee, R.W. Baker, and H.K. Lonsdale. Membranes for power generation by pressure-retarded osmosis. *Journal of Membrane Science*, 8:141–171, 1981.

[5] H.K. Lonsdale, U. Merten, and R.L. Riley. Transport properties of cellulose acetate osmotic membranes. *Journal of Applied Polymer Science*, 9(4):1341–1362, 1965.

[6] U. Merten. *Desalination by reverse osmosis.* MIT Press, 1966.

[7] S. Kimura and S. Sourirajan. Analysis of data in reverse osmosis with porous cellulose acetate membranes used. *American Institute of Chemical Engineers Journal*, 13(3):497–503, 1967.

[8] O. Kedem and A. Katchalsky. Thermodynamic analysis of the permeability of biological membranes to non-electrolytes. *Biochimica et Biophysica Acta*, 27(0):229–246, 1958.

[9] J.G. Wijmans and R.W. Baker. The solution-diffusion model: a review. *Journal of Membrane Science*, 107(1-2):1–21, 1995.

[10] D.R. Paul. Reformulation of the solution-diffusion theory of reverse osmosis. *Journal of Membrane Science*, 241(2):371–386, 2004.

[11] G. Mauviel, J. Berthiaud, C. Vallieres, D. Roizard, and E. Favre. Dense membrane permeation: From the limitations of the permeability concept back to the solution-diffusion model. *Journal of Membrane Science*, 266(1-2):62–67, 2005.

[12] A. Yaroshchuk. Influence of osmosis on the diffusion from concentrated solutions through composite/asymmetric membranes: Theoretical analysis. *Journal of Membrane Science*, 355(1-2):98–103, 2010.

[13] E. Nagy. *Basic equations of the mass transport through a membrane layer.* Elsevier, 2012.

[14] E. Lyster and Y. Cohen. Numerical study of concentration polarization in a rectangular reverse osmosis membrane channel: Permeate flux variation and hydrodynamic end effects. *Journal of Membrane Science*, 303 (1-2):140–153, 2007.

[15] S.S. Sablani, M.F.A. Goosen, R. Al-Belushi, and M. Wilf. Concentration polarization in ultrafiltration and reverse osmosis: a critical review. *Desalination*, 141 (3):269–289, 2001.

[16] L. Song and C. Liu. A total salt balance model for concentration polarization in crossflow reverse osmosis channels with shear flow. *Journal of Membrane Science*, 401-402(0):313–322, 2012.

[17] H.J. Oh, T.M. Hwang, and S. Lee. A simplified simulation model of RO systems for seawater desalination. *Desalination*, 238(1-3):128–139, 2009.

[18] A. Matin, G. Ozaydin-Ince, Z. Khan, S.M.J. Zaidi, K. Gleason, and D. Eggenspiler. Random copolymer films as potential antifouling coatings for reverse osmosis membranes. *Desalination and Water Treatment*, 34(1-3):100–105, 2011.

[19] S. Sundaramoorthy, G. Srinivasan, and D.V.R. Murthy. An analytical model for spiral wound reverse osmosis membrane modules: Part I - model development and parameter estimation. *Desalination*, 280 (1-3):403–411, 2011.

[20] A. Chatterjee, A. Ahluwalia, S. Senthilmurugan, and S.K. Gupta. Modeling of a radial flow hollow fiber module and estimation of model parameters using numerical techniques. *Journal of Membrane Science*, 236 (1-2):1–16, 2004.

[21] M.G. Marcovecchio, N.J. Scenna, and O.A. Aguirre. Improvements of a hollow fiber reverse osmosis desalination model: Analysis of numerical results. *Chemical Engineering Research and Design*, 88 (7):789–802, 2010.

[22] M. Sekino. Precise analytical model of hollow fiber reverse osmosis modules. *Journal of Membrane Science*, 85 (3):241–252, 1993.

[23] M. Wilf and C. Bartels. Optimization of seawater RO systems design. *Desalination*, 173 (1):1–12, 2005.

[24] M. Li. Reducing specific energy consumption in reverse osmosis (RO) water desalination: An analysis from first principles. *Desalination*, 276 (1-3):128–135, 2011.

[25] M. Li. Optimal plant operation of brackish water reverse osmosis (BWRO) desalination. *Desalination*, 293 (0):61–68, 2012.

[26] M. Li and B. Noh. Validation of model-based optimization of brackish water reverse osmosis (BWRO) plant operation. *Desalination*, 304 (0):20–24, 2012.

[27] Y. Lu, A. Liao, and Y. Hu. Optimization design of RO system for water purification. In *Proceedings of the 11th International Symposium on Process Systems Engineering*, 2012.

[28] M.H. Sharqawy, S.M. Zubair, and J.H. Lienhard V. Second law analysis of reverse osmosis desalination plants: An alternative design using pressure retarded osmosis. *Energy*, 36:6617–6626, 2011.

[29] W.M. Kays and A.L. London. *Compact Heat Exchangers 3rd ed.* McGraw-Hill, 1984.

[30] R.A. Robinson and R.H. Stokes. *Electrolyte solutions.* Dover Publications Inc., 2002.

[31] J.H. Lienhard IV and J.H. Lienhard V. *A Heat Transfer Textbook 3rd ed.* Phlogiston Press, 2008.

[32] J. Kucera. *Reverse osmosis: industrial applications and processes.* Scrivener Publishing, 2010.

[33] H. El-Dessouky and H. Ettouney. *Fundamentals of salt water desalination.* Elsevier, 2002.

[34] S. Loeb. Osmotic power plants. *Science*, 189:654–655, 1975.

[35] G.D. Mehta and S. Loeb. Internal polarization in the porous substructure of a semipermeable membrane under pressure-retarded osmosis. *Journal of Membrane Science*, 4:261–265, 1978.

[36] J.R. McCutcheon and M. Elimelech. Influence of concentrative and dilutive internal concentration polarization on flux behavior in forward osmosis. *Journal of Membrane Science*, 284:237–247, 2006.

[37] S. Qianhong, Y.K.W. Wong, S. Zhao, and C.Y. Tang. Organic fouling in pressure retarded osmosis: Experiments, mechanisms, and implications. *Journal of Membrane Science*, 428:181–189, 2013.

[38] V. Parida and H.Y. Ng. Forward osmosis fouling: Effects of organic loading, calcium, and membrane orientation. *Desalination*, 312:88–98, 2013.

[39] A. Nguyen, S. Azari, and K. Zou. Coating zwitterionic amino acid L-DOPA to increase fouling resistance of forward osmosis membrane. *Desalination*, 312:82–87, 2013.

[40] L.A. Hoover, J.D. Schiffman, and M. Elimelech. Nanofibers in thin-film composite membrane support layers: Enabling expanded application of forward and pressure retarded osmosis. *Desalination*, 308:73–81, 2013.

[41] S. Chou, R. Wang, L. Shi, Q. She, C.Y. Tang, and A.G. Fane. Thin-film composite hollow fiber membranes for pressure retarded osmosis (PRO) process with high power density. *Journal of Membrane Science*, 389:25–33, 2012.

[42] K.Y. Wang and T.S. Chung. Developing thin-film composite forward osmosis membranes on the PES/SPSf substrate through interfacial polymerization. *American Institute of Chemical Engineers Journal*, 58:770–781, 2012.

[43] D.H. Jung, J. Lee, D.Y. Kim, Y.G. Lee, M. Park, S. Lee, D.R. Yang, and J.H. Kim. Simulation of forward osmosis membrane process: Effect of membrane orientation and flow direction of feed and draw solutions. *Desalination*, 277:83–91, 2011.

[44] B. Gu, D. Kim, and D. Yang. Mathematical model of flat sheet membrane modules for FO process: Plate-and-frame module and spiral-wound module. *Journal of Membrane Science*, 379:403–415, 2011.

[45] M.F. Gruber, C.J. Johnson, C.Y. Tang, M.H. Jensen, L. Yde, and C. Helix-Nielsen. Computational fluid dynamics simulations of flow and concentration polarization in forward osmosis membrane systems. *Journal of Membrane Science*, 379:488–495, 2011.

[46] A. Sagiv and R. Semiat. Finite element analysis of forward osmosis process using NaCl solutions. *Journal of Membrane Science*, 379:86–96, 2011.

[47] S. van der Zwan, I.W.M. Pothof, B. Blankert, and J.I. Bara. Feasibility of osmotic power from a hydrodynamic analysis at module and plant scale. *Journal of Membrane Science*, 389:324–333, 2012.

[48] S.A. Klein. Engineering equation solver v8.881-3d. F-Chart Software, February 2011.

[49] S.E. Skilhagen, J.E. Dugstad, and R.J. Aaberg. Osmotic power - power production based on the osmotic pressure difference between waters with varying salt gradients. *Desalination*, 220:476–482, 2007.

[50] L.D. Banchik and J.H. Lienhard V. "Thermodynamic Analysis of a Reverse Osmosis Desalination System Using Forward Osmosis for Energy Recovery". In *Proc. ASME 2012 Intl. Mech. Engr. Cong. & Exp., IMECE2012-86987, Houston*, November 2012.

[51] W.A. Waqas, M.H. Sharqawy, and J.H. Lienhard V. Energy utilization from disposed brine of MSF desalination plant using pressure retarded osmosis. In *IDA World Congress, Tianjin, China, under review*, 2013.

[52] J.R. McCutcheon and M. Elimelech. Modeling water flux in forward osmosis: implications for improved membrane design. *American Institute of Chemical Engineers Journal*, 53:1736–1744, 2007.

[53] R.E. Pattle. Production of electric power by mixing fresh and salt water in the hydroelectric pile. *Nature*, 174:660, 1954.

[54] A. Achilli, T.Y. Cath, and A.E. Childress. Power generation with pressure retarded osmosis: An experimental and theoretical investigation. *Journal of Membrane Science*, 343:42–52, 2009.

[55] S. Zhao, L. Zou, C.Y. Tang, and D. Mulcahy. Recent developments in forward osmosis: Opportunities and challenges. *Journal of Membrane Science*, 396:1–21, 2012.

[56] G.Z. Ramon, B.J. Feinberg, and E.M. V. Hoek. Membrane-based production of salinity-gradient power. *Energy & Environmental Science*, 4:4423–4434, 2011.

[57] J.W. Post, J.Veerman, H.V.M. Hamelers, G.J.W. Euverink, S.J. Metz, K. Nymeijer, and C.J.N. Buisman. Salinity-gradient power: Evaluation of pressure-retarded osmosis and reverse electrodialysis. *Journal of Membrane Science*, 288:218–230, 2007.

[58] R.L. McGinnis, J.R. McCutcheon, and M. Elimelech. A novel ammonia-carbon dioxide osmotic heat engine for power generation. *Journal of Membrane Science*, 305:13–19, 2007.

[59] K.H. Mistry, R.K. McGovern, G.P. Thiel, E.K. Summers, S.M. Zubair, and J.H. Lienhard V. Entropy generation analysis of desalination technologies. *Entropy*, 13(10):1829–1864, 2011.

[60] N.Y. Yip and M. Elimelech. Thermodynamic and energy efficiency analysis of power generation from natural salinity gradients by pressure retarded osmosis. *Environmental Science and Technology*, 46:5230–5239, 2012.

[61] R. Labrecque. Exergy as a useful variable for quickly assessing the theoretical maximum power of salinity gradient energy systems. *Entropy*, 11:798–806, 2009.

[62] M. Wilf. *The Guidebook to Membrane Desalination Technology*. Balaban Desalination Publications, 2007.

[63] M.H. Sharqawy, J.H. Lienhard V, and S.M. Zubair. Thermophysical properties of seawater: A review of existing correlations and data. *Desalination and Water Treatment*, 16:354–380, 2010.

[64] B. Liberman and G. Greenberg. Recovery of osmotic power in SWRO plants. In *IDA World Congress/Perth Convention and Exhibition Centre (PCEC)*, 2011.

[65] T.Y. Cath, A.E. Childress, and M. Elimelech. Forward osmosis: Principles, applications, and recent developments. *Journal of Membrane Science*, 287:70–87, 2006.

[66] J.R. McCutcheon, R.L. McGinnis, and M. Elimelech. Desalination by ammonia-carbon dioxide forward osmosis: Influence of draw and feed solution concentrations on process performance. *Journal of Membrane Science*, 278:114–123, 2006.

[67] Robert L. McGinnis and Menachem Elimelech. Energy requirements of ammonia-carbon dioxide forward osmosis desalination. *Desalination*, 207:370–382, 2007.

[68] O.A. Bamaga, A. Yokochi, B. Zabara, and A.S. Babaqi. Hybrid FO/RO desalination system: Preliminary assessment of osmotic energy recovery and designs of new FO membrane module configurations. *Desalination*, 268:163–169, 2011.

[69] S. Loeb. Large-scale power production by pressure-retarded osmosis, using river water and sea water passing through spiral modules. *Desalination*, 143:115–122, 2002.

[70] H. Enomoto, M. Fujitsuka, T. Hasegawa, M. Kuwada, A. Tanioka, and M. Minagawa. A feasibility study of pressure-retarded osmosis power generation system based on measuring permeation volume using reverse osmosis membrane. *Electrical Engineering in Japan*, 173:1129–1138, 2010.

[71] A. Achilli and A.E. Childress. Pressure retarded osmosis: From the vision of Sidney Loeb to the first prototype installation – review. *Desalination*, 261:205–211, 2010.

[72] B. Liberman. Present and future: Energy efficient seawater desalination. In *Desalination: an energy solution.* International Desalination Association, 2010.

[73] ERI. Energy Recovery Inc. reverse osmosis with pressure exchanger model. *http://www.energyrecovery.com/index.cfm/0/0/56-Power-Model.html*, April 2012.

[74] F.J. Millero and W.H. Leung. The thermodynamics of seawater at one atmosphere. *American Journal of Science*, 276:1035–1077, 1976.

[75] K.S. Pitzer. *Thermodynamics 3rd ed.* McGraw-Hill, 1995.